Diagnosing electronic phases of matter using photonic correlation functions

Gautam Nambiar,[1] Andrey Grankin,[1] and Mohammad Hafezi[1]

[1]*Joint Quantum Institute, University of Maryland, College Park, Maryland 20742, USA*

In the past couple of decades, there have been significant advances in measuring quantum properties of light, such as quadratures of squeezed light and single-photon counting. Here, we explore whether such tools can be leveraged to probe electronic correlations in the many-body quantum regime. Specifically, we show that it is possible to probe certain spin, charge, and topological orders in an electronic system by measuring the quadrature and correlation functions of photons scattered off it. We construct a mapping from the correlation functions of the scattered photons to those of a correlated insulator, particularly for Mott insulators described by a single-band Hubbard model at half-filling. We show how frequency filtering before photodetection plays a crucial role in determining this mapping. If the ground state of the insulator is a gapped spin liquid, we show that a $G^{(2)}$ (two-photon coherence) measurement can detect the presence of anyonic excitations with fractional mutual statistics. We also show that homodyne measurements can be used to detect expectation values of static spin chirality operators on both the kagome and triangular lattices, thus being useful in detecting chiral spin liquids. Moreover, a slew of hitherto unmeasured spin-spin and spin-charge correlation functions of the material can be extracted from photonic correlations. This work opens up access to probe correlated materials, beyond the linear response paradigm, by detecting quantum properties of scattered light.

I. INTRODUCTION

Strongly interacting quantum many-body systems can host a variety of exotic phases of matter. However, there exists a gap between theoretical models and experimental observations in terms of accessible physical observables. A hallmark example is topologically ordered phases, beginning with the experimental observation of the Fractional Quantum Hall effect, whose excitations exhibit fractional statistics [1–6]. There are strong theoretical reasons [7–9] to expect that spin systems dubbed "quantum spin liquids" also host topological order and other exotic gapless field theories [10–16]. However, experimental verification of such claims has been extremely challenging. At the same time, other unconventional phases, including high-temperature superconductors and correlated insulators, have been experimentally observed in cuprate-like strongly correlated materials [17], and more recently in moiré materials [18, 19]. While there is a thriving theoretical effort to explain many of these phases, conclusively matching theory to experiment is generally difficult. The main challenge stems from the fact that the nontrivial nature of many of these phases is encoded in correlation functions that are difficult to measure experimentally. Conventionally, probes for accessing electronic correlation functions work within the linear response paradigm. For example, Raman scattering has been employed to study potential spin liquid candidates [20–25]. However, given how difficult it is to characterize exotic phases, it is important to (1) develop novel experimental protocols to measure a wider class of correlation functions and (2) understand how these new correlation functions can assist in diagnosing the phase of matter under study.

A promising approach is to move beyond the linear-response paradigm by studying the nonlinear response to an external electromagnetic drive [26–47]. One example
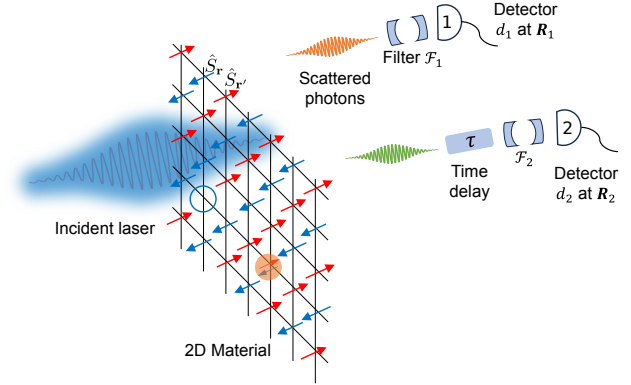

Figure 1. A system of itinerant electrons is irradiated with a laser. Conventionally, photodetectors measure the intensity of the scattered photons, and the correlations are ignored. In this paper, we propose a Hanbury Brown-Twiss-type setup to measure correlations between pairs of photons. We allow for frequency filters, $\mathcal{F}_1$ and $\mathcal{F}_2$, before detection, and a time delay, τ, between detection events.

is two-dimensional coherent spectroscopy, an extension of pump-probe spectroscopy [48–50], in which two pump pulses, separated by a fixed time delay, are applied to the sample, followed by a probe measurement at a fixed delay relative to the last pulse. A recent work predicted that a setup like this can be used to detect anyonic excitations [46, 47]. It is also possible to go beyond the linear-response paradigm by studying higher-order correlations within the output signal generated by external stimuli. A classic example is shot noise in electric current [51] that has been used to detect fractionally charged excitations [52, 53], Cooper pairing in normal state [54, 55] and absence of quasiparticles [56].

Thus, it is intriguing to ask whether quantum correlations between scattered photons could carry useful in-

formation beyond what can be obtained from linear response. It is known in quantum optics that when two or more photons are scattered off an optically nonlinear medium, they can become correlated [57]. Our work demonstrates that when this medium is a strongly correlated electronic system, its nontrivial correlations are inherited by the scattered photons. Therefore, analyzing photonic correlations in the outcome of spectroscopy experiments provides an alternative approach for studying many-body phases of matter.

The paradigmatic setup for the detection of the photonic correlations consists of a Hanbury Brown-Twiss interferometer where the scattered photons are divided into two separate paths [58] (See Fig. 1). Then, the photons are detected in each path separately. In this work, we also allow for the possibility of frequency and polarization filtering before detection. This scheme allows for the measurement of a four-point correlation function $G^{(2)}_{d_1,d_2}(\tau) = \langle \hat{a}^\dagger_{d_1}(0)\hat{a}^\dagger_{d_2}(\tau)\hat{a}_{d_2}(\tau)\hat{a}_{d_1}(0)\rangle$, where $\hat{a}_{d_j}$ are the annihilation operators of the filtered photonic mode in the corresponding (j-th) interferometer arm. τ denotes the time delay between the detection events[59]. We note that in addition to $G^{(2)}$, the described setup allows for the measurement of correlation functions of electromagnetic quadrature including $\langle \hat{a}_{d_1}(0)\rangle$ and $\langle \hat{a}_{d_2}(\tau)\hat{a}_1(0)\rangle$. This is done by mixing the scattered photons with a strong reference coherent field having a fixed phase.

In this work, we first develop a systematic procedure to map these photonic correlators to dynamical correlation functions of the material in its undriven state. As a specific example, we provide the mapping for a single-band Hubbard model at half-filling in a Mott insulator state. Furthermore, we demonstrate that frequency filtering plays a crucial role in determining the mapping. We show that depending on the filtering, the resulting correlation functions can be either purely in the spin sector or can be in the mixed spin-charge sector.

We then present several salient applications: (1) The first one is the measurement of spin chirality operators. These operators have nonzero expectation values in chiral spin liquids [60–66], and play the role of chiral mass terms in $U(1)$ Dirac spin liquids [67, 68]. We show that using first and second-order photonic homodyne correlations, one can measure the static expectation value of spin chirality operator on the kagome and triangular lattices respectively. (2) We show how optical correlations in scattered photons can measure mixed spin-charge correlators, which provide insight into the dynamics of a hole and a doubly-occupied site (called a doublon) in a Mott insulator. (3) We show that the $G^{(2)}$ correlation function can be also used to diagnose whether the state in the spin sector is a spin liquid with excitations carrying fractional mutual statistics. For this, we follow the semiclassical argument in Refs. [46, 47] for pump-probe spectroscopy, and show that it also applies for $G^{(2)}$ spectroscopy.

II. SUMMARY OF THE PAPER

In this section, we provide an overview of the main results of this paper, along with sufficient background and context to allow each of the remaining sections to be read independently.

A. The setting

We now consider the problem of photon scattering off a 2-dimensional strongly correlated electronic system, as shown in Fig. 1. The material, initially prepared in a thermal equilibrium state, is irradiated by a monochromatic laser having polarization $\mathbf{e}_L$ and frequency ω_L. The laser driving is weak, in the sense that $g_L \equiv \sqrt{2\pi I_L \alpha}\mathbf{a}/\omega_L \ll 1$, where I_L is the laser intensity, α is the fine-structure constant and $\mathbf{a}$ is the lattice spacing of the electronic system. Throughout this work, we assume the initial state of the electromagnetic field to be in either a Fock state $|\mathcal{N}_L\rangle = (\mathcal{N}_L!)^{-1/2}(\hat{a}^\dagger_L)^{\mathcal{N}_L}|0\rangle$ or in a coherent state $e^{\phi_L \hat{a}^\dagger_L - \phi^*_L \hat{a}_L}|0\rangle$, where $|0\rangle$ is the vacuum and $\hat{a}_L$ is the annihilation operator of the laser mode (see Appendix A for a more careful treatment of the laser as a wavepacket). Since the driving is weak, we can restrict our consideration to the subspace containing at most 2 scattered photons [69, 70]. These photons, before being detected, are separated into the two arms of a Hanbury Brown-Twiss interferometer, each containing frequency and polarization filters. Suppose $\mathcal{F}_j(\omega - \omega_j)$ is the filter function before detector d_j centerd around frequency ω_j with possibly some spread. The filter function is causal in the sense that $\tilde{\mathcal{F}}_j(t) \equiv \int^\infty_{-\infty} \frac{d\omega}{2\pi}\mathcal{F}_j(\omega - \omega_j)e^{-i(\omega - \omega_j)t}$ is 0 when $t < 0$. Then the photon annihilation operator of detector, $\hat{a}_{d_j}$ is roughly of the form $\hat{a}_{d_j} \sim i\sum_{\mathbf{k}}\mathcal{F}_j(\omega_{\mathbf{k}} - \omega_j)\hat{a}_{\mathbf{k},\mathbf{e}_j}$, i.e., a superposition of normal modes of free space $\hat{a}_{\mathbf{k},\mathbf{e}_j}$ labeled by momenta $\mathbf{k}$ and polarization $\mathbf{e}_j$. For a precise definition of $\hat{a}_{d_j}$, see Eq. (9, 11). Measurements are made in the state $|\text{out}\rangle$ in the asymptotic future, (formally defined in Sec. III A).

For the matter side, the general form of our results applies to any correlated insulator with an optical gap. For concreteness, we consider a 2-dimensional system of strongly interacting itinerant electrons in a Mott-insulator state, which we model by the single-band Hubbard model at half-filling [71, 72]. In the limit of strong on-site interaction $U \gg \mathtt{t}$, where $\mathtt{t}$ is the tunneling amplitude between nearest sites, the many-body energy spectrum splits into sectors having a definite number of doubly occupied sites ("doublon excitations"). The lowest energy manifold ("spin sector") is represented by the pure spin excitations described by the Heisenberg model. Depending on the lattice geometry, and strengths of tunnelings between next-nearest neighbors and beyond, there are several possibilities for the ground state of the spin sector. It could be a magnetically ordered state such as a Néel or a 120° antiferromagnet, in which case its ex-

citations are magnons. It could also be a quantum spin liquid whose excitations are charged under an emergent gauge group, or have fractional statistics or both.

Let us suppose the laser frequency ω_L is slightly detuned from the optical gap U. Specifically, we assume $\mathtt{t} \ll |\omega_L - U| \ll U$. Since a photon cannot get resonantly absorbed, it off-resonantly couples the two matter sectors (spin and charge sectors for the Hubbard model) shown in Fig. 2 and the photon gets inelastically scattered. The amplitudes for inelastic, i.e., Raman scattering depend on the finer structure within the spin and charge sectors. We note that in contrast to the conventional Raman spectroscopy, we are interested in the scattering of multiple photons which, as we demonstrate, provides additional information on the state electronic system. The relation between the inelastic photon scattering amplitudes and the matter correlations constitutes the main focus of this work and will be reviewed in the section below.

B. Mapping between photonic and matter correlators (Input-output relations)

Assuming $\mathtt{t} \ll |\omega_L - U| \ll U$, we can perform a systematic expansion of the photonic correlation functions with respect to the drive strength. We start by providing a qualitative picture of the laser-induced processes. Emission of a photon by the driven material, order by order in the drive strength, can result from one of the three pathways shown in Fig. 2(a-c). Fig. 2(a) is a Raman scattering process, where one photon is absorbed off-resonantly from the laser, and another photon of frequency ω_λ is emitted, and in the process, the material transitions from a state $|I\rangle$ to $|J\rangle$ in the same sector. Then, $\omega_\lambda = \omega_L + E_I - E_J$, and therefore the emitted photon has frequency close to ω_L. Fig. 2(b) is one order higher in the drive strength, as it involves absorption of two photons from the laser, and emission of a photon so that the material transitions from state $|I\rangle$ in the lower energy sector into $|K\rangle$ in the higher energy sector. Here, $\omega_\lambda = 2\omega_L + E_I - E_K$, and thus is of the order $2\omega_L - U$. To see how Fig. 2(c) arises, we can suppose that the process in Fig. 2(b) already happened. Then the material can come back to the lower energy sector by emitting a photon of frequency $E_K - E_I$, which is roughly U. Therefore, the intensity of emitted photons as a function of frequency has a profile as shown in Fig. 2(d-f). Because processes in Fig. 2(b-c) are one order higher in laser-material coupling than the one in Fig. 2(a), the heights of the peaks around $2\omega_L - U$ and U are lower than the central peak around ω_L. The microscopic details of these processes in the Hubbard model at half-filling will be the subject of Sec. V. In Sec. IV B, IV C and later VI, we obtain the mapping from photonic correlation functions to matter correlation functions resulting from the above processes. To do so, we use a $\hat{\mathcal{T}}$-matrix formalism. But for now, we will shortcut our way to the answer by writing the following effective Hamiltonian describing light emission in the *interaction picture* that captures all the processes in Fig. 2.

$$\hat{H}_{\mathrm{eff}}^I(t) = \sum_\lambda \hat{M}_\lambda(t)\hat{a}_\lambda^\dagger e^{i\omega_\lambda t} + \mathrm{h.c.} \tag{1}$$

Recall that in the interaction picture, $\hat{A}(t) = e^{i\hat{H}_0 t}\hat{A}e^{-i\hat{H}_0 t}$, where $\hat{H}_0$ is the Hamiltonian that excludes light-matter interactions. In the above equation, the operator $\hat{a}_\lambda^\dagger$ creates a photon in mode λ, which is a composite index for momentum and polarization. $\hat{M}_\lambda$ is a pure matter operator given by

$$\hat{M}_\lambda(t) = \left[e^{-i\omega_L t}\hat{A}_\lambda(t) + e^{-2i\omega_L t}\hat{B}_\lambda(t) + \hat{C}_\lambda(t)\right] + \mathrm{h.c.} \tag{2}$$

The operator $\hat{A}_\lambda$ [Fig. 2(a)] couples state $|I\rangle$ to $|J\rangle$ within the same lower energy sector. Operator $\hat{B}_\lambda$ [Fig. 2(b)] on the other hand takes $|I\rangle$ in the lower energy sector to $|K\rangle$ in the higher energy sector. Operator $\hat{C}_\lambda$ [Fig. 2(c)] takes $|K\rangle$ in the higher energy sector to $|I\rangle$ in the low energy sector. Operators $\hat{B}_\lambda$ and $\hat{C}_\lambda$ thus implement photon emission into the sidebands in Fig. 2(e) and Fig. 2(f) respectively. For the energy scales we consider in this work, the dependence of the matter operators on λ comes entirely through the polarization, since the momentum imparted to an electron from photons is negligible. So we will later replace the subscript λ by $j \in \{1, 2\}$ which determines whether the operator couples to the polarization of detector d_1 or d_2.

To determine the mapping between photonic and matter operators, let us apply the effective Hamiltonian, Eq. (1), to first order in perturbation theory. To detect a photon at time τ, it must have been emitted at some earlier time, say $\tau - t$ for $t > 0$, spending the remaining time in the filter. The greater the frequency resolution in the filter, the greater the uncertainty in this t. Conversely, if there is no frequency resolution, t is constrained to be 0. This relationship is expressed mathematically by the following correspondence:

$$\hat{a}_{d_j}(\tau) \mapsto \int_0^\infty \mathrm{d}t\, \tilde{\mathcal{F}}_j(t)e^{-i\omega_j t}\hat{M}_j(\tau - t). \tag{3}$$

In other words, to extract a matter correlator from a photonic correlator, the photonic operator $\hat{a}_{d_j}$ is replaced by the convolution of the (Fourier-transformed) filter function and the matter operator $\hat{M}_j$. The resulting mapping is summarized in Table I.

As shown earlier in Fig. 2, the frequency of emitted photons is either around the central peak ω_L, or located in pairs of sidebands, near $2\omega_L - U$ and U. The corresponding matter operators $\hat{A}_j$, $\hat{B}_j$ and $\hat{C}_j$ have distinct physical structure, which we study in details for the single-band Hubbard model in Sec. V. Let us summarize the main points here. The operator $\hat{A}_j$ is a
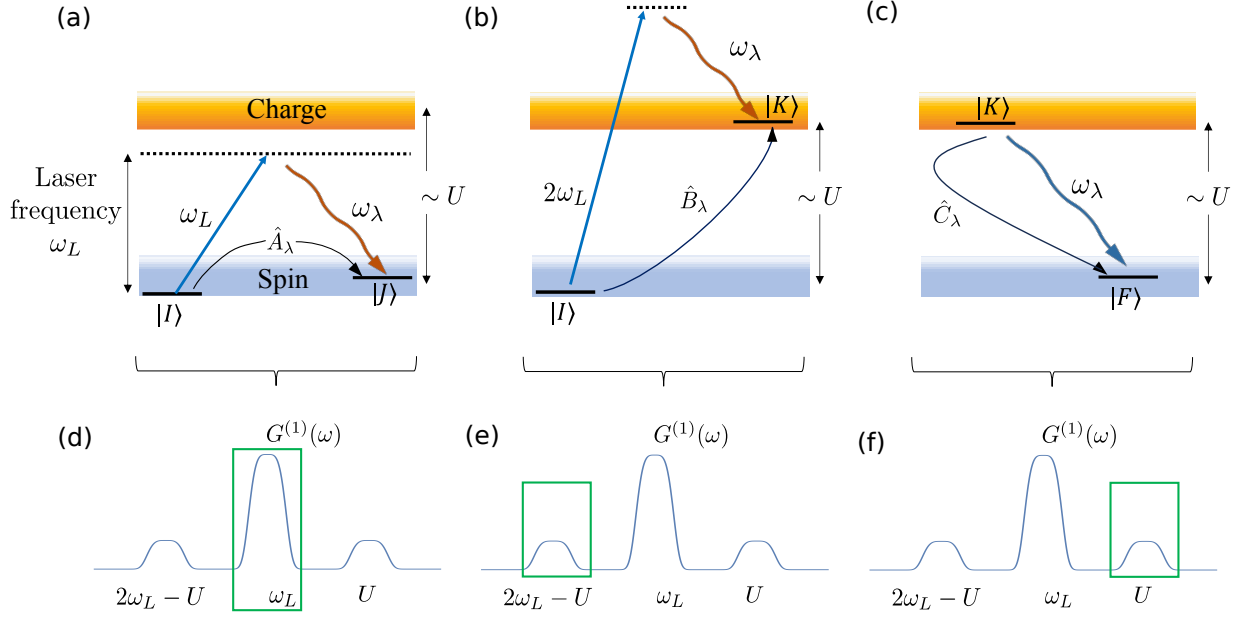
Figure 2. **(a-c)**The sectors shaded blue and orange are the lower and higher energy sectors respectively separated by an optical gap of order U. For the Hubbard model at half-filling, U is the Hubbard gap, and the low and high energy sectors are spin and charge sectors respectively. But in general, our formalism works for any insulator with an optical gap. The drive frequency ω_L is detuned from U. Different pathways leading to emission of a photon are shown. **(a)**: Raman process – absorption of a laser photon followed by emission of a photon of frequency around ω_L. This results in an effective matter operator $\hat{A}_\lambda$ that has a matrix element taking state $|I\rangle$ to $|J\rangle$ both within the same (lower energy) sector. **(b)**: Absorption of two photons followed by emission of a photon of frequency near $2\omega_L - U$. The effective matter operator $\hat{B}_\lambda$ takes $|I\rangle$ in the lower energy sector to $|K\rangle$ in the higher energy sector. **(c)**: Emission of a photon of frequency near U starting from a state $|K\rangle$ in the higher energy sector that was reached using process (b). The effective matter operator $\hat{C}_\lambda$ takes $|K\rangle$ to $|F\rangle$ in the lower energy sector. The corresponding schematic for the intensity vs frequency profile is shown in **(d-f)**. We see that the emission into sideband (e) always occurs together with emission into sideband (f).

sum of spin singlet terms modulated by the polarizations of the incoming laser and the detected photon. We suppose $\hat{\mathbf{S}}_\mathbf{r}$ is the spin of an electron at site $\mathbf{r}$. To leading order in $\mathtt{t}/|\omega_L - U|$, $\hat{A}_j \sim \frac{\mathtt{t}^2}{\omega_L - U} \sum_{\mathbf{r},\boldsymbol{\mu}} (\boldsymbol{\mu} \cdot \mathbf{e}_j^*)(\boldsymbol{\mu} \cdot \mathbf{e}_L)\left(4\hat{\mathbf{S}}_\mathbf{r} \cdot \hat{\mathbf{S}}_{\mathbf{r}+\boldsymbol{\mu}} - 1\right)$, where $\boldsymbol{\mu}$ runs through the directions available for electron-tunneling. This is the Loudon-Fleury operator [22, 23, 73], which is defined in detail in Eq. (53)). This operator $\hat{A}_j$ can be seen as a sum of 2×2 tensors in the polarization directions, i.e., $(e_j^*)^u (e_L)^v$ for $u, v \in \{x, y\}$. It can thus be decomposed into channels that are irreducible representations of the crystalline point group of the lattice. One can check that the above term in the channel $(e_j^*)^x(e_L)^y - (e_j^*)^y(e_L)^x$ (invariant under spatial rotations but odd under reflection) is zero for all lattices. Ref. [24] showed that on the kagome lattice, the leading order term in this channel, appearing at $\mathtt{t}^4/(\omega_L - U)^3$ is a sum of spin chirality operators $\sim \hat{\mathbf{S}}_\mathbf{r} \cdot \left(\hat{\mathbf{S}}_{\mathbf{r}'} \times \hat{\mathbf{S}}_{\mathbf{r}''}\right)$. We will shortly use this fact.

Next, operator $\hat{B}_j$ is a mixed spin-charge operator that involves both a spin operator and electron tunneling creating a doublon-hole pair (shown in Fig. 7, 8, and defined

precisely in Eq. (54)). Finally, $\hat{C}_j$ is a sum of electron tunneling operators and is proportional to the total electric current [Eq. (55)]. Given that $\hat{A}_j$ acts within a single sector, while $\hat{B}_j$ and $\hat{C}_j$ couples the two sectors, it is useful to treat them separately. Therefore, we specialize to the case where the filter functions have enough resolution to distinguish the three peaks in Fig. 2, while within each peak, the filter may be either broad or narrow. Then,

$$\hat{M}_j(t) = \begin{cases} e^{-i\omega_L t}\hat{A}_j(t) & \text{if detector } d_j \text{ detects near } \omega_L \\ e^{-2i\omega_L t}\hat{B}_j(t) & \text{if detector } d_j \\ & \quad \text{detects near } 2\omega_L - U \\ \hat{C}_j(t) & \text{if detector } d_j \text{ detects near } U. \end{cases}$$
$$(4)$$

This mapping is also summarized in Table I, which is presented later in Sec. VI [Eqs. (58, 61, 65, 72 and C19)].

To gain some intuition for these expressions, let us suppose the matter operator $\hat{M}_j(t)$ associated with photon emission creates an excitation. Two-photon correlations should then probe the dynamics of pairs of such excitations. One might naïvely think that the delay τ between the detection of the two photons is the same as the delay between the two matter excitation events. However, this

Photonic correlator	Matter correlator
Intensity $G^{(1)}_{d_j}(0) = \left\langle \hat{a}^\dagger_{d_j}(0)\hat{a}_{d_j}(0)\right\rangle_{\text{out}}$	$\iint_0^\infty \mathrm{d}t\,\mathrm{d}t'\,\tilde{\mathcal{F}}_j(t)\left[\tilde{\mathcal{F}}_j(t')\right]^* e^{-i\omega_j(t-t')}\left\langle \left[\hat{M}_j(-t')\right]^\dagger \hat{M}_j(-t)\right\rangle_0$
Second-order coherence $G^{(2)}_{d_1,d_2}(\tau) = \left\langle \hat{a}^\dagger_{d_1}(0)\hat{a}^\dagger_{d_2}(\tau)\hat{a}_{d_2}(\tau)\hat{a}_{d_1}(0)\right\rangle_{\text{out}}$	$\iiiint_0^\infty \mathrm{d}t_1\,\mathrm{d}t_2\,\mathrm{d}t'_1\,\mathrm{d}t'_2\,\tilde{\mathcal{F}}_1(t_1)\tilde{\mathcal{F}}_2(t_2)[\tilde{\mathcal{F}}_1(t'_1)]^*[\tilde{\mathcal{F}}_2(t'_2)]^* e^{i\omega_1(t'_1-t_1)}e^{i\omega_2(t'_2-t_2)}$ $\times \left\langle \bar{\mathbb{T}}\left[\hat{M}^\dagger_1(-t'_1)\hat{M}^\dagger_2(\tau-t'_2)\right]\mathbb{T}\left[\hat{M}_2(\tau-t_2)\hat{M}_1(-t_1)\right]\right\rangle_0$
First-order homodyne: $\left\langle \hat{a}_{d_j}(0)\right\rangle_{\text{out}}$	$\mathcal{F}_j(\omega_L-\omega_j)\left\langle \hat{M}_j(0)\right\rangle_0$
Second-order homodyne (photon number conserving): $\left\langle \hat{a}^\dagger_{d_2}(\tau)\hat{a}_{d_1}(0)\right\rangle_{\text{out}}$	$\iint_0^\infty \mathrm{d}t_1\,\mathrm{d}t_2\,\tilde{\mathcal{F}}_1(t_1)\left[\tilde{\mathcal{F}}_2(t_2)\right]^* e^{i(\omega_2 t_2-\omega_1 t_1)}\left\langle \hat{M}^\dagger_2(\tau-t_2)\hat{M}_1(-t_1)\right\rangle_0$
Second-order homodyne (photon number non-conserving): $\left\langle \hat{a}_{d_2}(\tau)\hat{a}_{d_1}(0)\right\rangle_{\text{out}}$	$\iint_0^\infty \mathrm{d}t_1\,\mathrm{d}t_2\,\tilde{\mathcal{F}}_1(t_1)\tilde{\mathcal{F}}_2(t_2)e^{-i(\omega_1 t_1+\omega_2 t_2)}\left\langle \mathbb{T}\left[\hat{M}_2(\tau-t_2)\hat{M}_1(-t_1)\right]\right\rangle_0$

Table I. Dictionary between photonic correlators obtained from light-matter scattering (left column) and matter correlation functions in equilibrium (right column). Here $\mathbb{T}[\ ]$ denotes time ordering of operators inside $[\ ]$ and $\bar{\mathbb{T}}[\ ]$ denotes anti-time-ordering. Note that $G^{(1)}_{d_j}(0)$ is the same as intensity of Raman-scattered photons [22, 23].

is not the case when frequency filtering occurs before detection. The higher the frequency resolution, the greater is the importance of interference between amplitudes for excitations created at different times. This is also true for two-photon scattering from a two-level system, where the correlation function depends on filtering [74–76]. Furthermore, spectral resolution enables selection of the energy window of excitations (see Eq. (4) above). Thus, even though light-matter interaction occurred well before photodetection, the frequency filter placed before detection can drastically affect the information obtained about the matter.

C. Applications

Given this new access to matter correlation functions, what do we learn that cannot be obtained from photon intensity measurements alone? Here, we summarize key applications for Mott insulators in both the spin and charge sectors. We also show how photonic $G^{(2)}$ and homodyne correlation functions can reveal concrete signatures of spin liquids, which are generally notoriously difficult to observe otherwise.

1. Measuring static spin chirality

Chiral spin liquid is the equivalent of a 1/2- bosonic fractional quantum Hall state occuring in an electrically neutral system [60]. Often in chiral spin liquids, scalar spin chirality operators defined earlier (odd under time-reversal) spontaneously acquire nonzero expectation value [61–66]. So far, there are proposals to use neutron scattering [77] and Raman scattering [$G^{(1)}(0)$ in our notation] [24] to measure the fluctuations in spin chirality. Here, we show that homodyne measurements

can directly measure the *static* expectation values of spin chirality in both kagome and triangular lattice.

Recall from Table I and Eq. (4) that when the detector detects near ω_L, the first order homodyne measurement $\left\langle \hat{a}_{d_j}(0)\right\rangle_{\text{out}}$ directly measures the static expectation value of operator $\hat{A}_j$. Ref. [24] showed that on the kagome lattice in the channel $(e^*_j)^x(e_L)^y-(e^*_j)^y(e_L)^x$, operator $\hat{A}_j$ is, to leading order, a sum of spin chirality terms. Therefore, our first order homodyne correlator can directly measure this.

For the triangular lattice, on the other hand, the spin chirality terms vanish at order $\mathtt{t}^4/(\omega_L-U)^3$ in this channel [24]. In our work (Sec. VII), we show that static spin chirality can still be measured using $\text{Im}\left[\langle \hat{a}_{d_2}(0)\hat{a}_{d_1}(0)\rangle\right]$, i.e., second order homodyne correlation between a pair of photons in the sidebands, where the detector d_1 first detects near frequency $2\omega_L-U$ and the detector d_2 then detects near U, with no time delay $\tau=0$. In contrast to the fractional statistics detection scheme below, the filters here are only sharp enough to select the sidebands, but are broad within each sideband.

Note that because $\tau=0$, the doublon-hole pair created during the first photon emission has to immediately recombine during the second. Hence our result that the net operator (spin-chirality) lies entirely in the spin sector. Below, we discuss the general case (when $\tau \neq 0$), when the net operator is in the charged sector.

2. Charged sector dynamics

By detecting a photon pair in the sidebands, one can extract a mixed spin-charge correlation function. For example, for a Mott insulator, the emission of one photon can be accompanied by the creation of a doublon-hole pair at a bond, followed by application of specific spin op-

erators on sites neighboring this bond. These operators include spin singlet projectors. The doublon-hole pair can then propagate till it is forced to recombine by emitting the second photon. The resulting correlator can potentially capture information about possible bound states in the charge sector called Mott excitons [78–91] and their dependence on the spin background. We show the general form of such mixed spin-charge operators in Sec. V C. However, making quantitative predictions for the charged sector of correlated insulators is the subject of future research.

3. Anyonic excitations – detecting fractional statistics in spin liquid candidates

If the ground state in the spin sector is topologically ordered, its excitations can have fractional statistics. To detect such statistics, one first needs to subtract any contribution due to trivial excitations. We show in Sec. VIII A that the connected correlator $\mathcal{G}^{(2)}_{d_1,d_2}(\tau) \equiv G^{(2)}_{d_1,d_2}(\tau) - G^{(1)}_{d_1}(0)G^{(1)}_{d_2}(0)$ is zero when the excitations are non-interacting bosons, provided four conditions are met: (1) both the detectors have sharp frequency filters around ω_1 and ω_2 respectively, (2) $\omega_j \neq \omega_L$, i.e., no elastic scattering, (3) $\omega_1 \neq \omega_2$, and (4) the polarization symmetry channels (discussed in Sec. II B) for the two detectors are distinct. In this limit of sharp spectral resolution, the dependence on the time delay τ drops out due to energy-time uncertainty.

Now, if the material is topologically ordered, the emission of each photon can be accompanied by the creation of an anyon pair. As these anyons propagate, an anyon created during one photon emission can braid nontrivially with an anyon created during another photon emission. Based our discussion above, a nonzero contribution to the connected $\mathcal{G}^{(2)}_{d_1,d_2}$ should come from either nontrivial mutual statistics during such a braid, or from interactions between excitations. Using ideas in Ref. [46, 47], we show in Sec. VIII B that non-trivial braiding leads to a universal singularity as a function of detected frequencies ω_1 and ω_2. We define the Raman shifts $\Omega_j = \omega_L - \omega_j$ for $j \in \{1, 2\}$. Then, $G^{(2)}_{d_1,d_2}(\Omega_1, \Omega_2) \sim \theta(\Omega_1 - \Delta_1)\theta(\Omega_2 - \Delta_2)\left[K_2(\Omega_2)(\Omega_1 - \Delta_1)^{-3/2} + (1 \leftrightarrow 2)\right]$. Here, $\theta(\omega)$ is the Heaviside step function, Δ_1 and Δ_2 are energy thresholds for creating anyon pairs via operators $\hat{A}_1$ and $\hat{A}_2$ respectively, and $K_j(\Omega_j)$ are system-specific functions. This singularity is a sharp signature for fractional mutual statistics in a spin liquid candidate.

III. THE FORMALISM AND DEFINITIONS IN DETAIL

In this section, we first lay out the $\hat{\mathcal{T}}$-matrix formalism that we will use to model the scattering process. Then

we will carefully define the photonic correlators studied in this work.

A. Review of formalism

We model the experimental scenario as a scattering process under a time-independent Hamiltonian $\hat{H} \equiv \hat{H}_0 + \hat{V}$, where $\hat{H}_0$ is the Hamiltonian for light and matter excluding light-matter interactions, and $\hat{V}$ is the light-matter interaction. The initial state $|\Psi(t = -T/2)\rangle$ at time $t = -T/2$ (in the limit $T \to \infty$) has light and matter decoupled – with light being in a laser-produced wavepacket state spatially far away from the material [Fig. 3(a)]. We suppose the initial state of matter is an energy eigenstate $|I\rangle$ of energy E_I. This can be readily extended to any mixed initial state diagonal in the eigenstate basis.

Around the time $t = 0$ for a duration proportional to the length of the laser wavepacket (which we later take to ∞), the wavepacket spatially overlaps with the material and interacts with it. In the asymptotic future, the electromagnetic part of the state is once again composed of wavepackets spatially far away from the material. However, at $t = T/2$, the electromagnetic sector is entangled with the matter sector because of the interactions that happened around $t = 0$ [Fig. 3(b)]. Optical measurements are made at $t = T/2$ in the state $|\Psi(t = T/2)\rangle \equiv e^{-i\hat{H}T} |\Psi(t = -T/2)\rangle$. The detected photons inherit correlations from the material.

As explained in Appendix A, it is convenient to define $|\text{out}\rangle \equiv e^{i\hat{H}_0 T/2} |\Psi(t = T/2)\rangle$ and $|\text{in}\rangle \equiv e^{-i\hat{H}_0 T/2} |\Psi(t = -T/2)\rangle$. Let the expectation value of energy in the initial state be $E^0_{\text{in}} \equiv \langle\text{in}|\hat{H}_0|\text{in}\rangle$. If the duration of the experiment is long enough, i.e., when the uncertainty in energy $(\delta E_{\text{in}}) \ll 1/T$, we can use the $\hat{\mathcal{T}}$-matrix formalism [92] to approximate $|\text{out}\rangle$. We suppose $|\Psi^0_j\rangle$ (defined in the full light-matter Hilbert space) is an energy eigenstate of $\hat{H}_0$ with energy E^0_j. Then, as shown in Appendix A,

$$|\text{out}\rangle = |\text{in}\rangle - \sum_{j,k} 2\pi i \delta(E^0_j - E^0_k) |\Psi^0_k\rangle \langle\Psi^0_k| \hat{\mathcal{T}} |\Psi^0_j\rangle \langle\Psi^0_j|\text{in}\rangle,$$
(5)

where $\hat{\mathcal{T}}$, or the $\hat{\mathcal{T}}$-matrix is given by

$$\hat{\mathcal{T}} = \hat{V} + \hat{V}\frac{1}{E^0_{\text{in}} - \hat{H}_0 - \hat{V} + i0^+}\hat{V}$$
$$= \hat{V} + \hat{V}\hat{\mathbb{G}}_0\hat{V} + \hat{V}\hat{\mathbb{G}}_0\hat{V}\hat{\mathbb{G}}_0\hat{V} + \hat{V}\hat{\mathbb{G}}_0\hat{V}\hat{\mathbb{G}}_0\hat{V}\hat{\mathbb{G}}_0\hat{V} + \dots,$$
(6)

where $\hat{\mathbb{G}}_0 \equiv \left(E^0_{\text{in}} - \hat{H}_0 + i0^+\right)^{-1}$. Eq. (5) is a generalization of Fermi's Golden rule to all orders in $\hat{V}$. In Appendix A, we provide a review of the $\hat{\mathcal{T}}$-matrix formalism along with a derivation of Eq. (5). In Sec. III B,
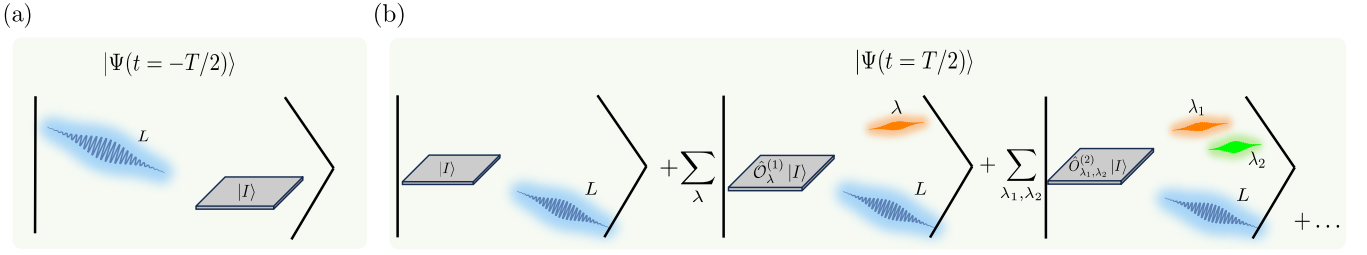
Figure 3. **(a)** The initial state in the asymptotic past (at time $t = -T/2$, in the limit where it approaches $-\infty$), $|\Psi(t = -T/2)\rangle$ consists of the electromagnetic field in a laser-produced wavepacket state far away from the material. For illustration, the material is assumed to be in an energy eigenstate $|I\rangle$. Around time $t = 0$, the wavepacket spatially overlaps with the material and interacts with it for a duration proportional to the length of the wavepacket, which we assume to be much larger than its central wavelength **(b)** At $t = T/2$, in the asymptotic future, light and the material are entangled with each other and the resulting superposition is schematically depicted in the figure. The expansion depicted here is in the number of photon modes in the final state. The first term corresponds to elastic scattering of light. The second set of terms corresponds to the emission of a photon in mode λ, leaving the material in state $\hat{\mathcal{O}}_\lambda^{(1)} |I\rangle$, where $\hat{\mathcal{O}}_\lambda^{(1)}$ is some operator that acts purely in the matter sector. Therefore, the probability of detection of a photon in mode k is proportional to $\langle \hat{\mathcal{O}}_\lambda^{(1)\dagger} \hat{\mathcal{O}}_\lambda^{(1)} \rangle$, which is a matter correlation function. The third set corresponds to the emission of a pair of photons in modes λ_1 and λ_2, whose probability is $\langle \hat{\mathcal{O}}_{\lambda_1,\lambda_2}^{(2)\dagger} \hat{\mathcal{O}}_{\lambda_1,\lambda_2}^{(2)} \rangle$, again a matter correlation function. In this paper, we present a formalism to derive expressions for these matter correlation functions.

we write $G^{(1)}$, $G^{(2)}$ and homodyne measurements as expectation values of operators in the $|out\rangle$ state. Later, in Sec. V, we relate these measurements to matter correlation functions by simplifying Eq. (6).

B. Definitions of photonic correlation functions

Our measurement scheme is shown Fig. 1. However, the photonic correlation function (to be introduced in Eq. (15), (17), and (19-21)) are general and applicable to a wider class of measurement schemes. We suppose the detectors d_1 and d_2 are located at $\mathbf{R}_1$ and $\mathbf{R}_2$ respectively (Fig. 1). The spatial origin is chosen to be at the center of mass of the material. The annihilation part of the frequency-filtered electric field operator (in the Interaction picture) along the direction of the detected polarization $\mathbf{e}_j$, seen by the detector d_j at location $\mathbf{R}_j$ (for $j \in \{1, 2\}$), is given by

$$\mathbf{e}_j^* \cdot \hat{\mathbf{E}}^{(+)} \left(\mathbf{R}_j, \frac{T}{2}\right)$$
$$= i \sum_{\mathbf{k}} \sqrt{\frac{\omega_{\mathbf{k}}}{2\varepsilon\mathcal{V}}} \hat{a}_{(\mathbf{k},\mathbf{e}_j)} e^{i\left(\mathbf{k}\cdot\mathbf{R}_j - \omega_{\mathbf{k}}\frac{T}{2}\right)} f_j(\omega_{\mathbf{k}} - \omega_j), \quad (7)$$
$$\hat{\mathbf{E}}^{(-)}(\mathbf{R}_j) \equiv \left[\hat{\mathbf{E}}^{(+)}(\mathbf{R}_j)\right]^\dagger,$$

where $\hat{a}_{(\mathbf{k},\mathbf{e}_j)}$ is a photon annihilation operator for each orthogonal plane-wave mode of momentum $\mathbf{k}$ and polarization $\mathbf{e}_j$, and $\omega_{\mathbf{k}} = c|\mathbf{k}|$. Here, ε is the dielectric constant and $\mathcal{V}$ is the mode-volume of free-space (which can be taken to infinity at a suitable point). $f_j(\omega - \omega_j)$, is a dimensionless frequency filter function which reflects the fact that each detector j could have its own sensitivity profile for modes of different frequencies. Here, ω_j is

a reference frequency about which the sensitivity of detector j is peaked. Causality implies that the poles of $f_j(\omega - \omega_j)$, when seen as a function of complex frequency ω, can only lie in the lower half-plane.

We suppose $|\mathbf{R}_1| = cT/2$. Since the material is located around $\mathbf{R} = \mathbf{0}$, classically, the modes that reach the detector at time $T/2$ are those with momentum $\mathbf{k}$ parallel to $\mathbf{R}_1$. Quantum mechanically, there will be wavepacket spreading, i.e., modes with $\mathbf{k}$ pointed slightly away from the detector could also reach the detector. But terms involving those modes in Eq. (7) oscillate rapidly as a function of T, and as we argue in Appendix A, they can be ignored in the $T \to \infty$ limit. Therefore, we assume that the direction of $\mathbf{k}$ lies within a thin solid angle $\delta\Omega_1$ around the direction of $\mathbf{R}_1$. Similarly, for detector 2, we only need to consider modes $\mathbf{k}$ along $|\mathbf{R}_2|$ up to a solid angle $\delta\Omega_2$. We suppose the second detector detects a photon time $\tilde{\tau}$ after the first detector does. The time-dependent phase for detector 2 would then be $e^{i|\mathbf{k}|[|\mathbf{R}_2| - c(T/2 + \tilde{\tau})]}$. This equals $e^{i\omega_{\mathbf{k}}[|\mathbf{R}_2|/c - |\mathbf{R}_1|/c + \tilde{\tau}]}$. Therefore, to simplify notation, let us define a retarded time τ as

$$\tau \equiv \tilde{\tau} - \frac{|\mathbf{R}_2| - |\mathbf{R}_1|}{c}. \quad (8)$$

Let us also define the annihilation operator for detector d_j (which is related to the local electric field as shown below):

$$\hat{a}_{d_j} \equiv i \sum_{\mathbf{k}}' \sqrt{\frac{c\omega_{\mathbf{k}}}{2\mathcal{V}}} f_j(\omega_{\mathbf{k}} - \omega_j) \hat{a}_{\mathbf{k},\mathbf{e}_j}, \quad (9)$$

where $\sum_{\mathbf{k}}'$ restricts the direction of $\mathbf{k}$ to be within a solid angle $\delta\Omega_j$ from the direction $\mathbf{R}_j$. This solid angle could be controlled by a lens that collects the output photons.

For later use, we also note that when the sum over $\mathbf{k}$ is converted into an integral over frequencies $\omega_{\mathbf{k}}$, one gets

$$\sideset{}{'}\sum_{\mathbf{k}} \sqrt{\frac{c\omega_{\mathbf{k}}}{2\mathcal{V}}} \longrightarrow \delta\Omega_j \int \mathrm{d}\omega_{\mathbf{k}} \sqrt{\frac{c\omega_{\mathbf{k}}\mathcal{V}}{2}}\rho(\omega_{\mathbf{k}}). \qquad (10)$$

Here, $\rho(\omega)$ is the density of states of light modes per unit volume. In free space, $\rho(\omega) = \omega^2/(2\pi c)^3$. But more generally, it can be modified to a different function by say, a cavity. We are allowed to do the above conversion into an integral over frequencies because we will find that all the matrix elements containing $\hat{a}_{\mathbf{k},\mathbf{e}_j}$ will depend on $\mathbf{k}$ only through $\omega_{\mathbf{k}}$. To simplify future expressions, we introduce the following effective filter function (for $j \in \{1,2\}$):

$$\mathcal{F}_j(\omega - \omega_j) \equiv 2\pi c\rho(\omega)\delta\Omega_j f_j(\omega - \omega_j). \qquad (11)$$

An example of such an effective filter function is a Lorentzian which arises naturally when the filter is a Fabry-Pérot cavity which selects frequencies close to the cavity resonance frequency ω_j. Specifically,

$$\mathcal{F}_{j,\text{ Lorentzian}}(\omega - \omega_j) = \frac{i\mathsf{K}_j\Gamma_j}{\omega - \omega_j + i\Gamma_j}, \qquad (12)$$

where

$$\mathsf{K}_j \equiv 2\pi c\rho(\omega_j)(\delta\Omega)_j. \qquad (13)$$

In writing so, we have assumed that the photonic density of states near ω_j does not vary much within the window in frequency where the detector is sensitive. One could similarly consider other causal effective filter functions with different selectivity profiles.

With this setup in mind, we are now ready to define our correlation functions.

1. Photon intensity $G^{(1)}(0)$

The intensity of light detected by the detector d_j of polarization $\mathbf{e}_j$, located at point $\mathbf{R}$ is

$$G^{(1)}_{d_j}(0) \equiv c\varepsilon$$
$$\times \langle\Psi(t = T/2)| \mathbf{e}_j \cdot \hat{\mathbf{E}}^{(-)}(\mathbf{R})\mathbf{e}_j^* \cdot \hat{\mathbf{E}}^{(+)}(\mathbf{R}) |\Psi(t = T/2)\rangle. \qquad (14)$$

Simplifying this using the definitions of $|\text{in}\rangle$, $|\text{out}\rangle$ and of the mode $\hat{a}_{d_j}$ detected by the detector in (9), the definition of $G^{(1)}$ simplifies to:

$$G^{(1)}_{d_j}(0) = \langle\text{out}| \hat{a}^{\dagger}_{d_j}(0)\hat{a}_{d_j}(0) |\text{out}\rangle. \qquad (15)$$

2. Second-order coherence $G^{(2)}(\tau)$

Similarly, one define the following second-order coherence function corresponding to detecting one photon of

polarization $\mathbf{e}_1$ at the detector at $\mathbf{R}_1$, followed by another photon of polarization $\mathbf{e}_2$ at the detector at $\mathbf{R}_2$, after a time $\tilde{\tau}$:

$$G^{(2)}_{d_1,d_2}(\tilde{\tau}) = c^2\varepsilon^2$$
$$\times \langle\Psi(t = T/2)| \left[\mathbf{e}_1 \cdot \hat{\mathbf{E}}^{(-)}(\mathbf{R}_1)\right] e^{i\hat{H}\tilde{\tau}} \left[\mathbf{e}_2 \cdot \hat{\mathbf{E}}^{(-)}(\mathbf{R}_2)\right]$$
$$\times \left[\mathbf{e}_2^* \cdot \hat{\mathbf{E}}^{(+)}(\mathbf{R}_2)\right] e^{-i\hat{H}\tilde{\tau}} \left[\mathbf{e}_1^* \cdot \hat{\mathbf{E}}^{(+)}(\mathbf{R}_1)\right] |\Psi(t = T/2)\rangle. \qquad (16)$$

The insertion of $e^{-i\hat{H}\tilde{\tau}}$ in the above definition is because the whole system continues to evolve between the detection of the first and second photons. However, as is clear from Fig. 3(b), at time $t = T/2$, the wavepackets of the scattered photons are far away from the material. Therefore, the light-matter interaction $\hat{V}$ has almost zero support in the final state, and thus does not have any effect after $t = T/2$. Therefore, we can replace $e^{-i\hat{H}\tilde{\tau}}$ with the free evolution $e^{-i\hat{H}_0\tilde{\tau}}$ in the above definition. The definition Eq. (16) can be simplified in the interaction picture, by going to the retarded time τ [Eq. 8], and using Eq. (9) to obtain:

$$G^{(2)}_{d_1,d_2}(\tau) = \langle\text{out}| \hat{a}^{\dagger}_{d_1}(0)\hat{a}^{\dagger}_{d_2}(\tau)\hat{a}_{d_2}(\tau)\hat{a}_{d_1}(0) |\text{out}\rangle. \quad (17)$$

As we discuss later, we only focus on the connected component of the above correlator, i.e.,

$$\mathcal{G}^{(2)}_{d_1,d_2}(\tau) \equiv G^{(2)}_{d_1,d_2}(\tau) - G^{(1)}_{d_1}(0)G^{(1)}_{d_2}(0). \qquad (18)$$

3. Homodyne detection

So far, we have looked at photonic correlation functions $G^{(1)}(0)$ and $G^{(2)}(\tau)$, which are related to photon *number* and its *fluctuations* respectively, and lack information about the phase of the electric field. In fact, the electric field (as opposed to its absolute value squared), and generally, any electromagnetic quadrature and its fluctuations can be directly measured. This is done using homodyne detection – by beating the detected signal with the electric field of a local oscillator (see for example, Chapter 4 of Ref. [93] and Chapter 9 of Ref. [94]). This way, for a mode $\hat{a}_\lambda$, one can measure an arbitrary quadrature, $\hat{a}_\lambda e^{i\phi} + \text{h.c.}$, for any ϕ. Thus, it is possible to measure the following three correlation functions:

$$X^+_{d_j}(0) = \langle\text{out}| \hat{a}_{d_j}(0) |\text{out}\rangle, \qquad (19)$$

$$X^{++}_{d_1,d_2}(\tau) = \langle\text{out}| \hat{a}_{d_2}(\tau)\hat{a}_{d_1}(0) |\text{out}\rangle, \qquad (20)$$

$$X^{-+}_{d_1,d_2}(\tau) = \langle\text{out}| \hat{a}^{\dagger}_{d_2}(\tau)\hat{a}_{d_1}(0) |\text{out}\rangle. \qquad (21)$$

IV. LIGHT SCATTERING OFF A SINGLE-BAND HUBBARD MODEL AT HALF-FILLING

To establish a connection between matter correlation functions and photonics correlators, $G^{(1)}$[Eq. (15)], $G^{(2)}$

[Eq. (17)] and the homodyne correlations [Eq. (19-21)], it is necessary to know the $\hat{\mathcal{T}}$-matrix that acts on $|\text{in}\rangle$. This requires knowledge of the material's Hamiltonian $\hat{H}_0$ and light-matter interaction $\hat{V}$. In this paper, we consider $\hat{H}_0$ to be a single-band Hubbard model at half-filling, and the light-matter interaction $\hat{V}$ as the Peierls substitution expanded up to second order in the vector potential. We explicitly work out the mapping between photonic and matter correlations for this specific $\hat{H}_0$ and $\hat{V}$. The procedure can then be readily adapted to any other system as long as its ground state is an insulator. Specifically, we consider the following Hamiltonian,

$$
\hat{H}_0 = \sum_{\langle \mathbf{r}, \mathbf{r}' \rangle, \sigma} \left[-\frac{\mathtt{t}}{2} \hat{c}_{\mathbf{r}'\sigma}^\dagger \hat{c}_{\mathbf{r}\sigma} + \text{h.c.} + U \sum_{\mathbf{r}} \hat{n}_{\mathbf{r},\uparrow} \hat{n}_{\mathbf{r},\downarrow} \right]
$$
$$
+ \sum_{\mathbf{k}, \mathbf{e_k}} \omega_{\mathbf{k}} \left(\hat{a}_{\mathbf{k}, \mathbf{e_k}}^\dagger \hat{a}_{\mathbf{k}, \mathbf{e_k}} + \frac{1}{2} \right),
\tag{22}
$$

where $\mathtt{t}$ is the tunneling coefficient along a nearest neighbor bond $\langle \mathbf{r}, \mathbf{r}' \rangle$ and $\hat{n}_{\mathbf{r}\sigma} \equiv \hat{c}_{\mathbf{r}\sigma}^\dagger \hat{c}_{\mathbf{r}\sigma}$. Under the Peierls substitution, the full light-matter Hamiltonian $\hat{H}$ is obtained by the substituting $\mathtt{t}$ in every bond $\langle \mathbf{r}, \mathbf{r}' \rangle$ with

$$
\mathtt{t} \to \mathtt{t} e^{i q_e \int_{\mathbf{r}}^{\mathbf{r}'} d\mathbf{x} \cdot \hat{\mathbf{A}}(\mathbf{x})},
\tag{23}
$$

where q_e is the charge of the electron, $\hat{\mathbf{A}}(\mathbf{r})$ is the vector potential of the electromagnetic field in Coulomb gauge and $\hat{a}_{\mathbf{k}, \mathbf{e_k}}$ are its normal modes. In free space, $\hat{\mathbf{A}}(\mathbf{r})$ can be expanded as

$$
\hat{\mathbf{A}}(\mathbf{r}) = \sum_{\mathbf{k}, \mathbf{e_k}} \frac{1}{\sqrt{2\varepsilon \mathcal{V} \omega_{\mathbf{k}}}} \left(\mathbf{e_k} \hat{a}_{\mathbf{k}, \mathbf{e_k}} e^{i\mathbf{k} \cdot \mathbf{r}} + \mathbf{e_k^*} \hat{a}_{\mathbf{k}, \mathbf{e_k}}^\dagger e^{-i\mathbf{k} \cdot \mathbf{r}} \right).
\tag{24}
$$

For spin-1/2 electrons, let us also define their spin as

$$
\hat{\mathbf{S}}_{\mathbf{r}} = \frac{1}{2} \sum_{\alpha, \beta} \hat{c}_{\mathbf{r}, \alpha}^\dagger \boldsymbol{\sigma} \hat{c}_{\mathbf{r}, \beta},
\tag{25}
$$

where $\boldsymbol{\sigma}$ is a vector formed by the three Pauli matrices. Expanding the light matter interaction in powers of q_e, the terms linear ("paramagnetic") and quadratic ("diamagnetic") in $\hat{\mathbf{A}}(\mathbf{x})$ in the Coulomb gauge in Eq. (22) are

$$
\hat{V} = \frac{\mathtt{t}}{2} \sum_{\langle \mathbf{r}, \mathbf{r}' \rangle, \sigma} \left\{ -i \left(\hat{c}_{\mathbf{r}'\sigma}^\dagger \hat{c}_{\mathbf{r}\sigma} - \hat{c}_{\mathbf{r}\sigma}^\dagger \hat{c}_{\mathbf{r}'\sigma} \right) (\mathbf{r}' - \mathbf{r}) \cdot q_e \hat{\mathbf{A}}_{\mathbf{r}, \mathbf{r}'} \right.
$$
$$
\left. + \left(\hat{c}_{\mathbf{r}'\sigma}^\dagger \hat{c}_{\mathbf{r}\sigma} + \hat{c}_{\mathbf{r}\sigma}^\dagger \hat{c}_{\mathbf{r}'\sigma} \right) \left[(\mathbf{r}' - \mathbf{r}) \cdot q_e \hat{\mathbf{A}}_{\mathbf{r}, \mathbf{r}'} \right]^2 \right\},
\tag{26}
$$

where $\hat{\mathbf{A}}_{\mathbf{r}, \mathbf{r}'} \equiv \hat{\mathbf{A}} \left(\frac{\mathbf{r} + \mathbf{r}'}{2} \right)$. We denote the paramagnetic term by $\hat{V}_P$ and the diamagnetic term by $\hat{V}_D$. Let us define

$$
\hat{\mathcal{J}}_{\boldsymbol{\mu}} \equiv \sum_{\mathbf{r}, \sigma} \left(\hat{c}_{\mathbf{r}+\boldsymbol{\mu}, \sigma}^\dagger \hat{c}_{\mathbf{r}\sigma} - \hat{c}_{\mathbf{r}\sigma}^\dagger \hat{c}_{\mathbf{r}+\boldsymbol{\mu}, \sigma} \right),
\tag{27}
$$

where $\boldsymbol{\mu}$ joins lattice site $\mathbf{r}$ to each of its neighbors. $\hat{\mathcal{J}}_{\boldsymbol{\mu}}$ is proportional to the global electric current in the direction $\boldsymbol{\mu}$. We argue in Sec. V A that the spatial dependence of the electromagnetic field can be ignored (dipole approximation). In that case, the paramagnetic term is

$$
\hat{V}_P \approx -ig\mathtt{t} \sum_{\boldsymbol{\mu}} \left[\hat{\mathcal{J}}_{\boldsymbol{\mu}} \bar{\boldsymbol{\mu}} \cdot \sum_{\lambda} \left(\mathbf{e}_{\lambda} \hat{a}_{\lambda} + \mathbf{e}_{\lambda}^* \hat{a}_{\lambda}^\dagger \right) \right],
\tag{28}
$$

where $\bar{\boldsymbol{\mu}} \equiv \boldsymbol{\mu}/\mathtt{a}$. Also, we use a convention for summation over $\mathbf{r}$ and $\boldsymbol{\mu}$, so that each bond $(\mathbf{r}, \boldsymbol{\mu})$ is counted exactly once (and not double-counted). Let us also define the total tunneling term along $\boldsymbol{\mu}$ as

$$
\hat{\mathcal{H}}_{\boldsymbol{\mu}} \equiv \sum_{\mathbf{r}, \sigma} \left(\hat{c}_{\mathbf{r}+\boldsymbol{\mu}, \sigma}^\dagger \hat{c}_{\mathbf{r}\sigma} + \hat{c}_{\mathbf{r}\sigma}^\dagger \hat{c}_{\mathbf{r}+\boldsymbol{\mu}, \sigma} \right).
\tag{29}
$$

Then, the diamagnetic term is

$$
\hat{V}_D \approx g^2 \mathtt{t} \sum_{\boldsymbol{\mu}} \left\{ \hat{\mathcal{H}}_{\boldsymbol{\mu}} \left[\bar{\boldsymbol{\mu}} \cdot \sum_{\lambda} \left(\mathbf{e}_{\lambda} \hat{a}_{\lambda} + \mathbf{e}_{\lambda}^* \hat{a}_{\lambda}^\dagger \right) \right]^2 \right\}.
\tag{30}
$$

In this implementation of light-matter interaction, the diamagnetic term couples to the point-split density $\frac{1}{2} \sum_{\sigma} \left(\hat{c}_{\mathbf{r}'\sigma}^\dagger \hat{c}_{\mathbf{r}\sigma} + \hat{c}_{\mathbf{r}\sigma}^\dagger \hat{c}_{\mathbf{r}'\sigma} \right)$ as opposed to just the density in the free-electron gas.

Third or higher order terms in $\hat{\mathbf{A}}$ obtained by expanding the Peierls substitution in Eq. (23) should be taken with caution. This is because the single-band Hubbard model should be viewed as the projection of a continuum model into a single band. Determining the true light-matter coupling term in such projected models is not trivial. For example, light-matter coupling could modulate longer-range hoppings and generically even modify the interaction terms [95, 96]. For the purposes of this paper, we will only consider the paramagnetic and diamagnetic terms in Eq. (26).

A. Overview of energy scales and sectors

Following Ref. [22–24], we work with Eq. (22), the single band Hubbard for spin-$\frac{1}{2}$ electrons at half-filling (i.e., the number of electrons equals the number of lattice sites) in the limit $t \ll U$, where the ground state is a Mott-insulator. In this limit, the manifold of of energy eigenstates *that can be accessed by applying local operators on the ground state* split up into sectors as shown in Fig. 4.

In the lowest energy sector (shaded blue), the charge degree of freedom is frozen and the excitations lie purely in the spin sector. If the ground state is a conventionally ordered state, these excitations are magnons and if the ground state is a quantum spin liquid, then these states can be composites of fractionalized excitations. The band-width of this sector is of the order of $J \approx \mathtt{t}^2/U$.

The sector shaded yellow, roughly separated by an energy U from the spin sector, consists of states where one site is doubly occupied (called doublon) and one site is empty (called hole). The states in this sector include bound-states of doublons and holes, called Mott excitons [78–91], as well as their scattering states. We expect the bandwidth of this sector to be of order $\mathtt{t}$. The sector shaded red consists of states with two doublon-hole pairs and have an energy of order $2U$ relative to the spin states.

Similar to Ref. [22–24], we assume that the laser frequency ω_L satisfies

$$\mathtt{t} \ll |U - \omega_L| \ll U. \tag{31}$$

In other words, the laser is detuned from the Hubbard gap U, and the detuning, though small compared to U, is large compared to $\mathtt{t}$. This assumption allows us to do perturbation theory in both $\mathtt{t}/|U - \omega_L|$ and $\mathtt{t}/U$.

The second small parameter is the laser-matter coupling that is involved during each photon absorption. Recall that the laser-matter coupling is $\sim \mathtt{t}\frac{q_e \mathtt{a}}{\sqrt{2\varepsilon \mathcal{V} \omega_L}} \hat{a}_L \hat{c}_{\mathbf{r}}^\dagger \hat{c}_{\mathbf{r}'}$. For a Fock-state input, $\hat{a}_L$ can be replaced by $\sqrt{\mathcal{N}_L}$, where $\mathcal{N}_L$ is the number of photons in the laser mode, i.e., the number of incident photons. Similarly, if the laser mode were in a coherent state, i.e., $e^{\phi_L \hat{a}_L^\dagger - \phi_L^* \hat{a}_L} |0\rangle$, then $\hat{a}_L$ can be replaced by ϕ_L. Now, the intensity of the laser is $I_L = \frac{\mathcal{N}_L \omega_L c}{\mathcal{V}}$, when modeled as a Fock state and $I_L = \frac{\phi_L^2 \omega_L c}{\mathcal{V}}$, when modeled as a coherent state. Thus, we can define a dimensionless laser-matter coupling:

$$g_L = \frac{q_e \mathtt{a} \sqrt{\mathcal{N}_L}}{\sqrt{2\varepsilon \mathcal{V} \omega_L}} \equiv \frac{\sqrt{2\pi I_L \alpha}\,\mathtt{a}}{\omega_L}, \tag{32}$$

where $\mathtt{a}$ is the lattice spacing and where $\alpha = \frac{q_e^2}{4\pi\varepsilon c}$ is the fine-structure constant. We can also interpret g_L as the ratio of the effective Rabi frequency of the laser drive to the laser frequency ω_L. In this work, we will assume that $g_L \ll 1$.

Similarly, the interaction term corresponding to a photon emission into an unoccupied mode $(\mathbf{k}, \mathbf{e}_j)$ is $\sim \mathtt{t}\frac{q_e \mathtt{a}}{\sqrt{2\varepsilon \mathcal{V} \omega_{\mathbf{k}}}} \hat{a}_{\mathbf{k}, \mathbf{e}_j}^\dagger \hat{c}_{\mathbf{r}}^\dagger \hat{c}_{\mathbf{r}'}$. This suggests another dimensionless coupling in the problem: $\frac{q_e \mathtt{a}}{\sqrt{2\varepsilon \mathcal{V} \omega_{\mathbf{k}}}}$, which we rewrite as $\sqrt{\pi\alpha}\mathtt{a}\sqrt{\frac{2c}{\omega_{\mathbf{k}} \mathcal{V}}}$. We see from Eq. (9),(10),(11) that the factor $\sqrt{\frac{2c}{\omega_{\mathbf{k}} \mathcal{V}}}$ will get cancelled in the final expressions for $G^{(1)}$ and $G^{(2)}$. Hence we define the following dimensionful light-matter coupling

$$g \equiv \sqrt{\pi\alpha}\mathtt{a}, \tag{33}$$

with the understanding that the dimensionless small parameter corresponding to g is essentially $\sqrt{\alpha}$.

To summarize, in this paper, we are going to provide expressions for $G^{(1)}$, $G^{(2)}$ and homodyne correlations only to leading order in the small parameters $\mathtt{t}/U$, $\mathtt{t}/|U - \omega_L|$, g_L and g.
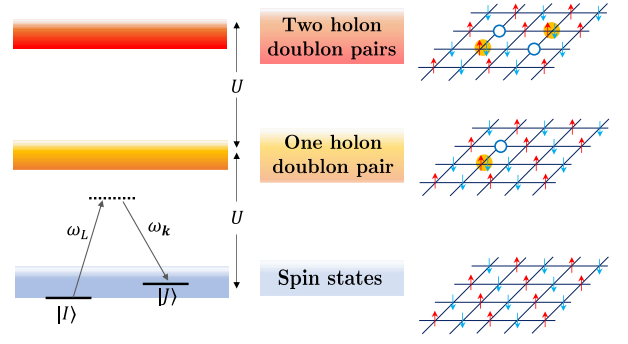

Figure 4. The energy eigenstates that can be accessed by applying local operators to the ground state of the Hubbard model at half-filling split up into sectors as shown here. The bottom-most sector (light blue) consists of spin states, i.e., the states in this sector have their charge degree of freedom frozen. The next two sectors (orange and red) are each separated energetically by roughly U, and these sectors have one and two doublon-hole pairs respectively. We schematically show a Raman process. Starting from a state $|I\rangle$ in the spin-sector, a photon absorption results in virtual occupation of a state in the sector of one doublon-hole pair. Then a photon emission into mode $\mathbf{k}$ results in the material returning to a possibly different state $|J\rangle$ in the spin sector.[a]

[a] Here we have used the convention in AMO physics for depicting a virtually occupied state, i.e., the dotted line is positioned such that its energy is $E_I + \omega_L$, even though there is no state at that energy.

B. Form of relevant terms in the $\hat{\mathcal{T}}$-matrix

In the expansion of $\hat{\mathcal{T}}$, the emission of each additional photon comes with a multiplicative factor of g. Therefore, we will only consider those processes that lead to an emission of at most two photons, the minimum number required to obtain a nonzero value of $G^{(2)}$.

With this in mind, let us examine the relevant terms in the expression $\hat{\mathcal{T}} = \hat{V} + \hat{V}\hat{\mathbb{G}}_0\hat{V} + \hat{V}\hat{\mathbb{G}}_0\hat{V}\hat{\mathbb{G}}_0\hat{V} + \hat{V}\hat{\mathbb{G}}_0\hat{V}\hat{\mathbb{G}}_0\hat{V}\hat{\mathbb{G}}_0\hat{V} + \ldots$. From Fig. 4, we see that starting from a state in the spin sector, emitting one photon requires the absorption of one photon from the laser. Therefore, to leading order,

$$\hat{V}\hat{\mathbb{G}}_0\hat{V} = \sum_{\mathbf{k}} \hat{R}_{(\mathbf{k}, \mathbf{e}_j)}^{(1)} \otimes \hat{a}_{\mathbf{k}, \mathbf{e}_j}^\dagger \hat{a}_L \sqrt{\frac{2c}{\mathcal{V}\omega_{\mathbf{k}}\mathcal{N}_L}} + \ldots, \tag{34}$$

where $\mathbf{e}_j$ is the polarization selected by the detector. We have chosen the normalization factor of $\sqrt{\frac{2c}{\mathcal{V}\omega_{\mathbf{k}}\mathcal{N}_L}}$ just to simplify future expressions.

Let us now consider processes leading to the emission of two photons. In this work, we assume that the detector filters out any photon whose frequency is outside the window $\omega_L \pm O(|\omega_L - U|)$. This means that a photon of frequency $2\omega_L - U$ is detected, but one of frequency $\omega_L/2$ is not. Under these conditions, we can see that (1) it is sufficient to consider processes where two photons are absorbed, and (2) after absorbing two photons and

emitting two photons, the final state of the material is in the spin sector. $\mathtt{t}/U$.

Thus, the term in $\hat{\mathcal{T}}$ that contributes to the emission of two photons takes the following form (we use the short-hand notation λ_j for the mode $(\mathbf{k}, \mathbf{e}_{\lambda_j})$ of frequency ω_{λ_j}, where $\mathbf{e}_{\lambda_j}$ is the polarization detected by detector j):

$$
\hat{V}_P \hat{\mathbb{G}}_0 \hat{V}_D \hat{\mathbb{G}}_0 \hat{V}_P + \hat{V}_P \hat{\mathbb{G}}_0 \hat{V}_P \hat{\mathbb{G}}_0 \hat{V}_P \hat{\mathbb{G}}_0 \hat{V}_P
$$
$$
= \sum_{\lambda_1, \lambda_2} \hat{R}^{(2)}_{\lambda_1, \lambda_2} \otimes \frac{\hat{a}^\dagger_{\lambda_1} \hat{a}^\dagger_{\lambda_2} (\hat{a}_L)^2}{2\sqrt{\mathcal{N}_L(\mathcal{N}_L - 1)}} \frac{2c}{\mathcal{V}\sqrt{\omega_{\lambda_1} \omega_{\lambda_2}}} + \ldots \quad (35)
$$

where $\hat{R}^{(2)}_{\lambda_1, \lambda_2}$ is a pure matter operator and will be calculated in the next section. $\hat{R}^{(2)}_{\lambda_1, \lambda_2}$ is symmetric in λ_1 and λ_2. Here, $\hat{a}^\dagger_{\lambda_1} \hat{a}^\dagger_{\lambda_2} (\hat{a}_L)^2$ signifies that two photons are absorbed from the laser and two photons are emitted into modes λ_1 and λ_2. The remaining factors are due to our normalisation convention. We note that while summing over modes λ_1 and λ_2, one can fix the polarizations as dictated by the detector, and only sum over the corresponding momenta.

C. Simplified expressions for photonic correlation functions

We now use the form of the $\hat{\mathcal{T}}$-matrix in Eqs. (34) and (35) to simplify the photonic correlation functions defined in Eqs. (15), (17), (19), (20) and (21). For this, we need the knowledge of the $|\text{out}\rangle$ state. First of all, let's suppose that the $|\text{in}\rangle$ state is a product state between the matter and light sectors.

$$
|\text{in}\rangle = |I\rangle_M \otimes |\psi_L^{(0)}\rangle_R, \quad (36)
$$

where $|I\rangle_M$ is an energy eigenstate of the matter part of $\hat{H}_0$ (hence subscript M) with energy E_I. $|\psi_L^{(0)}\rangle_R$ is a state in the electromagnetic sector with the laser mode occupied (we use subscript L to denote "laser" and subscript R to denote the "radiation" sector). Since Eq. (5) is easiest to apply for an $|\text{in}\rangle$ state that is an eigenstate of $\hat{H}_0$, we can consider $|\psi_L^{(0)}\rangle_R$ to be a Fock state with $\mathcal{N}_L$ photons in laser mode L, a mode with well-defined wavevector and polarization, i.e.,

$$
|\psi_L^{(0)}\rangle_R = \frac{1}{\sqrt{\mathcal{N}_L!}} \left(\hat{a}^\dagger_L \right)^{\mathcal{N}_L} |0\rangle_R. \quad (37)
$$

In Appendix B, we show that we can also have the laser mode L to be populated with a coherent state and still be able to calculate $|\text{out}\rangle$ to use Eq. (5). In that case,

$$
|\psi_L^{(0)}\rangle_R = e^{\phi_L \hat{a}^\dagger_L - \phi_L^* \hat{a}_L} |0\rangle_R. \quad (38)
$$

For either case, using Eq. (34), (35) and Eq. (5), to leading order in g, we get the $|\text{out}\rangle$ state to be a superposition of the unscattered $|\text{in}\rangle$ state, and states resulting

from one and two-photon scattering:

$$
|\text{out}\rangle = |I\rangle \otimes |\psi_L^{(0)}\rangle
$$
$$
- 2\pi i \sum_\lambda \sum_F \delta(E_{FI} + \omega_\lambda - \omega_L) |F\rangle
$$
$$
\times \sqrt{\frac{2c}{\mathcal{V}\omega_\lambda}} \langle F| \hat{R}^{(1)}_\lambda |I\rangle \otimes \hat{a}^\dagger_\lambda |\psi_L^{(1)}\rangle
$$
$$
- 2\pi i \sum_{\lambda_1, \lambda_2} \sum_F \delta(E_{FI} + \omega_{\lambda_1} + \omega_{\lambda_2} - 2\omega_L) |F\rangle
$$
$$
\times \frac{2c}{\mathcal{V}\sqrt{\omega_{\lambda_1} \omega_{\lambda_2}}} \langle F| \hat{R}^{(2)}_{\lambda_1, \lambda_2} |I\rangle \otimes \frac{\hat{a}^\dagger_{\lambda_1} \hat{a}^\dagger_{\lambda_2}}{2} |\psi_L^{(2)}\rangle. \quad (39)
$$

We have used the notation $E_{FI} \equiv E_F - E_I$. Here, if $|\psi_L^{(0)}\rangle$ is a Fock state as in Eq. (37), then $|\psi_L^{(1)}\rangle$ and $|\psi_L^{(2)}\rangle$ are the corresponding Fock states with $\mathcal{N}_L - 1$ and $\mathcal{N}_L - 2$ photons respectively in mode L. On the other hand, if $|\psi_L^{(0)}\rangle$ is a coherent state as in Eq. (38), then both $|\psi_L^{(1)}\rangle$ and $|\psi_L^{(2)}\rangle$ are equal to $|\psi_L^{(0)}\rangle$.

It is important to note that the photonic operators measured in X^+ [Eq. (19)] and X^{++} [Eq. (20)] do not conserve the total number of photons. Thus, from Eq. (39), we see that getting a nonzero value here requires $|\psi_L^{(0)}\rangle$ to be in a coherent state, and not a Fock state. On the other hand, the photonic operators measured $G^{(1)}$ [Eq. (15)], $G^{(2)}$ [Eq. (17)] and X^{-+} [Eq. (21)] do conserve total photon number, so both coherent state and Fock state inputs can lead to a nonzero measurement. With this in mind, we can use Eq. (39) to simplify the correlators defined in Eqs. (15), (17) and (19-21) as below. Here, we have assumed that the dependence of the matter operators $\hat{R}^{(1)}_\lambda$ and $\hat{R}^{(2)}_{\lambda_1, \lambda_2}$ on the photonic mode λ is only through its frequency ω_λ and polarization $\mathbf{e}_\lambda$, an assumption that we will justify in Sec. V A. Therefore, using Eq. (10), the sums over modes can be converted to integrals over frequencies as below:

$$
G^{(1)}_{d_j}(0) \approx \sum_J \left| \int_{-\infty}^{\infty} d\omega_{\lambda_j} \mathcal{F}_j(\omega_{\lambda_j} - \omega_j) \right.
$$
$$
\left. \times \delta\left(E_{JI} + \omega_{\lambda_j} - \omega_L \right) \langle J| \hat{R}^{(1)}_{\lambda_j}(\omega_{\lambda_j}) |I\rangle \right|^2. \quad (40)
$$

A word on notation – recall that here, ω_j is the reference frequency for detector j, i.e., where its sensitivity is peaked. On the other hand, ω_{λ_j} is integrated over, and denotes the frequency of the photon emitted into mode

λ_j. Next,

$$G^{(2)}_{d_1,d_2}(\tau) \equiv \left\langle \hat{a}^\dagger_{d_1}(0)\hat{a}^\dagger_{d_2}(\tau)\hat{a}_{d_2}(\tau)\hat{a}_{d_1}(0) \right\rangle_{\text{out}}$$

$$\approx \sum_F \left| \iint_{-\infty}^{\infty} \frac{d\omega_{\lambda_1}\, d\omega_{\lambda_2}}{(2\pi)} \Big[\mathcal{F}_1(\omega_{\lambda_1} - \omega_1)\mathcal{F}_2(\omega_{\lambda_2} - \omega_2) \right.$$

$$\times \delta\left(E_{FI} + \omega_{\lambda_1} + \omega_{\lambda_2} - 2\omega_L\right)$$

$$\left. \times\, e^{i\omega_{\lambda_1}\tau} \left\langle F|\hat{R}^{(2)}_{\lambda_1,\lambda_2}(\omega_{\lambda_1},\omega_{\lambda_2})|I\right\rangle \Big] \right|^2.$$

$$(41)$$

This expression is similar to Eq. (40) for $G^{(1)}$, except that here two photons are detected. The photon in mode λ_2 is detected after time τ following the photon detection in mode λ_1, leading to the phase $e^{i\omega_{\lambda_1}\tau}$ coming from time-evolution in between [97].

Next, for a coherent state input, the photon non-conserving homodyne correlations are:

$$\left\langle \hat{a}_{d_j}(0) \right\rangle_{\text{out}} \approx \mathcal{F}_j(\omega_L - \omega_j)\left\langle I|\hat{R}^{(1)}_{\lambda_j}(\omega_L)|I\right\rangle. \qquad (42)$$

$$\langle \hat{a}_{d_2}(\tau)\hat{a}_{d_1}(0)\rangle_{\text{out}} \approx i \iint_{-\infty}^{\infty} \frac{d\omega_{\lambda_1}\, d\omega_{\lambda_2}}{(2\pi)} \Big[e^{-i\omega_{\lambda_2}\tau}$$

$$\times \mathcal{F}_1(\omega_{\lambda_1} - \omega_1)\mathcal{F}_2(\omega_{\lambda_2} - \omega_2)\delta\left(\omega_{\lambda_1} + \omega_{\lambda_2} - 2\omega_L\right) \quad (43)$$

$$\times\, \left\langle I|\hat{R}^{(2)}_{\lambda_1,\lambda_2}(\omega_{\lambda_1},\omega_{\lambda_2})|I\right\rangle \Big].$$

Lastly, the photon number-conserving second-order homodyne correlation defined in Eq. (21), which reduces to $G^{(1)}_{d_1}(\tau)$ when the detectors d_1 and d_2 are identical, is

$$\left\langle \hat{a}^\dagger_{d_2}(\tau)\hat{a}_{d_1}(0) \right\rangle_{\text{out}}$$

$$\approx \sum_J \int_{-\infty}^{\infty} d\omega_{\lambda_1} \left[\mathcal{F}_1(\omega_{\lambda_1} - \omega_1)\mathcal{F}_2^*(\omega_{\lambda_1} - \omega_2)e^{i\omega_{\lambda_1}\tau} \right.$$

$$\left. \times\, \delta\left(E_{JI} + \omega_{\lambda_1} - \omega_L\right) \left\langle I\right| \left[\hat{R}^{(1)}_{\lambda_2}\right]^\dagger |J\rangle\langle J|\, \hat{R}^{(1)}_{\lambda_1}|I\rangle \right].$$

$$(44)$$

Here, the mode λ_2 is such that $\omega_{\lambda_1} = \omega_{\lambda_2}$, but the polarizations of λ_1 and λ_2 can be different.

V. MICROSCOPIC STRUCTURE OF MATTER OPERATORS $\hat{R}^{(1)}$ AND $\hat{R}^{(2)}$

In this section, we provide the explicit expressions for the matter operators $\hat{R}^{(1)}_{\lambda_1}$ and $\hat{R}^{(2)}_{\lambda_1,\lambda_2}$ for the single-band Hubbard model at half-filling defined in Sec. IV.

Let us first examine the terms in the expansion of $\hat{\mathcal{T}} = \hat{V} + \hat{V}\hat{\mathbb{G}}_0\hat{V} + \hat{V}\hat{\mathbb{G}}_0\hat{V}\hat{\mathbb{G}}_0\hat{V} + \hat{V}\hat{\mathbb{G}}_0\hat{V}\hat{\mathbb{G}}_0\hat{V}\hat{\mathbb{G}}_0\hat{V} + \ldots$. From Eq. (26), we see that the paramagnetic term in $\hat{V}$ involves an electron hopping to its neighboring site by absorbing or emitting a photon. The diamagnetic term involves hopping of an electron by either absorbing two photons, emitting two photons or by absorbing one photon along with emitting another.

A. Matter operator $\hat{R}^{(1)}_\lambda$: Review of Raman scattering

To leading order in g, we consider processes leading to the emission of one photon. Processes involving absorption and emission of two or more photons would be of higher order in g.

At half-filling, electron tunneling would result in double occupancy at a site and this costs energy U. Since $\mathtt{t} \ll |U - \omega_L|$, just one insertion of $\hat{V}$ alone cannot result in a photon absorption. But two insertions of $\hat{V}$ via the term $\hat{V}\hat{\mathbb{G}}_0\hat{V}$ can result in absorption and emission of a photon. A laser photon can be absorbed off-resonantly via the paramagnetic term (first arrow from the left in Fig. 4). This should then be followed by an electron in the doubly occupied site returning to its empty neighbor by emitting a photon, thus leaving the material in a possibly different state in the spin sector (second arrow from the left in Fig. 4). This is the familiar superexchange, this time, mediated by photons. Therefore, to leading order in light-matter interaction g and $\mathtt{t}/|U - \omega_L|$, the main contribution to $\hat{R}^{(1)}_\lambda$ is from such a Raman process [22, 73]. To leading order in $\mathtt{t}/|\omega_L - U|$, upon simplifying $\hat{V}\hat{\mathbb{G}}_0\hat{V}$, one gets the Fleury-Loudon term, a sum of projectors to spin singlets, modulated by the polarizations of the incoming laser and the detected photon [22–24, 73]:

$$\hat{R}^{(1)}_{(\mathbf{k},\mathbf{e}_j)} = \sum_{(\mathbf{r},\boldsymbol{\mu})} \frac{\mathtt{t}^2 g_L g}{\omega_L - U} \left(4\hat{\mathbf{S}}_\mathbf{r} \cdot \hat{\mathbf{S}}_{\mathbf{r}+\boldsymbol{\mu}} - 1\right) \left(\mathbf{e}_j^* \cdot \boldsymbol{\mu}\right) \left(\mathbf{e}_L \cdot \boldsymbol{\mu}\right)$$

$$+ \ldots$$

$$\equiv \hat{A}_j.$$

$$(45)$$

Here, for every site $\mathbf{r}$ on the lattice, $\boldsymbol{\mu}$ runs through the vectors joining $\mathbf{r}$ to its neighbours. For example, for a square lattice, $\boldsymbol{\mu}$ runs through $\mathtt{a}(\pm 1, 0)$ and $\mathtt{a}(0, \pm 1)$. Throughout this paper, we will use $(\mathbf{r}, \boldsymbol{\mu})$ to denote a bond joining $\mathbf{r}$ and $\mathbf{r}+\boldsymbol{\mu}$. We also use the summation convention that $\sum_{(\mathbf{r},\boldsymbol{\mu})}$ runs through each bond exactly once. The "..." above denotes terms of order $\mathtt{t}^3/|\omega_L - U|^2$ and higher.

Note that in Eq. (45), we have omitted the factor $e^{i(\mathbf{k}_L - \mathbf{k})\cdot(\mathbf{r}+\boldsymbol{\mu}/2)}$ inside the summation, i.e., we have ignored the momentum transferred by photons to the electrons. This is because ω_L and ω_λ are of order U, the Hubbard interaction. For typical materials, the corresponding wavelength is several thousand lattice spacings. Hence, throughout this paper, we will ignore the spatial variation of the laser field. Therefore, $\hat{R}^{(1)}_{(\mathbf{k},\mathbf{e}_j)}$ depends on the emitted mode $(\mathbf{k}, \mathbf{e}_j)$, only through its polarization $\mathbf{e}_j$ and in general, the frequency $\omega_\mathbf{k}$ (although the above expression does not depend on $\omega_\mathbf{k}$). In the near future, in systems with much larger lattice spacings, such as Moiré materials, significant momentum transfer to electrons may become possible optically. In this case, our formalism can be adjusted to include finite-momentum matter operators.

B. Processes leading to the emission of two photons

Now, we describe the processes that contribute to $\hat{R}^{(2)}$, i.e., lead to the emission of two photons. $\hat{R}^{(2)}_{\lambda_1,\lambda_2}$ can be extracted from Eq. (35) by expanding $\hat{V}_P \hat{\mathbb{G}}_0 \hat{V}_P \hat{\mathbb{G}}_0 \hat{V}_P \hat{\mathbb{G}}_0 \hat{V}_P + \hat{V}_P \hat{\mathbb{G}}_0 \hat{V}_D \hat{\mathbb{G}}_0 \hat{V}_P$. First, we provide a qualitative overview. We will then state the result for $\hat{R}^{(2)}_{\lambda_1,\lambda_2}$ for the case of the single band Hubbard model at half-filling. Explicit details of the derivation are provided in Appendix C.

In Fig. 5, we show a schematic in terms of energy levels for the different two-photon emission processes. In Fig. 6, we show the corresponding microscopic processes. We will also show that the intensity of photons $G^{(1)}(0)$ as a function of frequency qualitatively looks like Fig. 5(e-f), i.e., has one central peak around ω_L with width $\sim \mathtt{t}^2/U$ (highlighted in Fig. 5(e)), and has two sidebands around $2\omega_L - U$ and U (highlighted in Fig. 5(f)). The central peak can be anticipated from our previous discussion of Raman scattering, where the emitted photon's frequency differs from the laser's frequency by an order of the spin excitation energy scale. In this section, we will infer the existence of the sidebands. We will soon see that they result from the processes in Fig. 5(b-d) leading to pairs of photons around frequencies $2\omega_L - U$ and U. Let us now study all the processes one by one.

1. Fig. 5(a) shows the Raman process occurring twice in succession. First, a doublon-hole pair is virtually created along a bond by a photon absorption via the paramagnetic term $\hat{V}_P$ (Fig. 6(a$_1$-a$_2$)). This pair then recombines via a photon emission, with the system returning to the spin sector – in a possibly excited state. This effectively results in the application of a spin operator on the system, which to leading order in $\mathtt{t}/|\omega_L - U|$ is the Fleury-Loudon sum of spin singlet projectors [73] $\hat{A}_1$ defined in Eq. [45, 53]. The system now time-evolves till a second Raman process occurs (Fig. 6(a$_5$)), resulting in application of a second Fleury-Loudon operator $\hat{A}_2$. We show this explicitly in Appendix C 1.

   In effect, both the photons emitted have frequencies close to ω_L (the central peak in Fig. 5(e)), and their difference from ω_L is of the order of $J \sim \mathtt{t}^2/U$, i.e., the energy scale of the spin sector.

2. The microscopic process corresponding to Fig. 5(b) is shown in Fig. 6(b$_1$-b$_6$). It starts off similar to the process in Fig. 5(a). The difference is that here, the two emitted photons are of frequencies of order $2\omega_L - U$ and U respectively [the sidebands in Fig. 5(e,f)]. These sidebands are reminiscent of the sidebands of the fluorescence triplet when a two level system is irradiated with light detuned from its gap [74]. In Appendix C 1, we show how this process comes out naturally in our formalism.

3. Fig. 5(c) shows a process where two photons (ω_L) are absorbed, successively creating two virtual doublon-hole pairs at different locations [Fig. 6(c$_2$-c$_3$, c$_2'$-c$_3'$)]. Then, one of the doublon-hole pairs recombines by emitting a photon. The recombining pair could be one of the two pairs that were originally created [Fig. 6(c$_4$)], in which case those two pairs could have been arbitrarily separated. Alternatively, the recombining pair could be made of a hole from one pair and a doublon from the other pair [Fig. 6(c$_4'$)]. This would require the two bonds to be located such that they are connected by a different bond [Fig. 6(c$_3'$)]. The photon emitted this way has frequency ω_{λ_1} to be of the order of $2\omega_L - U$. After the first photon emission, the material is in the single doublon-hole pair sector. It time-evolves here [Fig. 6(c$_5$, c$_5'$)] till the emission of a second photon of frequency of order U by the recombination of the doublon-hole pair, which by now has possibly moved to a far away bond [Fig. 6(c$_6$, c$_6'$)]. This process again corresponds to the sidebands in Fig. 5(f).

Again, since a state $|K\rangle$ in the single doublon-hole sector is resonantly accessed, in effect, photons couple to matter operators that can excite the system into the charge sector. We will evaluate these operators explicitly in Appendix C 2. Notice that the steps in Fig. 6(b$_4$-b$_6$) and 6(c$_4$-c$_6$) look identical. The operators coming from rows (b) and (c) in Fig. 6 have opposite signs (arising from opposite signs of detuning), and they almost cancel. The non-cancellation is due to the following difference. In Fig. 6(b$_2$) and 6(b$_4$), the two bonds along which light-assisted tunneling happens, can be arbitrary, and in principle can even share a site or coincide. But the bonds in Fig. 6(c$_2$) and 6(c$_3$) are required to not share a site in order to let two doublon-hole pairs to be created. Thus, the effect of combining oppositely signed rows (b) and (c) of Fig. 6 is that after the emission of the first photon, one is left with a sum of local operators involving spin singlet projection along a bond, say ($\mathbf{r}_1, \boldsymbol{\mu}_1$), followed by electron tunneling along a bond touching ($\mathbf{r}_1, \boldsymbol{\mu}_1$), as shown in Fig. 7.

Similarly, the steps shown in row c' of Fig. 6 up to the emission of the first photon, results in a sum of local terms involving a spin operator supported on a bond followed by an electron tunneling operator supported near that bond as shown in Fig. 8.

Finally, the recombination of the doublon-hole pair by emitting the second photon [Fig. 6 (b$_6$, c$_6$, c$_6'$) and as we show later, Fig. 6(d$_5$)] results in an electron tunneling operator proportional to the global electric current.

So far, the processes we have considered come from the term $\hat{V}_P \hat{\mathbb{G}}_0 \hat{V}_P \hat{\mathbb{G}}_0 \hat{V}_P \hat{\mathbb{G}}_0 \hat{V}_P$ in Eq. (35), and did not involve the diamagnetic term.
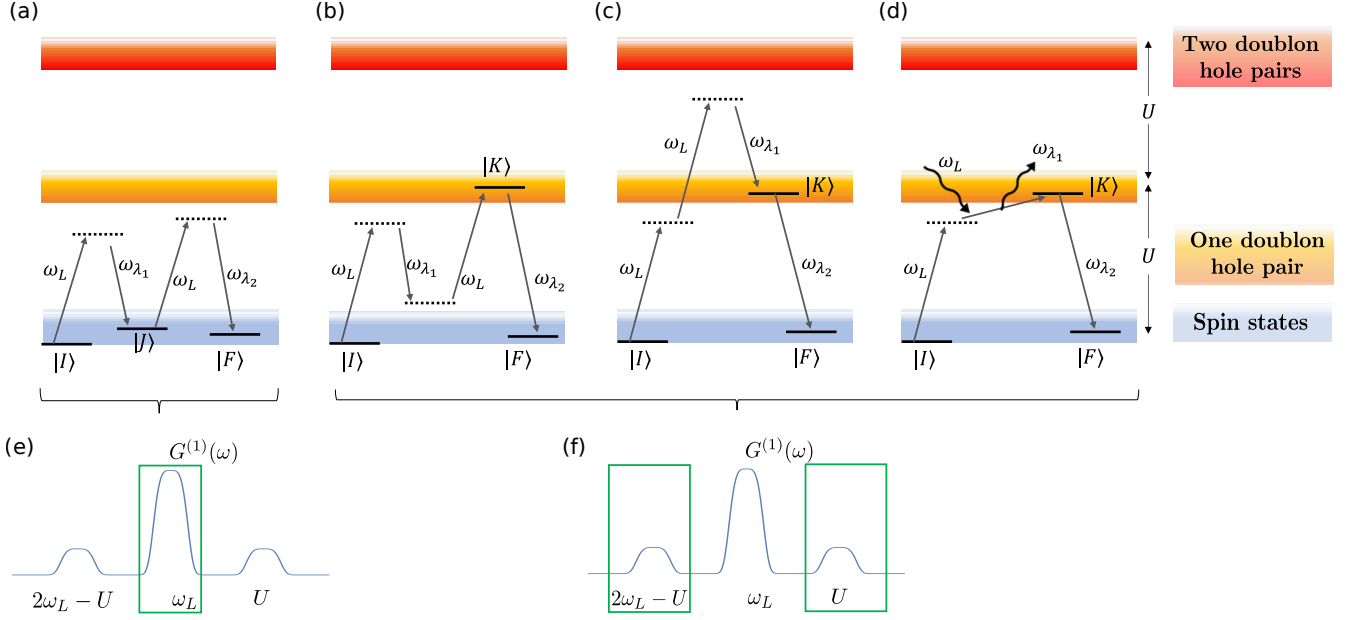
Figure 5. (a)-(d) show the four processes contributing to $G^{(2)}(\tau)$ to leading order in g_L and $\mathtt{t}/|\omega_L - U|$. (e) and (f) show a cartoon intensity profile of the emitted photons. Process (a) contributes to the central peak highlighted in (e) and processes (b-d) contribute to the sidebands highlighted in (f). **(a)**: Raman process occurring twice, with the intermediate state $|J\rangle$ being in the spin sector. **(b)**: Scattering of two photons, accompanied with the real, i.e., resonant excitation of a state $|K\rangle$ in charge sector. This is reminiscent of the sideband process in Ref. [74]. **(c)**: This process corresponds to successive absorption of two photons resulting in virtual occupation of the two doublon-hole sector, followed by emission of two photons into the sidebands in (f). **(d)**: This process differs from (a), (b) and (c) in that it involves the diamagnetic term. After a photon absorption and virtual occupation of the single doublon-hole sector, the diamagnetic term results in the scattering of a laser photon (wavy line labelled ω_L) into an emitted mode of frequency ω_{λ_1}, which lies in the sideband near $2\omega_L - U$. This results in occupation of a matter state $|K\rangle$ in the single doublon-hole sector. Finally, a photon of frequency ω_{λ_2} is emitted into the sideband around U. **(e)**: The central peak is highlighted, corresponding to photons of frequency around ω_L. **(f)**: The sidebands corresponding to pairs of photons of frequency around $2\omega_L - U$ and U are highlighted.

4. The process shown in Fig. 5(d) features the diamagnetic term, and is in fact the most leading order in $\mathtt{t}/|U - \omega_L|$. It is shown pictorially in Fig. 6(d$_1$-d$_5$). Here, an electron hops by absorbing a photon (of frequency ω_L) via the paramagnetic term. Then, via the diamagnetic term, a photon is absorbed (of frequency ω_L) and a photon of frequency ω_{λ_1} of the order of $2\omega_L - U$ is emitted. Finally, via the paramagnetic term, a photon is emitted, whose frequency ω_{λ_2}, is of the order of U, and the material returns to the spin sector. This process corresponds to $\hat{V}_P \hat{\mathbb{G}}_0 \hat{V}_D \hat{\mathbb{G}}_0 \hat{V}_P$ in Eq. (35). This process again corresponds to the sidebands in Fig. 5(e,f).

In summary, all the processes leading to emission into the sidebands [Fig. 5(b,c,d)] involve an intermediate step where the material resonantly transitions to a state $|K\rangle$ in the single doublon-hole sector. On the other hand, the process leading to emission into the central peak [Fig. 5(a)] involves only off-resonant occupation of the single doublon-hole sector. The physical implication of this is that in the processes in Fig. 5(b,c,d), light effectively couples to a mixed spin-charge operator. But in the process shown in Fig. 5(a), light effectively couples

to an operator living entirely in the spin sector. We will arrive at the same fact formally in Appendix C.

C. Microscopic expression for $\hat{R}^{(2)}$

Following the discussion above, we now provide the explicit expression for operator $\hat{R}^{(2)}_{\lambda_1,\lambda_2}$. The derivation is carried out by expanding the $\hat{\mathcal{T}}$-matrix, and is provided in Appendix C. We provide explicit expressions here so that even for a different microscopic system (whose charged excitations are gapped), the reader can follow our derivation in Appendix C and obtain the expressions analogous to what we provide below.

We saw in Sec. V B and Fig. 5, that processes leading to photon emission in the sidebands involve matter operators that create charge excitations when acting on the spin sector. Therefore, before writing down the expression for $\hat{R}^{(2)}$, it is useful to define below some of those operators which move an electron from one site to another, thereby taking a state from the spin sector into the single doublon-hole sector, and vice versa.

First, we define $\hat{\mathcal{H}}_{\mathbf{r},\mathbf{r}'}$, a local tunneling term defined
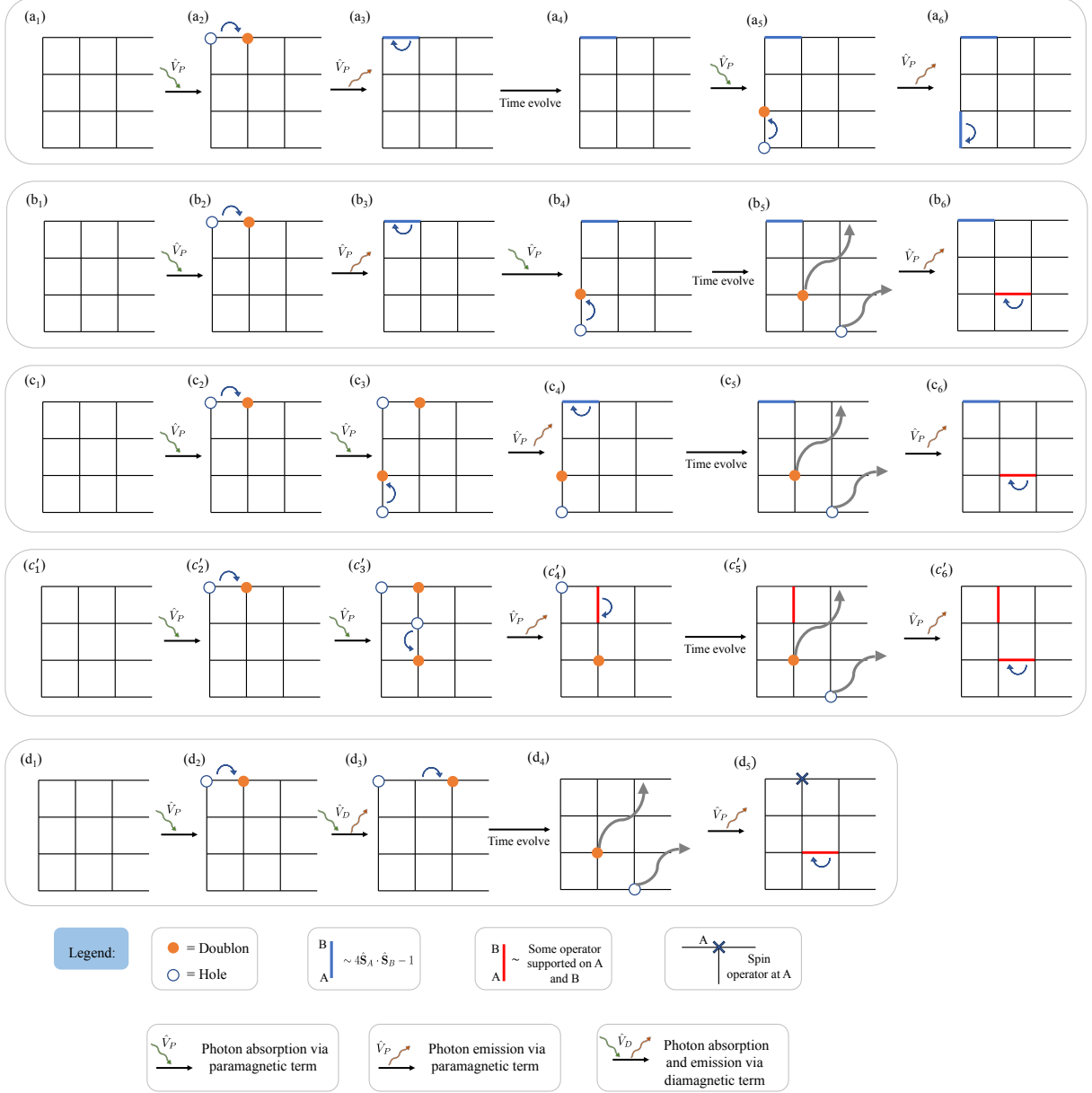
Figure 6. Microscopic processes corresponding to Fig. 5: We show the square lattice for concreteness, but our results are general. In all the subfigures, a curved blue arrow indicates that an electron *tunneled* from the tail to head of the arrow, and the configuration shown in a subfigure is a consequence of the hop shown in the *same* subfigure. The legend is provided at the bottom. We have organized the subfigures into rows on the basis of the subfigures of Fig. 5. ($\mathbf{a_1}$-$\mathbf{a_6}$): This row corresponds to Fig. 5(a). The system absorbs a photon via the paramagnetic term, virtually creating a doublon-hole pair (a_2). An electron then tunnels back emitting a photon. This results in applying the spin exchange operator $4\mathbf{S}_A \cdot \mathbf{S}_B - 1$ along the bond, say, AB colored blue in (a_3). A similar process then repeats along a different bond via absorption of a second laser photon, resulting in the emission of a second photon. ($\mathbf{b_1}$-$\mathbf{b_6}$): This row corresponds to Fig. 5(b). Here, the photons are emitted into the sidebands (see the discussion below Eq. (C7)). Next, the process in Fig. 5(c) amounts to two successive photon absorptions followed by the emission of two photons. This can occur in two distinct ways – (c_1-c_6) and (c'_1-c'_6). ($\mathbf{c_1}$-$\mathbf{c_5}$): Two doublon-hole pairs are created, and the same ones are annihilated. Note that during the time between emission of the two photons, the doublon-hole pair can move around (c_5). ($\boldsymbol{c'_1}$-$\boldsymbol{c'_5}$): Two doubon-hole pairs are created. A hole from one pair and a doublon from a different pair recombine (c'_4). ($\mathbf{d_1}$-$\mathbf{d_5}$): This row corresponds to Fig. 5(d). A doublon-hole pair is virtually created by absorbing a photon via the paramagnetic term. Then, either a doublon or a hole scatters to a different site by both absorbing and emitting a photon via the diamagnetic term (d_3). After time evolution, the doublon-hole pair recombines by emitting a photon via the paramagnetic term.
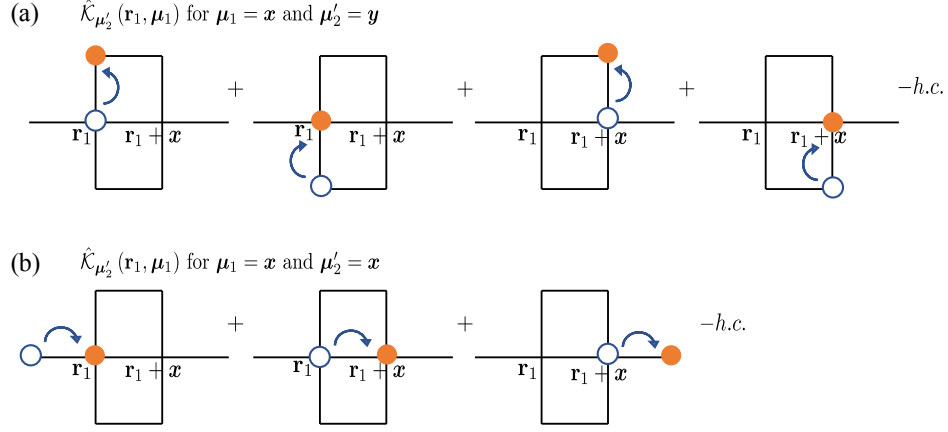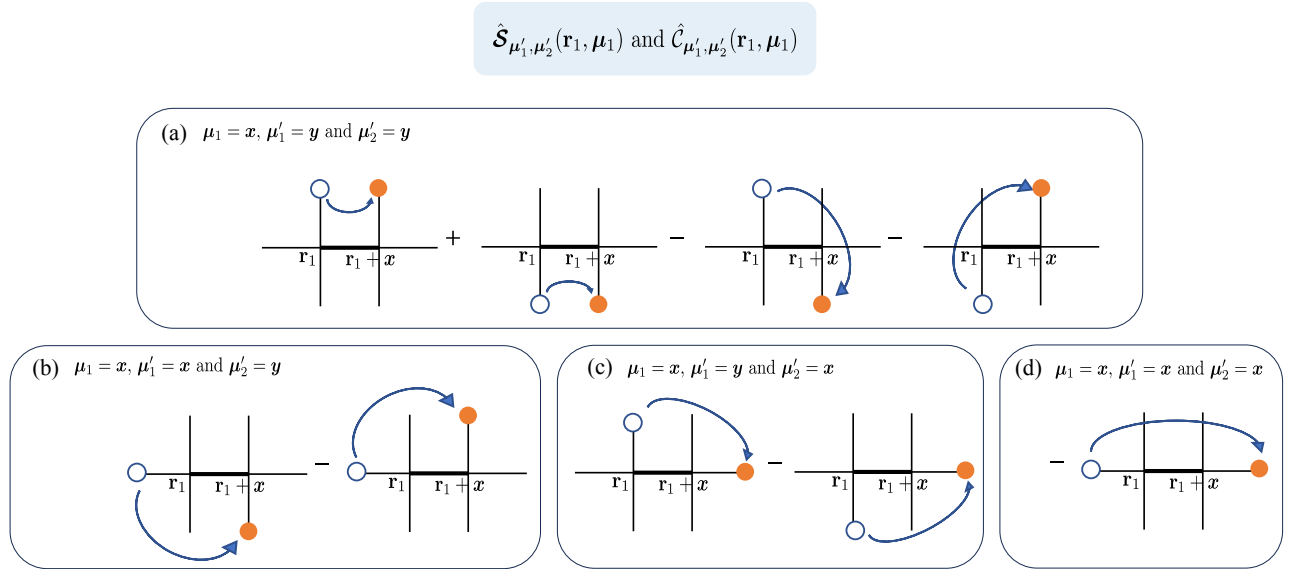
Figure 7. A visualization of the definition of the operator $\hat{\mathcal{K}}_{\boldsymbol{\mu}_2'}(\mathbf{r}_1, \boldsymbol{\mu}_1)$ (see Eq. (48)) on the square lattice. This is an operator that creates a doublon-hole pair when acting on the spin sector. **(a)**: $\boldsymbol{\mu}_1 = \boldsymbol{x}$ (lattice vector in the x-direction) and $\boldsymbol{\mu}_2' = \boldsymbol{y}$. **(b)**: $\boldsymbol{\mu}_1 = \boldsymbol{x}$ and $\boldsymbol{\mu}_2' = \boldsymbol{x}$.

Figure 8. A visualization of the definition of the operators $\hat{\boldsymbol{\mathcal{S}}}_{\boldsymbol{\mu}_1', \boldsymbol{\mu}_2'}(\mathbf{r}_1, \boldsymbol{\mu}_1)$ and $\hat{\mathcal{C}}_{\boldsymbol{\mu}_1', \boldsymbol{\mu}_2'}(\mathbf{r}_1, \boldsymbol{\mu}_1)$ (see Eq. (51) and Eq. (52)). Both the operators create a doublon-hole pair when acting on a state in the spin sector. $\hat{\boldsymbol{\mathcal{S}}}$ is a spin triplet operator, while $\hat{\mathcal{C}}$ is a spin triplet operator. Since this is the only difference between the two, we use the same figure to denote both $\hat{\boldsymbol{\mathcal{S}}}$ and $\hat{\mathcal{C}}$. The operators are specified by a bond $(\mathbf{r}_1, \boldsymbol{\mu}_1)$ and two additional lattice directions $\boldsymbol{\mu}_1'$ and $\boldsymbol{\mu}_2'$. The four subfigures show the definition for different choices of these directions.

for a pair of sites $\mathbf{r}$ and $\mathbf{r}'$, as

$$\hat{\mathcal{H}}_{\mathbf{r},\mathbf{r}'} \equiv \sum_\alpha \left(\hat{c}_{\mathbf{r}',\alpha}^\dagger \hat{c}_{\mathbf{r},\alpha} + \text{ h.c.} \right), \text{ and} \tag{46}$$

Similarly, we define a local (antihermitian) spin current from $\mathbf{r}$ to $\mathbf{r}'$:

$$\hat{\boldsymbol{\mathcal{J}}}_{\mathbf{r},\mathbf{r}'}^S \equiv \sum_{\alpha,\beta} \left(\hat{c}_{\mathbf{r}',\alpha}^\dagger \boldsymbol{\sigma}_{\alpha\beta} \hat{c}_{\mathbf{r},\beta} - \text{h.c.} \right). \tag{47}$$

Next, we define an operator $\hat{\mathcal{K}}_{\boldsymbol{\mu}_2'}(\mathbf{r}_1, \boldsymbol{\mu}_1)$ which is a sum of those operators that tunnel the electron along the

lattice vector $\boldsymbol{\mu}_2'$ with the following additional constraint. The constituent terms are localized to the vicinity of the bond $(\mathbf{r}_1, \boldsymbol{\mu}_1)$, in the sense that for each tunneling term in $\hat{\mathcal{K}}_{\boldsymbol{\mu}_2'}(\mathbf{r}_1, \boldsymbol{\mu}_1)$, the electron originates from or ends in either $\mathbf{r}_1$ or $\mathbf{r}_1 + \boldsymbol{\mu}_1$. See Fig. 7 for a visualization. The formal definition is

$$\hat{\mathcal{K}}_{\boldsymbol{\mu}_2'}(\mathbf{r}_1, \boldsymbol{\mu}_1)$$
$$\equiv \sum_{\mathbf{r}_2', \sigma_2'} \eta_{(\mathbf{r}_1, \boldsymbol{\mu}_1)}^{(\mathbf{r}_2', \boldsymbol{\mu}_2')} \left(\hat{c}_{\mathbf{r}_2' + \boldsymbol{\mu}_2', \sigma_2'}^\dagger \hat{c}_{\mathbf{r}_2' \sigma_2'} - \hat{c}_{\mathbf{r}_2' \sigma_2'}^\dagger \hat{c}_{\mathbf{r}_2' + \boldsymbol{\mu}_2', \sigma_2'} \right), \tag{48}$$

where we have introduced a symbol $\eta_{(\mathbf{r}_1, \boldsymbol{\mu}_1)}^{(\mathbf{r}_2', \boldsymbol{\mu}_2')}$ that is a func-

tion of two bonds $(\mathbf{r}_1, \boldsymbol{\mu}_1)$ and $(\mathbf{r}_2', \boldsymbol{\mu}_2')$, and is symmetric in its two arguments. It is defined as

$$
\eta_{(\mathbf{r}_1, \boldsymbol{\mu}_1)}^{(\mathbf{r}_2', \boldsymbol{\mu}_2')} = \begin{cases} 1, & \text{if bonds } (\mathbf{r}_2', \boldsymbol{\mu}_2') \text{ and } (\mathbf{r}_1, \boldsymbol{\mu}_1) \text{ have} \\ & \text{at least one site in common.} \\ 0, & \text{otherwise.} \end{cases}
\tag{49}
$$

Now, we define another set of tunneling operators — a spin triplet operator $\hat{\boldsymbol{\mathcal{S}}}_{\boldsymbol{\mu}_1', \boldsymbol{\mu}_2'}(\mathbf{r}_1, \boldsymbol{\mu}_1)$ and a spin singlet operator $\hat{\mathcal{C}}_{\boldsymbol{\mu}_1', \boldsymbol{\mu}_2'}(\mathbf{r}_1, \boldsymbol{\mu}_1)$, shown in Fig. 8. They tunnel an electron from one site adjacent to the bond $(\mathbf{r}_1, \boldsymbol{\mu}_1)$, to another site adjacent to the same bond – for example, from an empty circle to a filled circle in Fig. 8. These two sites are of the form $\mathbf{r}_1 \pm \boldsymbol{\mu}_1'$ and $\mathbf{r}_1 + \boldsymbol{\mu}_1 \pm \boldsymbol{\mu}_2'$, on the condition that these two sites, together with the sites of the bond $\mathbf{r}_1$ and $\mathbf{r}_1 + \boldsymbol{\mu}_1$, constitute four distinct sites. This is enforced using the following notation (for nonzero lattice vectors $\boldsymbol{\mu}$, $\boldsymbol{\nu}$ and $\boldsymbol{\rho}$):

$$
h(\boldsymbol{\mu}, \boldsymbol{\nu}, \boldsymbol{\rho}) = \begin{cases} 0, & \text{if } \boldsymbol{\mu} + \boldsymbol{\rho} = \mathbf{0}, \\ & \text{or if } \boldsymbol{\nu} = \boldsymbol{\mu} \\ & \text{or if } \boldsymbol{\mu} + \boldsymbol{\rho} = \boldsymbol{\nu}. \\ 1, & \text{otherwise.} \end{cases}
\tag{50}
$$

With this notation, $\hat{\boldsymbol{\mathcal{S}}}_{\boldsymbol{\mu}_1', \boldsymbol{\mu}_2'}(\mathbf{r}_1, \boldsymbol{\mu}_1)$ and $\hat{\mathcal{C}}_{\boldsymbol{\mu}_1', \boldsymbol{\mu}_2'}(\mathbf{r}_1, \boldsymbol{\mu}_1)$ are defined as

$$
\hat{\boldsymbol{\mathcal{S}}}_{\boldsymbol{\mu}_1', \boldsymbol{\mu}_2'}(\mathbf{r}_1, \boldsymbol{\mu}_1) = \frac{1}{2} \sum_{\substack{s_1' \in \{\pm 1\} \\ s_2' \in \{\pm 1\}}} s_1' s_2' \Bigg\{ \Bigg[h(\boldsymbol{\mu}_1, s_1'\boldsymbol{\mu}_1', s_2'\boldsymbol{\mu}_2')
$$
$$
\times \sum_{\alpha, \beta} \Big(\hat{c}_{\mathbf{r}_1 + \boldsymbol{\mu}_1 + s_2'\boldsymbol{\mu}_2', \alpha}^{\dagger} \boldsymbol{\sigma}_{\alpha\beta} \hat{c}_{\mathbf{r}_1 + s_1'\boldsymbol{\mu}_1', \beta} + \text{h.c.} \Big) \Bigg]
$$
$$
+ [\boldsymbol{\mu}_1' \leftrightarrow \boldsymbol{\mu}_2'] \Bigg\}, \text{ and}
\tag{51}
$$

$$
\hat{\mathcal{C}}_{\boldsymbol{\mu}_1', \boldsymbol{\mu}_2'}(\mathbf{r}_1, \boldsymbol{\mu}_1) = \frac{1}{2} \sum_{\substack{s_1' \in \{\pm 1\} \\ s_2' \in \{\pm 1\}}} s_1' s_2' \Bigg\{ \Bigg[h(\boldsymbol{\mu}_1, s_1'\boldsymbol{\mu}_1', s_2'\boldsymbol{\mu}_2')
$$
$$
\times \sum_{\alpha} \Big(\hat{c}_{\mathbf{r}_1 + \boldsymbol{\mu}_1 + s_2'\boldsymbol{\mu}_2', \alpha}^{\dagger} \hat{c}_{\mathbf{r}_1 + s_1'\boldsymbol{\mu}_1', \alpha} - \text{h.c.} \Big) \Bigg] + [\boldsymbol{\mu}_1' \leftrightarrow \boldsymbol{\mu}_2'] \Bigg\}.
\tag{52}
$$

With these local operators at hand, we define the following global (zero-momentum) matter operators $\hat{A}_j$, $\hat{B}_j$ and $\hat{C}_j$ that the photon detected by each of the two detectors $j \in \{1, 2\}$ couples to. The information about the detector j enters these operators through the polarization $\mathbf{e}_j$ of the detected photon. To leading order in laser-matter coupling g_L and $\mathtt{t}/|\omega_L - U|$, the operators are:

$$
\hat{A}_j = \frac{g_L \mathtt{g} \mathtt{t}^2}{\omega_L - U} \sum_{\mathbf{r}, \boldsymbol{\mu}} \Big(4\hat{\mathbf{S}}_{\mathbf{r}} \cdot \hat{\mathbf{S}}_{\mathbf{r}+\boldsymbol{\mu}} - 1 \Big) \big(\bar{\boldsymbol{\mu}} \cdot \mathbf{e}_L \big) \big(\bar{\boldsymbol{\mu}} \cdot \mathbf{e}_j^* \big),
\tag{53}
$$

The operator $\hat{A}_i$ acts purely within the spin sector, and was the same operator that showed up in $G^{(1)}$ of Raman scattering (Eq. (45)).

The operator $\hat{B}_j$, on the other hand, creates a doublon-hole pair, when acting on the spin sector. In addition, it also creates spin excitations, and is therefore a mixed spin-charge operator. It is defined below (where we make use of the definitions in Eq. (46), (47), (48), (52) and (51)).

$$
\hat{B}_j = g_L^2 \mathtt{t}^2 \mathtt{g} \Bigg\{ \sum_{\boldsymbol{\mu}', \boldsymbol{\mu}} \sum_{\substack{s, s'=\pm 1 \\ s\boldsymbol{\mu} \neq s'\boldsymbol{\mu}'}} \Bigg[\big(\bar{\boldsymbol{\mu}}' \cdot \mathbf{e}_L \big) \big(\bar{\boldsymbol{\mu}} \cdot \mathbf{e}_L \big) \big(\bar{\boldsymbol{\mu}} \cdot \mathbf{e}_j^* \big) ss' \sum_{\mathbf{r}} \Big[\frac{1}{2} \hat{\mathcal{H}}_{\mathbf{r}+s'\boldsymbol{\mu}', \mathbf{r}+s\boldsymbol{\mu}} - \hat{\boldsymbol{\mathcal{J}}}_{\mathbf{r}+s'\boldsymbol{\mu}', \mathbf{r}+s\boldsymbol{\mu}}^{S} \cdot \hat{\mathbf{S}}_{\mathbf{r}} \Big] \Bigg]
$$
$$
- \frac{\mathtt{t}}{\omega_L - U} \sum_{\boldsymbol{\mu}', \boldsymbol{\mu}} \Bigg[\big(\bar{\boldsymbol{\mu}}' \cdot \mathbf{e}_L \big) \big(\bar{\boldsymbol{\mu}} \cdot \mathbf{e}_L \big) \big(\bar{\boldsymbol{\mu}} \cdot \mathbf{e}_j^* \big) \sum_{\mathbf{r}} \hat{\mathcal{K}}_{\boldsymbol{\mu}'}(\mathbf{r}, \boldsymbol{\mu}) \Big(4\hat{\mathbf{S}}_{\mathbf{r}} \cdot \hat{\mathbf{S}}_{\mathbf{r}+\boldsymbol{\mu}} - 1 \Big) \Bigg]
$$
$$
- \frac{\mathtt{t}}{\omega_L - U} \sum_{\substack{\mathbf{r}, \boldsymbol{\mu}, \\ \boldsymbol{\mu}_1', \boldsymbol{\mu}_2'}} \Bigg[\big(\bar{\boldsymbol{\mu}}_1' \cdot \mathbf{e}_L \big) \big(\bar{\boldsymbol{\mu}}_2' \cdot \mathbf{e}_L \big) \big(\bar{\boldsymbol{\mu}} \cdot \mathbf{e}_j^* \big) \Big[\hat{\boldsymbol{\mathcal{S}}}_{\boldsymbol{\mu}_1', \boldsymbol{\mu}_2'}(\mathbf{r}, \boldsymbol{\mu}) \cdot \Big(\frac{\hat{\mathbf{S}}_{\mathbf{r}} - \hat{\mathbf{S}}_{\mathbf{r}+\boldsymbol{\mu}}}{2} - i\hat{\mathbf{S}}_{\mathbf{r}} \times \hat{\mathbf{S}}_{\mathbf{r}+\boldsymbol{\mu}} \Big)
$$
$$
+ \hat{\mathcal{C}}_{\boldsymbol{\mu}_1', \boldsymbol{\mu}_2'}(\mathbf{r}, \boldsymbol{\mu}) \Big(\hat{\mathbf{S}}_{\mathbf{r}} \cdot \hat{\mathbf{S}}_{\mathbf{r}+\boldsymbol{\mu}} - \frac{1}{4} \Big) \Big] \Bigg] \Bigg\}.
\tag{54}
$$

The first line in Eq. (54) comes from the process shown in Fig. 6(d$_1$-d$_5$), and involves scattering via the diamagnetic

term. The second line above, involving $\hat{\mathcal{K}}_{\boldsymbol{\mu}'}(\mathbf{r}, \boldsymbol{\mu})$ results from the incomplete cancellation of the processes in Fig. 6(b$_1$-b$_6$) and Fig. 6(c$_1$-c$_6$) (see Sec. V B for a discussion). The last two lines involving $\hat{\boldsymbol{\mathcal{S}}}_{\boldsymbol{\mu}'_1, \boldsymbol{\mu}'_2}(\mathbf{r}, \boldsymbol{\mu})$ and $\hat{\mathcal{C}}_{\boldsymbol{\mu}'_1, \boldsymbol{\mu}'_2}(\mathbf{r}, \boldsymbol{\mu})$ come from the process shown in Fig. 6(c$'_1$-c$'_6$).

Finally, the operators $\hat{C}_j$ also take a state in the spin sector into one in the single doublon-hole sector, and vice versa. They are defined below:

$$\hat{C}_j = \frac{g\mathtt{t}}{\omega_L - U} \sum_{\boldsymbol{\mu}} \left(\bar{\boldsymbol{\mu}} \cdot \mathbf{e}_j^* \right) \hat{\mathcal{J}}_{\boldsymbol{\mu}}. \tag{55}$$

As a reminder, $\hat{\mathcal{J}}_{\boldsymbol{\mu}}$ was defined in Eq. (27), and is proportional to the global electron current in the direction $\boldsymbol{\mu}$.

Having defined the above matter operators, we are ready to return to the matter operator $\hat{R}^{(2)}$ that dictates the two-photon scattering amplitude. The matrix elements of $\hat{R}^{(2)}$ between matter energy states $|I\rangle$ and $|K\rangle$ (both in the spin sector) are of the following form (see Appendix C):

$$\langle F|\hat{R}^{(2)}_{\lambda_1, \lambda_2}|I\rangle$$
$$= -\sum_J \left[\frac{\langle F|\hat{A}_2|J\rangle \langle J|\hat{A}_1|I\rangle}{\omega_{\lambda_1} - (\omega_L - E_{JI} + i0^+)} + (1 \leftrightarrow 2) \right]$$
$$- \sum_K \left[\frac{\langle F|\hat{C}_2|K\rangle \langle K|\hat{B}_1|I\rangle}{\omega_{\lambda_1} - (2\omega_L - E_{KI} + i0^+)} + (1 \leftrightarrow 2) \right], \tag{56}$$

where $|I\rangle$, $|J\rangle$ and $|F\rangle$ are many-body eigenstates of the Hubbard model that all lie in the spin sector. $|K\rangle$ on the other hand is a many-body eigenstate in the charge-sector, containing one doublon-hole pair. Here, E_{JI} is of order $\mathtt{t}^2/U$, while E_{KI} is of order $U \pm \text{order}(\mathtt{t})$. Therefore, we see from Eq. (56) that photon pair emitted into the central peak [Fig. 5(e)], i.e., of frequency near ω_L, couples to pure spin operators $\hat{A}_j$. On the other hand, a photon pair emitted into the sidebands [Fig. 5(f)], i.e., of frequency near $2\omega_L - U$ and U, couples to the mixed spin-charge operator $\hat{B}_j$ and current operator $\hat{C}_j$ respectively.

The energy dependent factors in Eq. (56) can be absorbed into the Heisenberg evolution of the matter operators (see Appendix C for a derivation), and can be written as

$$\langle F|\hat{R}^{(2)}_{\lambda_1, \lambda_2}|I\rangle$$
$$= -i \int_{-\infty}^{\infty} \mathrm{d}t\, e^{-i(\omega_{\lambda_1} - \omega_L)t} \langle F|\mathbb{T}\left[\hat{A}_2(0)\hat{A}_1(-t) \right]|I\rangle$$
$$- i \int_{-\infty}^{\infty} \mathrm{d}t \langle F| \left[\theta(t)e^{-i(\omega_{\lambda_1} - 2\omega_L)t}\hat{C}_2(0)\hat{B}_1(-t) \right.$$
$$\left. + \theta(-t)e^{-i\omega_{\lambda_1} t}\hat{C}_1(-t)\hat{B}_2(0) \right]|I\rangle. \tag{57}$$

where $\mathbb{T}[\,]$ denotes time ordering of operators inside $[\,]$.

Note that the formula for $G^{(2)}(\tau)$ in Eq. (41) involves an integral over ω_{λ_1} and ω_{λ_2}, i.e., coherent superpositions of the different $\hat{R}^{(2)}_{\lambda_1, \lambda_2}$'s. Therefore, the frequency filter functions $\mathcal{F}_i(\omega)$ of the detectors will play a crucial role in determining $G^{(2)}(\tau)$. With this in mind, we will study the temporal structure of the matter correlation functions obtained by measuring $G^{(2)}(\tau)$, paying special attention to their dependence on the frequency filter functions of the detectors.

VI. TEMPORAL STRUCTURE OF CORRELATION FUNCTIONS

In this section, we combine the matter operators $\hat{R}^{(1)}$ and $\hat{R}^{(2)}$ from Sec. V C with the formulas for photonic correlators from Sec. IV [Eq. (40-43)] to derive the final expressions summarized in Table I.

It is useful to work with the Fourier transform of the filter function defined as $\tilde{\mathcal{F}}_j(t) = \int_{-\infty}^{\infty} \frac{\mathrm{d}\omega}{2\pi} \mathcal{F}_j(\omega)e^{-i\omega t}$. In order to simplify the expressions, we will absorb phases such as $e^{-iE_{JI}t}$ into Heisenberg time-evolution of the operators involved in the correlation functions. The result is summarized below.

A. Intensity $G^{(1)}$

The expression for $G^{(1)}_{d_j} = \langle \text{out}| \hat{a}^\dagger_{d_j}(0)\hat{a}_{d_j}(0) |\text{out}\rangle$ in Eq. (40) can be simplified to

$$G^{(1)}_{d_j} \approx \iint_{-\infty}^{\infty} \mathrm{d}t\, \mathrm{d}t'\, \tilde{\mathcal{F}}_j(t) \left[\tilde{\mathcal{F}}_j(t') \right]^* e^{i(\omega_L - \omega_j)(t - t')}$$
$$\times \langle I| \left[\hat{A}_j(-t') \right]^\dagger \hat{A}_j(-t)|I\rangle. \tag{58}$$

Recall that $\hat{A}_j$ was defined in Eq. (45). Here, we have used the definition of a Heisenberg-evolved operator $\hat{A}(t) \equiv e^{i\hat{H}_0 t}\hat{A}e^{-i\hat{H}_0 t}$. To connect to known results [22–24], let us take the case of a Lorentzian effective filter function as defined in Eq. (12) that is peaked in frequency around ω_j with a width Γ_j, such that the filter gets more and more selective as $\Gamma_j \to 0$. In time domain, this filter function is

$$\tilde{\mathcal{F}}_{j,\,\text{Lorentzian}}(t) = \mathtt{K}_j \Gamma_j \theta(t)e^{-\Gamma_j t}. \tag{59}$$

Eq. (58) then simplifies to:

$$G^{(1)}(\omega_j) \approx |\mathsf{K}_j|^2 \Gamma_j / 2$$
$$\times \int_{-\infty}^{\infty} \mathrm{d}t \, e^{-\Gamma_j|t|} e^{i(\omega_L - \omega_j)t} \left\langle \left[\hat{A}_j(t)\right]^\dagger \hat{A}_j(0) \right\rangle_0, \quad (60)$$

where K is a constant and was defined in Eq. (13). The expectation value is taken in a matter eigenstate $|I\rangle$ in the spin sector, or more generally, in any state in thermal equilibrium (hence, the subscript 0) within the spin sector. We thus recover the result of Ref. [22–24]. Thus, $G^{(1)}$ measures the dynamical fluctuations of spin singlet projection operators. In the special case of A_{2g} channel for the Kagome lattice, it measures the dynamical fluctuations of spin chirality operators.

B. First order homodyne correlator X^+

To write an expression for the correlator measured by homodyne detection, i.e., $\langle \mathrm{out}| \hat{a}_{d_j}(0) |\mathrm{out}\rangle$, we substitute $\hat{R}^{(1)}$ [Eq. (45)] into Eq. (42). We obtain:

$$\langle \mathrm{out}| \hat{a}_{d_j}(0) |\mathrm{out}\rangle = \mathcal{F}_j(\omega_L - \omega_j) \left\langle \hat{A}_j(0) \right\rangle_0. \quad (61)$$

We thus see that firstly, the signal for the homodyne correlator X^+ is peaked at the laser frequency ω_L, corresponding to *elastic* scattering of photons. Secondly, this correlator directly measures the static expectation value of the operator $\hat{A}_j$, which in most cases is a sum of spin singlet projection operators. But on the Kagome lattice in A_{2g} channel, i.e., in the $\left(e_j^x\right)^* e_L^y - \left(e_j^y\right)^* e_L^x$ channel, to leading order in $\mathsf{t}/|\omega_L - U|$, this operator is a linear combination of spin chirality operators [24]. While there have been proposals to measure fluctuations in spin chirality

using neutron scattering [77] and Raman scattering [24], the first order photonic homodyne correlator presented in our work allows a direct measurement of static spin chirality. Note that a nonzero signal in this channel is only possible if the ground state spontaneously breaks reflection and time reversal symmetry.

C. Second order coherence $G^{(2)}(\tau)$

To derive the matter correlator measured by $G^{(2)}_{d_1,d_2}(\tau) = \langle \mathrm{out}| \hat{a}_{d_1}^\dagger(0)\hat{a}_{d_2}^\dagger(\tau)\hat{a}_{d_2}(\tau)\hat{a}_{d_1}(0) |\mathrm{out}\rangle$, we substitute $\hat{R}^{(2)}_{\lambda_1,\lambda_2}$ [Eq. (56)] into the formula in Eq. (41). To do so, we need to first expand the following quantity in terms of matter operators $\hat{A}_j$, $\hat{B}_j$ and $\hat{C}_j$.

$$i \int_{-\infty}^{\infty} \frac{\mathrm{d}\omega_{\lambda_1}}{2\pi} \mathcal{F}_1(\omega_{\lambda_1} - \omega_1) \mathcal{F}_2(2\omega_L - \omega_{\lambda_1} - E_{FI} - \omega_2)$$
$$\times e^{i\omega_{\lambda_1}\tau} \langle F| \hat{R}^{(2)}_{\lambda_1,\lambda_2}(\omega_{\lambda_1}, \omega_{\lambda_2})|I\rangle. \quad (62)$$

Note that in the above-equation, we have used the δ-function to fix $\omega_{\lambda_2} = 2\omega_L - \omega_{\lambda_1} - E_{FI}$. Before proceeding, just like we did in Sec. V A, it is useful to work with the Fourier transforms of the filter functions.

From now on, we will assume that the filters $\mathcal{F}_i(\omega)$ are sensitive enough to distinguish frequencies around ω_L from those around $2\omega_L - U$ and from those around U. So we will ignore any interference between these sets of terms and treat terms of each window separately. Without loss of generality, we assume that $\tau > 0$, i.e., detector 2 clicks after detector 1.

Substituting the matrix element $\langle F| \hat{R}^{(2)}_{\lambda_1,\lambda_2}(\omega_{\lambda_1}, \omega_{\lambda_2})|I\rangle$ obtained in Eq. (57) into the expression in Eq. (62), and only keeping the term corresponding to the frequency range of interest, we get:

$$i \int_{-\infty}^{\infty} \frac{\mathrm{d}\omega_{\lambda_1}}{2\pi} \mathcal{F}_1(\omega_{\lambda_1} - \omega_1) \mathcal{F}_2(2\omega_L - \omega_{\lambda_1} - E_{FI} - \omega_2) e^{i\omega_{\lambda_1}\tau} \langle F| \hat{R}^{(2)}_{\lambda_1,\lambda_2}|I\rangle$$

$$= e^{i(2\omega_L - E_{FI})\tau} \int_0^\infty \int_0^\infty \mathrm{d}t_1 \, \mathrm{d}t_2 \, \tilde{\mathcal{F}}_1(t_1)\tilde{\mathcal{F}}_2(t_2) \langle F| \hat{M}^{(2)}_{d_1,d_2}(\tau - t_2, -t_1)|I\rangle, \quad \text{where}$$

$$\hat{M}^{(2)}_{d_1,d_2}(\tau - t_2, -t_1) = \begin{cases} e^{-i\omega_L\tau} e^{i[(\omega_L - \omega_1)t_1 + (\omega_L - \omega_2)t_2]} \mathbb{T}\left[\hat{A}_2(\tau - t_2)\hat{A}_1(-t_1)\right] \\ \quad \text{if both detectors detect near } \omega_L, \\[2mm] e^{i[(2\omega_L - \omega_1)t_1 - \omega_2 t_2]} \theta(t_1 + \tau - t_2) \hat{C}_2(\tau - t_2)\hat{B}_1(-t_1) \\ \quad \text{if detector 1 detects near } 2\omega_L - U \text{ and detector 2 detects near } U, \\[2mm] e^{-2i\omega_L\tau} e^{i[-\omega_1 t_1 + (2\omega_L - \omega_2)t_2]} \theta(t_2 - t_1 - \tau) \hat{C}_1(-t_1)\hat{B}_2(\tau - t_2) \\ \quad \text{if detector 1 detects near } U \text{ and detector 2 detects near } 2\omega_L - U. \end{cases} \quad (63)$$

The above operator is directly related to the operator $\hat{M}_j(t)$ introduced in Sec. II B [see Eq. (2) and Eq. (4)]:

$$\hat{M}^{(2)}_{d_1,d_2}(\tau - t_2, -t_1) = \mathbb{T}\left[\hat{M}_2(\tau - t_2)\hat{M}_1(-t_1)\right]. \quad (64)$$

From Eq. (41), we see that expression for $G^{(2)}(\tau)$ is obtained by taking the absolute value squared of the above expression and summing over F. The result is:

$$G^{(2)}_{d_1,d_2}(\tau) \approx \iint_0^\infty \iint_0^\infty dt_1\, dt_2\, dt_1'\, dt_2'\, \tilde{\mathcal{F}}_1(t_1)\tilde{\mathcal{F}}_2(t_2)[\tilde{\mathcal{F}}_1(t_1')]^*[\tilde{\mathcal{F}}_2(t_2')]^*\, \mathcal{C}^{(2)}_{d_1,d_2}(-t_1', \tau - t_2'; \tau - t_2, -t_1), \tag{65}$$

where

$$
\mathcal{C}^{(2)}_{d_1,d_2}(-t_1', \tau - t_2'; \tau - t_2, -t_1)
$$
$$
= \begin{cases}
e^{i\left[(\omega_L - \omega_1)(t_1 - t_1') + (\omega_L - \omega_2)(t_2 - t_2')\right]} \left\langle \bar{\mathbb{T}}\left[\hat{A}_1^\dagger(-t_1')\hat{A}_2^\dagger(\tau - t_2')\right] \mathbb{T}\left[\hat{A}_2(\tau - t_2)\hat{A}_1(-t_1)\right]\right\rangle_0 \\
\quad \text{if both detectors detect near } \omega_L, \\[1.5em]
\theta(t_1' + \tau - t_2')\theta(t_1 + \tau - t_2)e^{i\left[(2\omega_L - \omega_1)(t_1 - t_1') - \omega_2(t_2 - t_2')\right]} \left\langle \hat{B}_1^\dagger(-t_1')\hat{C}_2^\dagger(\tau - t_2')\hat{C}_2(\tau - t_2)\hat{B}_1(-t_1)\right\rangle_0 \\
\quad \text{if detector 1 detects near } 2\omega_L - U \text{ and detector 2 detects near } U, \\[1.5em]
\theta(t_2 - t_1 - \tau)\theta(t_2' - t_1' - \tau)e^{i\left[(2\omega_L - \omega_2)(t_2 - t_2') - \omega_1(t_1 - t_1')\right]} \left\langle \hat{B}_2^\dagger(\tau - t_2')\hat{C}_1^\dagger(-t_1')\hat{C}_1(-t_1)\hat{B}_2(\tau - t_2)\right\rangle_0 \\
\quad \text{if detector 1 detects near } U \text{ and detector 2 detects near } 2\omega_L - U.
\end{cases} \tag{66}
$$

Recall that the matter operators $\hat{A}_i$, $\hat{B}_j$ and $\hat{C}_i$ are matter operators that are defined in Eq. (53), (54) and (55) respectively, and $\tilde{\mathcal{F}}_j(t_j)$ for detector j is the Fourier transform of the frequency filter function $\mathcal{F}_j(\omega - \omega_j)$, w.r.t. the argument $\omega - \omega_j$.

The temporal structure is illustrated in Fig. 9. Given that the photonic correlator is of the form $\sim \left\langle \hat{a}_1^\dagger(0)\hat{a}_2^\dagger(\tau)\hat{a}_2(\tau)\hat{a}_1(0)\right\rangle$, we would have naïvely expected the matter correlator to be of the form $\sim \left\langle \hat{A}_1^\dagger(0)\hat{A}_2^\dagger(\tau)\hat{A}_2(\tau)\hat{A}_1(0)\right\rangle$. This structure is indeed correct if the filter functions are broad in frequency, and hence narrow in time. But in general, the photon could spend time in the causal filter, say a cavity, before getting detected. Therefore the time delay between the clicks of the detector does not necessarily equal the time between the emission of the two photons. In fact, if the filter's frequency selectivity window is narrower than $1/\tau$, then its Fourier transform can be so wide that the first photon to be emitted could be the second to be detected. Hence one needs the convolution of the matter operators with the Fourier transformed filter functions as written in Eq. (65, 66).

To gain some more concreteness, let us now consider Lorentzian effective filter functions as defined in Eq. (12), i.e., $\mathcal{F}_j(\omega) = i\mathsf{K}\Gamma_j/(\omega - \omega_j + i\Gamma_j)$, for detectors $j = 1$ and 2 respectively. Substituting its Fourier transform, Eq. (59) into Eq. (65), we get:

$$G^{(2)}_{d_1,d_2}(\tau) = |\mathsf{K}_1\mathsf{K}_2\Gamma_1\Gamma_2|^2 \int_0^\infty \int_0^\infty \int_0^\infty \int_0^\infty dt_1\, dt_2\, dt_1'\, dt_2' \left[\right.$$
$$\left. \times\, e^{-\left[\Gamma_1(t_1 + t_1') + \Gamma_2(t_2 + t_2')\right]} \mathcal{C}^{(2)}_{d_1,d_2}(-t_1', \tau - t_2'; \tau - t_2, -t_1) \right] \tag{67}$$

Let us now look at the different limiting cases of the frequency selectivity being broad (large Γ_j) and narrow (small Γ_j). In the large Γ_j limit, we will approximate $\theta(t)\Gamma_j e^{-\Gamma_j t} \approx \delta(t)$.[98]

1. Detector d_1 is broad in frequency

First, let us take the limit $\Gamma_1 \to \infty$. Then, Eq. (67) becomes

$$\left. G^{(2)}_{d_1,d_2}(\tau)\right|_{\Gamma_1 \to \infty} \approx |\mathsf{K}_1\mathsf{K}_2|^2\Gamma_2^2 \int_0^\infty dt_2 \int_0^\infty dt_2'\, e^{-\Gamma_2(t_2 + t_2')}$$
$$\times\, \mathcal{C}^{(2)}_{d_1,d_2}(0, \tau - t_2'; \tau - t_2, 0). \tag{68}$$

In this correlator, the operator that couples to the photon detected first (red dot in Fig. 9) is inserted at a fixed time 0, while the operator coupling to the photon detected second (red dot in Fig. 9) can come earlier than τ.

2. Detector d_2 is broad in frequency

Next, let us take the limit $\Gamma_2 \to \infty$. Then, Eq. (67) becomes

$$\left. G^{(2)}_{d_1,d_2}(\tau)\right|_{\Gamma_2 \to \infty} \approx |\mathsf{K}_1\mathsf{K}_2|^2\Gamma_1^2 \int_0^\infty dt_1 \int_0^\infty dt_1'\, e^{-\Gamma_1(t_1 + t_1')}$$
$$\times\, \mathcal{C}^{(2)}_{d_1,d_2}(-t_1', \tau; \tau, -t_1). \tag{69}$$

Here, the operators coupling to the second photon (blue dots in Fig. 9) are fixed to be at time τ, while the red dots can come earlier than time 0. Another difference
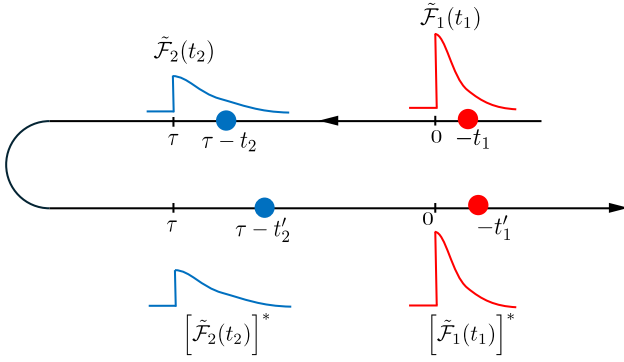
Figure 9. Time contour for the matter correlation function corresponding to $G^{(2)}_{d_1,d_2}(\tau)$, given by Eq. (65, 66). Here, time flows forward from right to left. The red and blue circles denote operators that couple to the photon detected first and second respectively. The forward time segment of the contour (top) is time-ordered, while the backward time segment (bottom) is anti-time-ordered. The profiles of the Fourier transformed *causal* filter functions $\tilde{\mathcal{F}}_j(t_j)$ are shown schematically. More selective the filter is in frequency, the broader its Fourier transform is in time. We see that even though the second detector clicks at time τ after the first, the insertion of the matter operator that couples to the second photon can occur earlier, i.e., at $\tau - t_2$. In fact, $\tau - t_2$ can even be earlier than the operator insertion corresponding to the first photon (at $-t_1$) if the width of frequency selectivity window is smaller than $1/\tau$. We look at some limiting cases in Eq. (69-71). When detector d_1 is broad in frequency selectivity, the red dot is forced to be at time 0 [Eq. (69)]. Similarly, when detector d_2 [Eq. (70)] is broad, the blue dot is forced to be at τ.

to note from the previous case is that the two operator insertions at the same time τ come consecutively. Hence temporally, Eq. (70) is more like a three-point correlator than a four-point one.

3. Both detectors are broad in frequency

Next, let us take the limit where both $\Gamma_1 \to \infty$ and $\Gamma_2 \to \infty$. Then, Eq. (67) becomes

$$G^{(2)}_{d_1,d_2}(\tau)\Big|_{\Gamma_1,\Gamma_2\to\infty} \approx |\mathsf{K}_1\mathsf{K}_2|^2 \mathcal{C}^{(2)}_{d_1,d_2}(0,\tau;\tau,0). \tag{70}$$

This has the structure $\sim \left\langle \hat{A}_1^\dagger(0)\hat{A}_2^\dagger(\tau)\hat{A}_2^\dagger(\tau)\hat{A}_1^\dagger(0) \right\rangle$, exactly mirroring the structure of the photonic correlator because the detection process is localized in time.

4. Both detectors are narrow in frequency

Now, let us consider the opposite limit of sharp frequency resolution, when both Γ_1 and Γ_2 are much less than $1/\tau$. We can shift t_2 and t_2' by τ in *Eq.* (67), pushing the τ dependence into the exponential factors like

$e^{\Gamma_2 t_2}$. But in the limit $\Gamma_1, \Gamma_2 \to 0$, the τ dependence in $G^{(2)}_{d_1,d_2}(\tau)$ [Eq. (67)] fades away, i.e.,

$$G^{(2)}_{d_1,d_2}\Big|_{\Gamma_1,\Gamma_2\to 0} \propto \iiint_{-\infty}^{\infty} \mathrm{d}t_2\,\mathrm{d}t_1'\,\mathrm{d}t_2'\, \mathcal{C}^{(2)}_{d_1,d_2}(-t_1',-t_2';-t_2,0). \tag{71}$$

But in practice, one should first calculate Eq. (67) using nonzero Γ_j and then take the limit $\Gamma_j \to 0^+$.

D. Second order photon number non-conserving homodyne correlation $X^{++}(\tau)$

Here, we derive the matter correlator measured by the second order photon non-conserving homodyne correlation function, i.e., $X^{++}_{d_1,d_2}(\tau) = \langle\mathrm{out}|\,\hat{a}_{d_2}(\tau)\hat{a}_{d_1}(0)\,|\mathrm{out}\rangle$. Substituting the expression for $\hat{R}^{(2)}_{\lambda_1,\lambda_2}$ [Eq. 56] into Eq. (43), and then using Eq. (63), we obtain:

$$\langle\hat{a}_{d_2}(\tau)\hat{a}_{d_1}(0)\rangle_{\mathrm{out}} \approx \iint_{-\infty}^{\infty} \mathrm{d}t_1\,\mathrm{d}t_2\, \tilde{\mathcal{F}}_1(t_1)\tilde{\mathcal{F}}_2(t_2)$$
$$\times \left\langle \hat{M}^{(2)}_{d_1,d_2}(\tau-t_2,-t_1) \right\rangle_0, \tag{72}$$

where $\hat{M}^{(2)}_{d_1,d_2}(\tau - t_2, -t_1)$ is a time-ordered product of operators, as defined in Eq. (63).

Like before, specializing to Lorentzian effective filters defined in Eq. (59), and taking the large Γ_1, Γ_2 limit, i.e., the limit of frequency selectivity being broad, the above equation becomes

$$\langle\hat{a}_{d_2}(\tau)\hat{a}_{d_1}(0)\rangle_{\mathrm{out}}\Big|_{\Gamma_1,\Gamma_2\to\infty}$$
$$\approx \mathsf{K}_1\mathsf{K}_2 \left\langle \hat{M}^{(2)}_{d_1,d_2}(0,-\tau) \right\rangle_0. \tag{73}$$

Lastly, we discuss the second order photon number conserving homodyne correlator $X^{-+}_{d_1,d_2}(\tau) = \langle\mathrm{out}|\,\hat{a}_{d_2}^\dagger(\tau)\hat{a}_{d_1}(0)\,|\mathrm{out}\rangle$ in Appendix C 4.

In summary, Eq. (58), (61), (65), and (72) map correlation functions of photons onto the right-hand-side which is a correlation function of the matter operators. The expectation value $\langle.\rangle_0$ in the right-hand side, in our derivation is taken in any unperturbed energy eigenstate $|I\rangle$ of the matter Hamiltonian that lies within the spin sector. As a corollary, the expectation value can also be taken in a mixed state (in the spin sector) that is diagonal in the energy eigenbasis, and in particular, in a thermal state. Thus, our formula also works at nonzero temperatures, as long as the temperature is much smaller than U.

VII. APPLICATION I: MEASURING STATIC SPIN CHIRALITY

In this section, we show that static spin chirality on the triangular lattice can be measured using a second-order
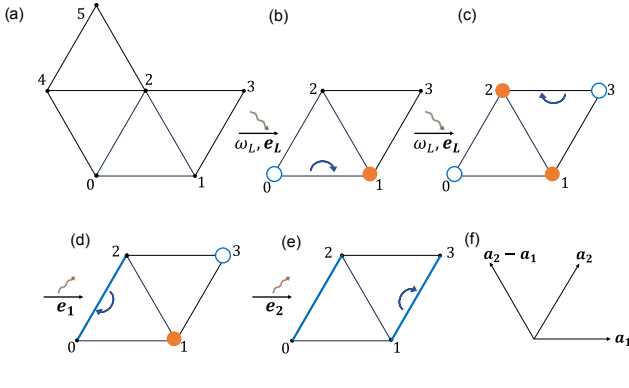
Figure 10. Processes leading to spin chirality matter operator: **(a)**: We study this motif. Later, one should translate the contribution from this motif by all lattice vectors of the triangular lattice. A black dot represents a singly occupied electron, i.e., a spin degree of freedom. Blue empty circle is a hole and an orange filled circle is a doubly occupied site (doublon). **(b)**: Upon absorption of a photon, an electron virtually hops from 0 to 1. **(c)**: Upon absorption of a second photon, an electron hops virtually from 3 to 0. **(d)**: The doublon-hole pair recombines along the bond from 2 to 0 by emitting a photon of polarization $\mathbf{e}_1$ and frequency around $2\omega_L - U$. **(e)**: This is similar to the previous step, but the frequency of the second photon is around U. **(f)**: Lattice vectors $\boldsymbol{a}_1$ and $\boldsymbol{a}_2$ of the triangular lattice. Also shown is the linear combination $\boldsymbol{a}_2 - \boldsymbol{a}_1$.

homodyne measurement $\mathrm{Im}\,\langle \hat{a}_{d_2}(0)\hat{a}_{d_1}(0)\rangle_{\mathrm{out}}$ if the system is driven by a coherent state input. The conditions are that the delay time $\tau = 0$, and the filters are such that d_1 and d_2 select the sidebands near $2\omega_L - U$, and U respectively, but are broad in their respective sidebands.

The contributing process is shown in Fig. 5(c), and microscopically corresponds to Fig. 6(c_1'-c_6'). The same process for the triangular lattice is shown here in Fig. 10. We have shown in Sec. V C that the correlations between photons emitted into the sidebands probe correlations between operators $\hat{B}_j$ [Eq. (54)] and $\hat{C}_j$ [Eq. (55)], both of which couple the spin sector to the charge sector. How could we then measure a pure spin correlator via photons in the sidebands? The reason lies in the two conditions we mentioned above. The absence of filtering implies that photons do not spend any additional time in the filter after they are emitted by the material. Furthermore, $\tau = 0$ implies that the doublon-hole pair formed at the time of the first photon emission should immediately (within a temporal uncertainty $\sim 1/|\omega_L - U|$) recombine to emit the second photon. In other words, the time evolution step between Fig. 6(c_4') and (c_5') is not present anymore. Thus the net result of the two-photon scattering on the material is the application of an operator purely in the spin sector. Further, we are able to circumvent the no-go result in Ref. [24] (where the spin chirality term was zero on the triangular lattice) because we have access to three polarizations $\mathbf{e}_L$, $\mathbf{e}_1$ and $\mathbf{e}_2$.

Using the mapping from photonic to electronic correlator, we have

$$\mathrm{Im}\,\langle \hat{a}_{d_2}(0)\hat{a}_{d_1}(0)\rangle_{\mathrm{out}} = \mathtt{K}_1\mathtt{K}_2\,\mathrm{Im}\,\left\langle \hat{C}_2(0)\hat{B}_1(0)\right\rangle_0. \quad (74)$$

The expression for $\hat{B}_1$ is given in Eq. (54). Operator $\hat{C}_2$ is the global electron current along the direction $\mathbf{e}_2$, consisting of nearest neighbor tunnelings. For the system to return to the spin sector after applying $\hat{C}_2$, the electron tunneling implemented by $\hat{B}_1$ should also be along a nearest neighbor bond. By symmetry, only the third line of Eq. (54) can contribute to nonzero spin chirality. In Eq. (54), tunneling along $\boldsymbol{\mu}_1'$ after absorbing a laser photon is shown in Fig. 10(b). We can now see from Fig. 10(c) that the tunneling direction due to the first and second photon absorptions are the same, i.e., $\boldsymbol{\mu}_2' = \boldsymbol{\mu}_1'$. Similarly, the electron tunneling direction during both the photon emissions — one in operator $\hat{B}_1$ and the other in operator $\hat{C}_2$ are the same. The term from $\hat{B}_1$ [Eq. (54)] which is relevant to Fig. 10 is (summation over spin indices of fermionic operators is implicit):

$$\frac{-g_L^2 \mathtt{t}^3 g}{2(\omega_L - U)}\left(\boldsymbol{a}_1 \cdot \mathbf{e}_L\right)^2\left(\boldsymbol{a}_2 \cdot \mathbf{e}_1^*\right)$$
$$\times \left(\hat{c}_1^\dagger \boldsymbol{\sigma} \hat{c}_3 + \hat{c}_3^\dagger \boldsymbol{\sigma} \hat{c}_1\right) \cdot \left(\frac{\hat{\mathbf{S}}_0 - \hat{\mathbf{S}}_2}{2} - i\mathbf{S}_0 \times \mathbf{S}_2\right). \quad (75)$$

Here, $\boldsymbol{a}_1$ and $\boldsymbol{a}_2$ are lattice vectors $(1,0)$ and $(1/2, \sqrt{3}/2)$ respectively [See Fig. 10(f)]. The term from $\hat{C}_2$ [Eq. (55)] which is relevant to Fig. 10 is:

$$\frac{g\mathtt{t}}{\omega_L - U}\left(\boldsymbol{a}_2 \cdot \mathbf{e}_2^*\right)\left(\hat{c}_3^\dagger \hat{c}_1 - \hat{c}_1^\dagger \hat{c}_3\right) \quad (76)$$

Now, we can see that the electron tunneling in Eq. (75) can be combined with that in Eq. (76) to give an operator lying purely in the spin sector. To do so, we use the following identity that holds at half-filling:

$$\left(\hat{c}_3^\dagger \hat{c}_1 - \hat{c}_1^\dagger \hat{c}_3\right)\left(\hat{c}_3^\dagger \boldsymbol{\sigma} \hat{c}_1 + \hat{c}_1^\dagger \boldsymbol{\sigma} \hat{c}_3\right) = \hat{\mathbf{S}}_3 - \hat{\mathbf{S}}_1 - 2i\hat{\mathbf{S}}_3 \times \hat{\mathbf{S}}_1. \quad (77)$$

Using this identity, the contribution from the process shown in Fig. 10 to $\hat{C}_2\hat{B}_1$ is:

$$\frac{g_L^2 g^2 \mathtt{t}^4}{(\omega_L - U)^2}\left(\boldsymbol{a}_1 \cdot \mathbf{e}_L\right)^2\left(\boldsymbol{a}_2 \cdot \mathbf{e}_1^*\right)\left(\boldsymbol{a}_2 \cdot \mathbf{e}_2^*\right)$$
$$\times \left(\frac{\hat{\mathbf{S}}_2 - \hat{\mathbf{S}}_0}{2} - i\mathbf{S}_2 \times \mathbf{S}_0\right) \cdot \left(\frac{\hat{\mathbf{S}}_3 - \hat{\mathbf{S}}_1}{2} - i\mathbf{S}_3 \times \mathbf{S}_1\right). \quad (78)$$

Now, for the same set of points $0, 1, 2, 3$ [Fig. 10], there is an alternative process where the laser-induced tunneling happens along bonds 02 and 13, while the tunneling during photon emission occurs along bonds 01 and 23. The resulting contribution to $\hat{C}_2\hat{B}_1$ is:

$$\frac{g_L^2 g^2 \mathtt{t}^4}{(\omega_L - U)^2}\left(\boldsymbol{a}_2 \cdot \mathbf{e}_L\right)^2\left(\boldsymbol{a}_1 \cdot \mathbf{e}_1^*\right)\left(\boldsymbol{a}_1 \cdot \mathbf{e}_2^*\right)$$
$$\times \left(\frac{\hat{\mathbf{S}}_3 - \hat{\mathbf{S}}_2}{2} - i\mathbf{S}_3 \times \mathbf{S}_2\right) \cdot \left(\frac{\hat{\mathbf{S}}_1 - \hat{\mathbf{S}}_0}{2} - i\mathbf{S}_1 \times \mathbf{S}_0\right). \quad (79)$$

Similarly, we will have the equivalent of the pair of terms as Eq. (78) and Eq. (79) for the set of points $0, 1, 2, 4$ [Fig. 10(a)]:

$$
\frac{g_L^2 g^2 \mathtt{t}^4}{(\omega_L - U)^2} \Bigg[(\boldsymbol{a}_1 \cdot \mathbf{e}_L)^2 \left((\boldsymbol{a}_2 - \boldsymbol{a}_1) \cdot \mathbf{e}_1^* \right) \left((\boldsymbol{a}_2 - \boldsymbol{a}_1) \cdot \mathbf{e}_2^* \right)
$$

$$
\times \left(\frac{\hat{\mathbf{S}}_4 - \hat{\mathbf{S}}_0}{2} - i \mathbf{S}_4 \times \mathbf{S}_0 \right) \cdot \left(\frac{\hat{\mathbf{S}}_2 - \hat{\mathbf{S}}_1}{2} - i \mathbf{S}_2 \times \mathbf{S}_1 \right)
$$

$$
+ \left((\boldsymbol{a}_2 - \boldsymbol{a}_1) \cdot \mathbf{e}_L \right)^2 (\boldsymbol{a}_1 \cdot \mathbf{e}_1^*)(\boldsymbol{a}_1 \cdot \mathbf{e}_2^*)
$$

$$
\times \left(\frac{\hat{\mathbf{S}}_2 - \hat{\mathbf{S}}_4}{2} - i \mathbf{S}_2 \times \mathbf{S}_4 \right) \cdot \left(\frac{\hat{\mathbf{S}}_1 - \hat{\mathbf{S}}_0}{2} - i \mathbf{S}_1 \times \mathbf{S}_0 \right) \Bigg].
\tag{80}
$$

Lastly, the contribution to $\hat{C}_2 \hat{B}_1$ from the set of points $0, 4, 5, 2$ [Fig. 10(a)] is:

$$
\frac{g_L^2 g^2 \mathtt{t}^4}{(\omega_L - U)^2} \Bigg[(\boldsymbol{a}_2 \cdot \mathbf{e}_L)^2 \left((\boldsymbol{a}_2 - \boldsymbol{a}_1) \cdot \mathbf{e}_1^* \right) \left((\boldsymbol{a}_2 - \boldsymbol{a}_1) \cdot \mathbf{e}_2^* \right)
$$

$$
\times \left(\frac{\hat{\mathbf{S}}_4 - \hat{\mathbf{S}}_0}{2} - i \mathbf{S}_4 \times \mathbf{S}_0 \right) \cdot \left(\frac{\hat{\mathbf{S}}_5 - \hat{\mathbf{S}}_2}{2} - i \mathbf{S}_5 \times \mathbf{S}_2 \right)
$$

$$
+ \left((\boldsymbol{a}_2 - \boldsymbol{a}_1) \cdot \mathbf{e}_L \right)^2 (\boldsymbol{a}_2 \cdot \mathbf{e}_1^*)(\boldsymbol{a}_2 \cdot \mathbf{e}_2^*)
$$

$$
\times \left(\frac{\hat{\mathbf{S}}_5 - \hat{\mathbf{S}}_4}{2} - i \mathbf{S}_5 \times \mathbf{S}_4 \right) \cdot \left(\frac{\hat{\mathbf{S}}_2 - \hat{\mathbf{S}}_0}{2} - i \mathbf{S}_2 \times \mathbf{S}_0 \right) \Bigg].
\tag{81}
$$

Now, the total contribution to $\hat{C}_2 \hat{B}_1$ in Eq. (74) is obtained by translating the motif shown in Fig. 10 by all integer multiples of the lattice vectors $\boldsymbol{a}_1$ and $\boldsymbol{a}_2$ and adding the sum of Eq. (78, 79, 80 and 81) for that motif. The resulting expression is a function of three polarizations $\mathbf{e}_L$, $\mathbf{e}_1^*$ and $\mathbf{e}_2^*$ of the form $(\mathbf{e}_L \cdot \boldsymbol{\mu}')^2 (\mathbf{e}_1^* \cdot \boldsymbol{\mu})(\mathbf{e}_2^* \cdot \boldsymbol{\mu})$. To isolate the scalar spin chirality, one must take linear combinations of the above terms for different directions of polarizations, and write them in terms of irreducible representations of the crystalline point group of the triangular lattice.

We focus on the imaginary part of $\langle \hat{a}_{d_2}(0) \hat{a}_{d_1}(0) \rangle_{\text{out}}$ here. We get scalar spin chirality operators in the following channel (invariant under rotations but odd under reflection, termed A_{2g} in Ref. [24]):

$$
\left[(e_1^x)^* (e_2^y)^* + (e_2^x)^* (e_1^y)^* \right] \left[(e_L^x)^2 - (e_L^y)^2 \right]
$$

$$
- \left[(e_1^x)^* (e_2^x)^* - (e_1^y)^* (e_2^y)^* \right] (2 e_L^x e_L^y).
\tag{82}
$$

In this channel,

$$
\text{Im}\, \langle \hat{a}_{d_2}(0) \hat{a}_{d_1}(0) \rangle_{\text{out}} = \frac{\sqrt{3} g_L^2 g^2 \mathtt{K}_1 \mathtt{K}_2 \mathtt{t}^4}{2(\omega_L - U)^2}
$$

$$
\tag{83}
$$

Here, we have used the notation $= \hat{\mathbf{S}}_{\mathbf{r}} \cdot \left(\hat{\mathbf{S}}_{\mathbf{r}+\boldsymbol{a}_1} \times \hat{\mathbf{S}}_{\mathbf{r}+\boldsymbol{a}_2} \right)$. g_L and g are light-matter couplings defined in Sec. IV A and $\mathtt{K}_1$ and $\mathtt{K}_2$ are constants related to detector efficiency and photonic density of states, defined in Eq. (13).

Generically, in a chiral spin liquid, the above expectation value will be nonzero. Hence, the above protocol can serve as an experimental scheme to detect a chiral spin liquid.

VIII. APPLICATION II: USING $G^{(2)}$ TO DETECT FRACTIONAL STATISTICS

In this section, we will show that if the ground state of the spin sector is topologically ordered, the existence of anyonic excitations with fractional mutual statistics can be detected using $G^{(2)}_{d_1, d_2}$. For this, we will show that the arguments of Ref. [46, 47] for pump-probe susceptibility can also be adapted for $G^{(2)}_{d_1, d_2}$.

Before we perform the analysis for topological excitations, we should make sure that there is a way to experimentally subtract off any contribution from topologically trivial non-interacting excitations. One subtraction scheme is the "connected" $\mathcal{G}^{(2)}$ correlator defined in Eq. (18), i.e., $\mathcal{G}^{(2)}_{d_1, d_2}(\tau) \equiv G^{(2)}_{d_1, d_2}(\tau) - G^{(1)}_{d_1}(0) G^{(1)}_{d_2}(0)$.

We would like this correlator to be unaffected by free bosonic excitations and to be dominated by (1) interactions between excitations and (2) fractional statistics (if any). But is that really so? In fact, for a general filter function, the connected $\mathcal{G}^{(2)}_{d_1, d_2}(\tau)$ can still be nonzero even for noninteracting magnons. However, we will show below that this contribution can be made 0 provided (1) the polarization symmetry channels for the two detectors are different and (2) frequency filters are sharp and centred away from the laser frequency ω_L.

A. Noninteracting magnons

The low energy Hamiltonian of the Hubbard model at half-filling, when projected to the spin sector is the Heisenberg model:

$$\hat{H}_{\text{Heisenberg}} = \frac{1}{2} \sum_{\mathbf{r},\mathbf{r}'} J_{\mathbf{r}\mathbf{r}'} \hat{\mathbf{S}}_{\mathbf{r}} \cdot \hat{\mathbf{S}}_{\mathbf{r}'}, \qquad (84)$$

where $J_{\mathbf{r}\mathbf{r}'} = 4\mathsf{t}_{\mathbf{r}\mathbf{r}'}^2/U$. Depending on the lattice geometry and the values of couplings beyond nearest neighbor and next nearest couplings, the Heisenberg model is believed to admit a variety of ground states – both ordered states and spin liquids. In this subsection, we consider the case when the ground state is ordered and the excitations are magnons. If one ignores magnon-magnon interactions, then the low energy Hamiltonian is (assuming the ground state energy is 0)

$$\hat{H}_{\text{low}} = \sum_{\mathbf{k}} \varepsilon_{\mathbf{k}} \hat{b}_{\mathbf{k}}^{\dagger} \hat{b}_{\mathbf{k}}. \qquad (85)$$

Here, $\hat{b}_{\mathbf{k}}^{\dagger}$ creates a magnon carrying momentum $\mathbf{k}$ and is generally a superposition of $\hat{S}_{\mathbf{k}}^{+}$ and $\hat{S}_{\mathbf{k}}^{-}$, where $\hat{S}_{\mathbf{k}}^{\pm} = \hat{S}_{\mathbf{k}}^{x} \pm i\hat{S}_{\mathbf{k}}^{y}$. This low energy Hamiltonian and the dispersion $\varepsilon_{\mathbf{k}}$ can be derived from the Heisenberg model by a standard linearized Holstein-Primakoff transformation followed by a Bogoliubov rotation [99, 100]. Recall that the spin sector operators entering photonic correlation functions are $\hat{A}_j$ given in Eq. (53). As discussed in Sec. V A, $\hat{A}_j$ can be decomposed into the irreducible representations of the crystalline point symmetry group. In this section, we will assume that this decomposition has been done (by taking linear combinations of experimental data for various directions of polarization) and $\hat{A}_j$ is in one such representation. We now rewriting $\hat{A}_j$ in terms of magnon operators. Up to second order in magnon operators, we have (in the interaction picture)

$$\hat{A}_j(-t) = \sum_{\mathbf{k};k_x \geq 0} \Big\{ \alpha_j(\mathbf{k}) e^{-2i\varepsilon_{\mathbf{k}}t} \hat{b}_{\mathbf{k}}^{\dagger} \hat{b}_{-\mathbf{k}}^{\dagger}$$
$$+ (\alpha'_j(\mathbf{k}))^* \hat{b}_{\mathbf{k}} \hat{b}_{-\mathbf{k}} e^{2i\varepsilon_{\mathbf{k}}t} \qquad (86)$$
$$+ \beta_j(\mathbf{k}) \left(\hat{b}_{\mathbf{k}}^{\dagger} \hat{b}_{\mathbf{k}} + \hat{b}_{-\mathbf{k}}^{\dagger} \hat{b}_{-\mathbf{k}} + 1 \right) \Big\},$$

where the coefficients $\alpha_j(\mathbf{k})$, $\alpha'_j(\mathbf{k})$ and $\beta_j(\mathbf{k})$ are determined by the Bogoliubov rotation performed in order to arrive at Eq. (85). By design, they are irreducible representations of the crystalline point symmetry group, and the vector (formed by coefficients at diferent momenta) for two distinct channels are orthogonal.

Let us work at zero temperature, i.e., the spin system is initially in its ground state. We define the Raman shift $\Omega_j \equiv \omega_L - \omega_j$. Using Eq. (58), we see that the Raman intensity $G^{(1)}$ detected in channel j for a Lorentzian filter (Eq. (12)) is given by

$$G_{d_j}^{(1)}(0) = |\mathsf{K}_j|^2 \sum_{\mathbf{k}} \frac{\Gamma_j^2 |\alpha_j(\mathbf{k})|^2}{\Gamma_j^2 + (\Omega_j - 2\varepsilon_{\mathbf{k}})^2}. \qquad (87)$$

So the photon emission can create a magnon pair, and $G^{(1)}(0)$ gets contributions from all magnon pair creations whose energy $2\varepsilon_{\mathbf{k}}$ is equal to the Raman shift Ω_j within an uncertainty Γ_j set by the frequency filter. Note that in the above equation, we have a discrete sum over momenta, where the number of terms is determined by the number of lattice sites N irradiated by the laser beam.

Let us look at the limits $\Gamma_j \to \infty$ (broad filter) and $\Gamma_j \to 0$ (sharp filter):

$$G_{d_j}^{(1)}(0) \xrightarrow{\Gamma_j \to \infty} N\mathsf{a}^2 |\mathsf{K}_j|^2 \int_{\text{B.Z.}} \frac{d^2k}{(2\pi)^2} |\alpha_j(\mathbf{k})|^2, \qquad (88)$$

where B.Z. stands for the first Brillouin zone of the lattice.

$$G_{d_j}^{(1)}(0) \xrightarrow{\Gamma_j \to 0} N\Gamma_j \mathsf{a}^2 |\mathsf{K}_j|^2 \int_{\text{B.Z.}} \frac{d^2k}{4\pi} \delta(2\varepsilon_{\mathbf{k}} - \Omega_j) |\alpha_j(\mathbf{k})|^2, \qquad (89)$$

and is thus the density of states of magnon pairs (of zero total momentum) at Ω_j, modulated by $|\alpha_j(\mathbf{k})|^2$. Note that in the sharp filter limit, Γ_j should not be made smaller than the level-spacing of magnons, which is $1/\sqrt{N}$ for linear dispersion, and $1/N$ for quadratic dispersion. Thus, $\Gamma_j N$ should remain nonzero even in the limit $\Gamma_j \to 0$.

Let us now come to $G_{d_1,d_2}^{(2)}(\tau)$. Recall that for a Lorentzian filter, it is given by

$$\mathcal{G}_{d_1,d_2}^{(2)}(\tau) = |\mathsf{K}_1 \mathsf{K}_2 \Gamma_1 \Gamma_2|^2 \iiiint_0^{\infty} dt_1\, dt_2\, dt_1'\, dt_2'$$
$$\times \Big\{ e^{-[\Gamma_1(t_1+t_1')+\Gamma_2(t_2+t_2')]} e^{i[\Omega_1(t_1-t_1')+\Omega_2(t_2-t_2')]}$$
$$\times \Big(\Big\langle \bar{\mathbb{T}} \left[\hat{A}_1^{\dagger}(-t_1') \hat{A}_2^{\dagger}(\tau-t_2') \right] \mathbb{T} \left[\hat{A}_2(\tau-t_2) \hat{A}_1(-t_1) \right] \Big\rangle_0$$
$$- \Big\langle \hat{A}_1^{\dagger}(-t_1') \hat{A}_1(-t_1) \Big\rangle_0 \Big\langle \hat{A}_2^{\dagger}(-t_2') \hat{A}_2(-t_2) \Big\rangle_0 \Big) \Big\}. \qquad (90)$$

Starting from the ground state of the spin system, the right-most operator (corresponding to the earliest photon emission) first creates a magnon pair. For $G_{d_1,d_2}^{(2)}$ to factorize, we want the emission of the next photon to correspond to the creation of an independent magnon pair, as opposed to destruction of the earlier created magnon pair. To ensure this, $\hat{A}_1$ and $\hat{A}_2$ should be in different symmetry channels so that by the orthogonality relations, if $\hat{A}_1$ creates a magnon pair, only $\hat{A}_1^{\dagger}$ can annihilate it and $\hat{A}_2$ cannot. With this condition imposed, the contributions to the connected $\mathcal{G}_{d_1,d_2}^{(2)}$ are the following. First, let us suppose $\hat{A}_1$ and $\hat{A}_2$ each create a magnon pair of different momenta, and then both magnon pairs are destroyed by $\hat{A}_1^{\dagger}$ and $\hat{A}_2^{\dagger}$ respectively. The term resulting from this process factorizes as $G_{d_1}^{(1)}(0)G_{d_2}^{(1)}(0)$. However if the momenta are the same, then it does not factorize, since $\langle 0|(\hat{b}_{\mathbf{k}}\hat{b}_{-\mathbf{k}})^2(\hat{b}_{\mathbf{k}}^{\dagger}\hat{b}_{-\mathbf{k}}^{\dagger})^2|0\rangle - \langle 0|\hat{b}_{\mathbf{k}}\hat{b}_{-\mathbf{k}}\hat{b}_{\mathbf{k}}^{\dagger}\hat{b}_{-\mathbf{k}}^{\dagger}|0\rangle = 3$, where $|0\rangle$ is a state with no magnons. For this non-cancellation to occur, both emitted photons should have the same frequency.

The second contribution to the connected $\mathcal{G}^{(2)}_{d_1,d_2}$ is when $\hat{A}_1$ creates a magnon pair, but $\hat{A}_2$ instead of creating an additional pair, simply elastically scatters off it [via the term $\beta_2(\mathbf{k})\left(\hat{b}^\dagger_\mathbf{k}\hat{b}_\mathbf{k} + \hat{b}^\dagger_{-\mathbf{k}}\hat{b}_{-\mathbf{k}} + 1\right)$]. The sum of these two contributions is generically nonzero and can potentially mask nontrivial topological contributions. To avoid this, the frequency filter functions for both detectors need to be sharp. This allows one to (1) filter out the case when the two magnon pairs created are identical by demanding that the frequencies of the detected photons are different, and (2) filter out elastic scattering (i.e., impose $\omega_1 \neq \omega_L$ and $\omega_2 \neq \omega_L$).

Under these conditions, the connected $G^{(2)}$ is zero for noninteracting bosonic excitations.

B. Anyonic excitations: Singularity from fractional statistics

As shown previously, the detection of a photon by detector d_j corresponds to the application of operator $\hat{A}_j$, (defined in Eq. (53)) on the material. As long as $\hat{A}_j$ does not commute with the Hamiltonian, $\hat{A}_j$ acting on the ground state will create excitations. If the material is topologically ordered, its excitations can be anyonic. We assume that the material is at zero temperature. Now, if $|I\rangle$ is the ground state, then $\hat{A}_j|I\rangle$ would generically have an overlap with a state consisting of an anyon pair, unless this is ruled out by symmetry. We will therefore suppose that $\hat{A}_1$ and $\hat{A}_2$ create pairs of anyons whose energy gaps are Δ_1 and Δ_2 respectively. For concreteness, if the ground state is a $\mathbb{Z}_2$ spin liquid, one can think of $\hat{A}_1$ and $\hat{A}_2$ as creating e and m anyon pairs respectively. These pairs get annihilated by $\hat{A}^\dagger_1$ and $\hat{A}^\dagger_2$ respectively [101]. We point out that Δ_1 and Δ_2 are the gaps within the spin sector and are much smaller than the optical gap U.

Eq. (90) for the connected $\mathcal{G}^{(2)}$ gets contributions from different worldlines of anyons obeying the constraint that the pair created at time $-t_1$ is annihilated at time $-t'_1$, and similarly the pair created at $\tau - t_2$ is annihilated at $\tau - t'_2$. Among these are those worldlines where one anyon *braids* nontrivially with another. Such paths come with an extra braiding phase. Ref. [46, 47] showed that this extra phase leads to a singularity in a certain pump-probe susceptibility – a 4-point correlator similar to $G^{(2)}$ but with a different temporal contour. In this section, we show that nontrivial mutual statistics leads to a singularity in the connected $\mathcal{G}^{(2)}$ as well: $\mathcal{G}^{(2)}_{d_1,d_2}(\Omega_1,\Omega_2) \sim \theta(\Omega_1 - \Delta_1)\theta(\Omega_2 - \Delta_2)\left[K_2(\Omega_2)(\Omega_1 - \Delta_1)^{-3/2} + (1 \leftrightarrow 2)\right]$, where $K_j(\Omega_j)$ are system-specific functions (recall that $\Omega_j = \omega_L - \omega_j$). In the limit of sharp frequency filters, we expect the dependence of $G^{(2)}$ on τ to drop out. Hence, we have set $\tau = 0$.

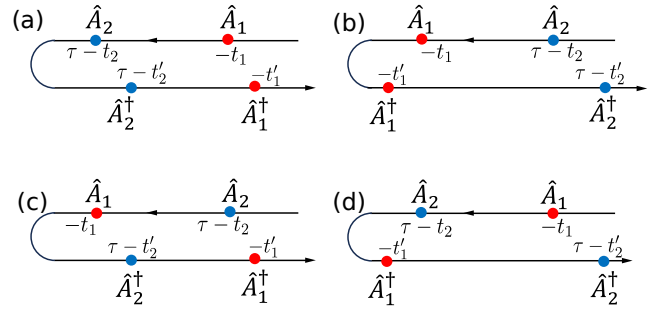We adapt the geometric argument in Ref. [46, 47] to show the above result. There are two main changes in

Figure 11. Four operator orderings in Eq. (90): **(a)**: $\tau - t_2 > -t_1$ and $\tau - t'_2 > -t'_1$, **(b)**: $-t_1 > \tau - t_2$ and $-t'_1 > \tau - t'_2$, **(c)**: $-t_1 > \tau - t_2$ and $\tau - t'_2 > -t'_1$, and **(d)**: $\tau - t_2 > -t_1$ and $-t'_1 > \tau - t'_2$.

our case. Firstly, the operators $\hat{A}_j$ can also contain terms that do not create any excitations, thereby leading to elastic scattering. We explained the conditions under which such contributions can be ruled out in Sec. VIII A. Secondly, since we are also frequency-filtering the first detected photon, $-t_1 \neq -t'_1$, i.e., the time of creation and annihilation respectively of the corresponding anyon pair are not equal.

The spin correlator extracted from $\mathcal{G}^{(2)}$, i.e., Eq. (90) is a sum of terms with four different operator orderings depending on the ordering within the pairs $(-t_1, -t'_1)$, and $(-t_2, -t'_2)$. These orderings are (suppressing the time arguments): $\langle \hat{A}^\dagger_1 \hat{A}^\dagger_2 \hat{A}_2 \hat{A}_1 \rangle$, $\langle \hat{A}^\dagger_2 \hat{A}^\dagger_1 \hat{A}_1 \hat{A}_2 \rangle$, $\langle \hat{A}^\dagger_1 \hat{A}^\dagger_2 \hat{A}_1 \hat{A}_2 \rangle$, and $\langle \hat{A}^\dagger_2 \hat{A}^\dagger_1 \hat{A}_2 \hat{A}_1 \rangle$ [Fig. 11 (a), (b), (c), (d) respectively].

First, let us consider the operator ordering in Fig. 11(a), i.e., $\langle \hat{A}^\dagger_1(-t'_1)\hat{A}^\dagger_2(-t'_2)\hat{A}_2(-t_2)\hat{A}_1(-t_1)\rangle$. In this correlator, first $\hat{A}_1$ and then $\hat{A}_2$ each create anyon pairs at time $-t_1$ and $-t_2$ respectively (shown as red and blue respectively in Fig. 12). The blue pair gets destroyed by $\hat{A}^\dagger_2$ at time $-t'_2$, and lastly, at time $-t'_1$, the red anyon pair gets destroyed by $\hat{A}^\dagger_1$. If one ignores anyon-anyon interactions, as shown in Sec. VIII A, the contributions from worldlines without any braiding get canceled when we look at the connected $\mathcal{G}^{(2)}$. Furthermore, the argument in Ref. [47] about the contribution from short-ranged interactions being less singular than the contribution from fractional statistics also applies in our setting. Therefore, we will only study worldlines involving nontrivial braiding of otherwise "non-interacting" anyons. Each such worldline contributes a topological factor of $(1 - \cos\alpha_{12})$ where $e^{i\alpha_{12}}$ is the braiding phase of a blue anyon going around the red one.

The connected part can be written as a path integral over all trajectories where the blue anyon pair braids around one of the red anyons. Recall that here, $t_1 - t_2 > 0$, and $t'_1 - t'_2 > 0$, but the orderings within the pairs (t_1, t'_1), and (t_2, t'_2) are left unspecified. For the recombination of the second (blue) anyon pair between t_2 and t'_2, just ballistic propagation is not enough
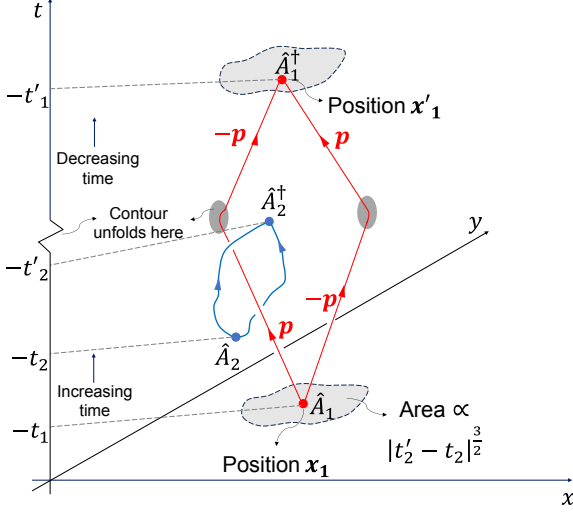
Figure 12. This figure is similar to Fig. 1 of Ref. [47], except the backward propagation is unfolded here. Without loss of generality, in this figure, $t_2 > t'_2$. In our time axis, from $-t'_2$, onwards, time decreases in the upward direction. For the operator ordering in Fig. 11(a), we depict a history of anyons that contributes to the connected $\mathcal{G}^{(2)}$. At time $-t_1$, operator $\hat{A}_1$ creates an anyon pair (red) at spatial point $\mathbf{x}_1$. Since $\hat{A}_1$ is a zero-momentum operator, $\mathbf{x}_1$ is integrated over the whole area of irradiation. At time $-t_2$, operator $\hat{A}_2$ (blue) creates a second anyon pair that recombines at $-t'_2$ due to wavepacket spreading. Let us consider a fixed worldline loop of the second pair. A path integral over all possible histories of the red anyons is dominated by those trajectories where a red anyon ballistically propagates through the blue loop till time $-t'_2$, and then turns around to recombine at time $-t'_1$. For a fixed momentum $\mathbf{p}$ of the red anyon, it has been shown geometrically that $\mathbf{x}_1$ can only be from within an area $\sim |t'_2 - t_2|^{3/2}$ [47]. Since $-t'_1$ and $-t_1$ are not necessarily equal, classically, the red anyons will not recombine if they exactly retrace their path during backward propagation. However, due to quantum wavepacket spreading, there is a nonzero amplitude of recombination, which we conjecture to be independent of t_2 and t'_2.

and wavepacket spreading is necessary (see Fig. 12). The amplitude of recombination of the blue pair by quantum wave-packet spreading is $\sim |t_2 - t'_2|^{-d/2}$ where spatial dimension $d = 2$.

To study the first (red) anyon pair, following Ref. [46, 47], one can do a semiclassical analysis in the limit where the time it takes for an anyon pair to recombine is much less than the time difference between creating the first and second anyon pairs, i.e., $|t_1 - t_2| \gg |t_2 - t'_2|$, $|t'_1 - t'_2| \gg |t_2 - t'_2|$, and $|t'_1 - t'_2| \gg |t_1 - t'_1|$. In principle, we also need to evaluate correlators outside this limit, since t_j and t'_j are integrated over. But as a first approximation, we obtain the correlator by extrapolating the expressions found in this limit.

The path integral is then dominated by those trajectories where one anyon from the red pair propagates ballistically with momentum $\mathbf{p}$ and passes through the closed

worldline of the blue anyon pair [46, 47]. At time $-t'_2$, the red anyons turn around to recombine at time $-t'_1$ (here, $\mathbf{p}$ is integrated over). One such trajectory is shown in Fig. 12. It was shown in Ref. [46, 47] that for a fixed momentum $\mathbf{p}$ of a red anyon, it can braid through the blue pair only if its starting location $\mathbf{x}_1$, i.e., the spatial position of creation of the red anyon pair, belongs to an area that scales as $\sim |t'_2 - t_2|^{3/2} F_1(p)$. Computing the function $F_1(p)$ is beyond the scope of this work, and its specific form is not important for our results. Combining all the factors, the overall amplitude for braiding scales as $\sim (1 - \cos\alpha_{12})|t_2 - t'_2|^{1/2} F_1(p) e^{i\Delta_2(t'_2 - t_2)}$.

One caveat in our case is that since $t'_1 \neq t_1$, we need to consider wavepacket spreading even in the red anyon pair to ensure recombination after backward propagation. We conjecture that this recombination amplitude only depends on $(t_1 - t'_1)$, and is independent of t_2 or t'_2. We present a semiclassical argument for this. The center of mass position of the red anyon pair should remain unchanged at the saddle point level, because the blue pair does not impart center of mass momentum to the red pair. If we consider the two red anyons to be moving with equal and opposite momenta $\mathbf{p}$ and $-\mathbf{p}$, each momentum $\mathbf{p}$ contributes an amplitude $e^{i(\frac{p^2}{m_1} + \Delta_1)(t'_1 - t_1)}$ towards recombination, where m_1 is the effective mass of a red anyon. This factor is independent of t_2 and t'_2. Combining all the above factors, we get

$$
\begin{aligned}
\sim &(1 - \cos\alpha_{12})|t_2 - t'_2|^{1/2} e^{i\left(\frac{p^2}{m_1} + \Delta_1\right)(t'_1 - t_1)} F_1(p) \\
&\times e^{i\Delta_2(t'_2 - t_2)}
\end{aligned} \quad (91)
$$

While the geometric argument captures the scaling $|t_2 - t'_2|^{1/2}$, it does not capture a phase jump $e^{i\frac{\pi}{4}\text{sign}(t_2 - t'_2)}$ when t_2 and t'_2 are exchanged. The phase jump is important to capture the Heaviside step functions $\theta(\Omega_1 - \Delta_1)\theta(\Omega_2 - \Delta_2)$ in our final result. Fixing the phase requires knowing what happens when $t_2 - t'_2$ is close to zero, but this regime is beyond the scope of the scaling argument. We get around this difficulty by an analyticity argument. For this, it is convenient to consider the correlator $\left\langle \hat{A}_1^\dagger(-t'_1)\hat{A}_2^\dagger(-t'_2)\hat{A}_2(-t_2)\hat{A}_1(-t_1) \right\rangle$ as an analytic continuation of a Euclidean-time correlation function. We analytic continue:

$$
t_j \to t_j + i\epsilon_j \equiv iu_j \text{ and } t'_j \to t'_j + i\epsilon'_j \equiv iu'_2, \quad (92)
$$

such that $0 < \epsilon_1 < \epsilon_2 < \epsilon'_2 < \epsilon'_1 \to 0^+$. This order of limits is required because a zero temperature correlation function $\left\langle \hat{P}_1(-iu_n)\hat{P}_2(-iu_{n-1})\dots\hat{P}_n(-iu_1) \right\rangle$ is well-defined only if the operators are time-ordered w.r.t. the arguments $\text{Re}\,u_n, \text{Re}\,u_{n-1}, \dots, \text{Re}\,u_1$, i.e., if $\text{Re}\,u_n > \text{Re}\,u_{n-1} > \dots \text{Re}\,u_1$. Here, we use the convention $\hat{P}_n(-iu_n) \equiv e^{u_n\hat{H}_0}\hat{P}_n e^{-u_n\hat{H}_0}$. Now, we know that the correlation function we are computing here is an analytic function of u_2 and u'_2 when $\text{Re}\,u'_2 > \text{Re}\,u_2$, i.e., $\epsilon'_2 > \epsilon_2$.

The factor of $\sim |t_2 - t_2'|^{1/2}$ obtained above should thus be replaced by $(u_2' - u_2)^{1/2}$, such that the branch-cut is in the unphysical region where $\mathrm{Re}(u_2' - u_2) < 0$. This method is agnostic to the ordering between real times t_2 and t_2'.

$$
\begin{aligned}
&\left\langle \hat{A}_1^\dagger(-iu_1') \hat{A}_2^\dagger(-iu_2') \hat{A}_2(-iu_2) \hat{A}_1(-iu_1) \right\rangle \\
&\sim N\mathsf{a}^2 (1 - \cos\alpha_{12}) e^{-\Delta_1(u_1' - u_1) - \Delta_2(u_2' - u_2)} \\
&\times (u_2' - u_2)^{1/2} \int \frac{\mathrm{d}^2 p}{(2\pi)^2} e^{-\frac{p^2}{m_1}(u_1' - u_1)} F_1(p).
\end{aligned}
\tag{93}
$$

Analytic continuing back to real-time, while maintaining $\mathrm{Re}(u_1' - u_1) > 0$ and $\mathrm{Re}(u_2' - u_2) > 0$, we get

$$
\begin{aligned}
&\left\langle \hat{A}_1^\dagger(-t_1') \hat{A}_2^\dagger(-t_2') \hat{A}_2(-t_2) \hat{A}_1(-t_1) \right\rangle \\
&\sim N\mathsf{a}^2 |t_2 - t_2'|^{1/2} e^{i\frac{\pi}{4}\mathrm{sign}(t_2 - t_2')} e^{i\Delta_2(t_2' - t_2 + i0^+)} \\
&\times (1 - \cos\alpha_{12}) \int \frac{\mathrm{d}^2 p}{(2\pi)^2} e^{i\left(\frac{p^2}{m_1} + \Delta_1\right)(t_1' - t_1 + i0^+)} F_1(p),
\end{aligned}
\tag{94}
$$

If we insert the above expression into Eq. (90), and perform the Fourier transform, we obtain that the contribution of the contour in Fig. 11(a) to the connected $\mathcal{G}^{(2)}$ is $\theta(\Omega_1 - \Delta_1)\theta(\Omega_2 - \Delta_2) K_1(\Omega_1)(\Omega_2 - \Delta_2)^{-3/2}$. Here, $K_1(\Omega_1)$ is a function obtained by integrating over momenta $\mathbf{p}$ of the red anyon and performing the Fourier-transform w.r.t. $t_1' - t_1$. One can now observe that the result for the contour in Fig. 11(b) can be obtained by swapping the roles of the red and blue anyons in the above calculation. The resulting contribution is $\theta(\Omega_1 - \Delta_1)\theta(\Omega_2 - \Delta_2) K_2(\Omega_2)(\Omega_1 - \Delta_1)^{-3/2}$.

Now, consider the contour in Fig. 11(c). Here, the blue anyon pair is created before the red pair is created and also annihilated before the red pair is annihilated. In this case, neither anyon can be treated ballistically. Even if one tries to naïvely apply the semiclassical argument from Ref. [46, 47], the location of creation of the red anyon pair is drawn from an area scaling as $(u_2' - u_1)(u_2' - u_2)^{1/2}$. This area is smaller than the factor $(u_2' - u_2)^{3/2}$ we found for the contour in Fig. 11(a). Thus, the resulting contribution to the connected $\mathcal{G}^{(2)}$ from Fig. 11(c) should also be less singular than that from Fig. 11(a). For the same reason, the contribution from Fig. 11(d) is also less singular. Therefore, our final estimate for the singular part of $\mathcal{G}^{(2)}$ is

$$
\begin{aligned}
\mathcal{G}^{(2)}_{d_1, d_2}(\Omega_1, \Omega_2) &\sim \theta(\Omega_1 - \Delta_1)\theta(\Omega_2 - \Delta_2) \\
&\times \left[K_2(\Omega_2)(\Omega_1 - \Delta_1)^{-3/2} + (1 \leftrightarrow 2) \right].
\end{aligned}
\tag{95}
$$

Thus, our result can serve as a test to detect fractional statistics in a spin system by measuring correlations between photons scattered off it. We note that the derivation of Eq. (95) involved an assumption that the extent of wavepacket spreading of the first anyon pair is independent of the time at which the second pair was created, as long as the two creation events are sufficiently spaced apart temporally. This assumption should be examined more carefully in future work.

1. Alternative protocol – hybrid filtering

We now suggest an alternative filtering protocol (compared to what we proposed above) for using $\mathcal{G}^{(2)}$ to detect fractional statistics. Instead of both filters being spectrally sharp, let us suppose the first detector is spectrally broad (hence temporally sharp), and the second detector is spectrally sharp. In this case, t_1 and t_1' are both 0. Thus, the above assumption used in the previous protocol is no longer needed. We would then expect a similar $(\Omega_2 - \Delta_2)^{-3/2}$ singularity in the limit of large τ, i.e., time delay between detection of the two photons. However, to make this claim precise, one must rule out any contributions from topologically trivial excitations (discussed in Sec. VIII A) that are equally or more singular. This is a direction for future work.

IX. DISCUSSION

We have demonstrated in this work that useful information about a many-body system can be extracted from correlations between photons scattered off it. We have developed a general formalism for mapping photonic correlators to electronic ones in an insulator, emphasizing the role of frequency filtering in determining this map. In particular, we considered the electronic system to be a single-band Hubbard model at half-filling. In the frequency window around the laser frequency ω_L, two-photon correlations can be used to measure dynamical correlators within the spin sector. On the other hand, if one photon is detected around a frequency $2\omega_L - U$ and the other around U, the photonic correlators probe the dynamics of a single doublon-hole pair conditioned on the application of spin operators nearby. As an application, we have shown that the static expectation value of scalar spin chirality can be measured on the kagome and triangular lattices using first and second order homodyne measurements respectively. Next, we showed that if the insulator is a spin liquid with anyonic excitations, the $G^{(2)}$ correlator in the sharp frequency filtering limit shows a well-defined singularity as a function of frequencies. To show this, we made a physically motivated assumption that the extents of wavepacket spreading in two anyons are independent of each other.

As remarked in Sec. IV, usually the starting lattice Hamiltonian for the material is obtained after projecting to a subset of the microscopic bands. The specific form of the light-matter interaction depends on the details of the projection. While our formalism for mapping photonic to electronic correlators is general, the specific form of operator in Eq. (54) should be reworked for any given microscopic model.

Since we are dealing with correlated systems, even if the microscopic Hamiltonian is given, the ground state is not a priori obvious (what symmetries it spontaneously breaks, whether it is a spin liquid, and so on). Our mapping between photonic and electronic correlators depends only on the microscopic Hamiltonian and is agnostic to the ansatz used for describing its ground state and excitations. It is an interesting direction to calculate these correlators for specific ansatzes of the ground state. For one dimensional systems, one can use tensor network methods. In two dimensions, controlled calculations are challenging, but uncontrolled calculations using parton construction might still provide useful predictions.

Understanding the dynamics of a single doublon-hole pair created on top of a state in the spin sector is a highly challenging problem. This problem can be a starting point to understand Mott insulators at nonzero doping. Calculating our correlators and checking them against experiment can serve as a useful testbed for the various theories proposed to solve the problem [102]. Another class of problems involving interesting interplay of charge and spin dynamics is that of Mott insulators close to the Mott transition, i.e., when $\mathtt{t}/U$ is order 1 [103]. In this limits, transitions between neutral chiral spin liquids and quantum Hall states have been predicted [104, 105]. It is interesting to ask if measuring our correlators could shed light on such transitions.

In our work, we focused on dynamical correlation functions of zero momentum operators. However, in the absence of strong Coulomb binding in photo-excited electron-hole pairs, the dipole approximation can be violated for itinerant electrons, and photon momentum and angular momentum can be imparted to electrons [106, 107]. Moreover, given the recent development of near-field spectroscopy [108], it is intriguing to explore spatially and spectrally resolved correlations. This question may be especially relevant today in the context of moiré materials which come with a much enlarged lattice spacing.

ACKNOWLEDGMENTS

Appendix A: Review on $\hat{\mathcal{T}}$-matrix formalism

In this appendix, we review scattering theory using the $\hat{\mathcal{T}}$-matrix formalism. This review is loosely based on Chapter 3 of Ref. [92]. The key takeaway from this appendix is Eq. (5) which serves as a generalization of Fermi's Golden Rule that works to all orders in perturbation theory.

Consider a Hamiltonian

$$\hat{H} = \hat{H}_0 + \hat{V}. \tag{A1}$$

For concreteness, one can imagine $\hat{H}_0$ to be the full Hamiltonian of light and matter separately, and $\hat{V}$ is the light-matter interaction. But this formalism is applicable to any quantum scattering problem. At time $-T/2$, we start with a state $|\Psi(t = -T/2)\rangle$ in the full (light + matter) Hilbert Space. Around $t = 0$, light and matter are interacting, and the scattered light is observed at $t = T/2$. The final state is $|\Psi(t = T/2)\rangle \equiv e^{-i\hat{H}T} |\Psi(t = -T/2)\rangle$. We are interested in the limit when $T \to \infty$. The final state will have several terms with oscillating prefactors of the type $e^{i(E_m^0 - E_n^0)T}$ where E_m^0 and E_n^0 are the energy eigenstates of $\hat{H}_0$. But we are interested in the limit $T \gg 1/(\delta E_{\rm in})$, ($\delta E_{\rm in}$ being the uncertainty in energy of the initial state) where this terms are fast-oscillating and average out to 0. Therefore, it is useful to have a formalism that directly computes the time-evolved state with such fast-oscillating terms filtered away. This is what the $\hat{\mathcal{T}}$-matrix formalism does.

We define states $|{\rm in}\rangle$ and $|{\rm out}\rangle$ as follows:

$$|\Psi(t = -T/2)\rangle \equiv e^{-i\hat{H}_0(-T/2)} |{\rm in}\rangle \tag{A2}$$

$$\langle\Psi(t = T/2)| \equiv \langle{\rm out}| e^{i\hat{H}_0 T/2}. \tag{A3}$$

The purpose of this trick is to allow one to define Heisenberg operators in terms of the eigenstates of $\hat{H}_0$ with respect to time $t = 0$, which is a time when the photon wave-packet and the material are already interacting. So $|{\rm in}\rangle$ is defined as the initial state evolved forward in time till $t = 0$ by the noninteracting Hamiltonian $\hat{H}_0$. In this state, the laser wavepacket spatially overlaps with the material [Fig. 13(a)]. Similarly, $|{\rm out}\rangle$ is defined by evolving the final state backward in time till $t = 0$ by the noninteracting Hamiltonian $\hat{H}_0$ [Fig. 13(b)]. We suppose the state $|{\rm in}\rangle$ is a wave-packet with a narrow spread of energy w.r.t $\hat{H}_0$ such that the energy is centred around $E_{\rm in}^0$. A non-zero width in energy (momentum of photon) in the wavepacket is mandatory at time $-T/2$ because otherwise, the wavefunction of light would not be localized far away from the material as we want it to. Generically, a narrow wavepacket gets wider with time (in real space). Since light is relativistic (i.e., the magnitude of velocity of all the component waves of the wavepacket are equal, so the uncertainty in velocity comes solely in its direction), the velocity of this spreading is maximum in the direction perpendicular to the velocity of the centre of the wavepacket. This spreading velocity has magnitude $\sim c\frac{\sigma_p}{p}$ where p is the mean momentum of the wavepacket and σ_p is its uncertainty in momentum. For small enough $\frac{\sigma_p}{p}$, the spreading of the wavepacket fails to catch up with the centre itself. Therefore, in the rest of this section, we will ignore wavepacket spreading. (Similar reasoning can also be used to neglect wavepacket spreading in the case of a non-relativistic scatterer.)

Consider the state at time $t = 0$:

$$|\Gamma_-\rangle \equiv e^{-i\hat{H}T/2} e^{i\hat{H}_0 T/2} |{\rm in}\rangle. \tag{A4}$$

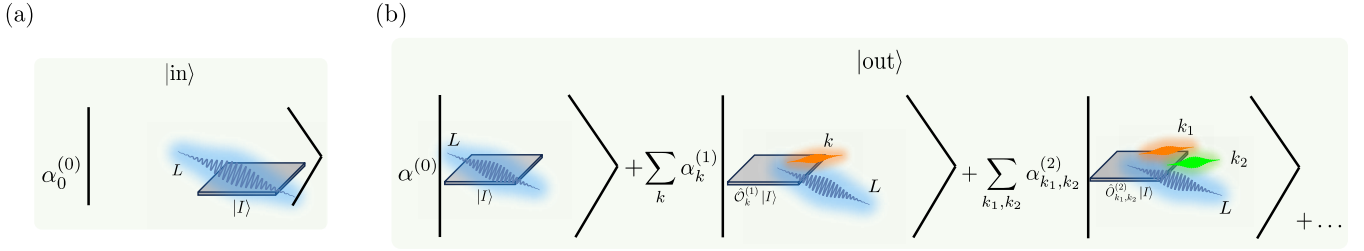Now, let us view $|\Gamma\rangle$ as a function of the initial time

Figure 13. **Fig. 3 in Interaction Picture**: Schematic depiction of (a) $|\text{in}\rangle \equiv e^{-i\hat{H}_0 T/2}|\Psi(t=-T/2)\rangle$ and (b) $|\text{out}\rangle \equiv e^{i\hat{H}_0 T/2}|\Psi(t=T/2)\rangle$. This is a mathematical trick used to bring all wavepackets to where it should have been at $t=0$, according to the noninteracting Hamiltonian $\hat{H}_0$. The states (a) and (b) are respectively obtained by evolving the initial and final states shown in Fig. 3(a) and 3(b) forward and backward respectively in time till $t=0$. States $|\text{in}\rangle$ and $|\text{out}\rangle$ are identical to Fig. 3(a) and (b) respectively, except that the light wavepackets have been shifted so as to be in the vicinity of the material. Further, upon doing so, the individual terms may have picked up additional phases $\alpha_k^{(1)}$ etc. (compared to the corresponding terms in Fig. 3) due to time-evolution.

$-T/2$. We rewrite the above expression by first differentiating w.r.t. t' (supposing $t'=-T/2$ in the above equation) and then integrating over t' from $-T/2$ to 0.

$$\partial_{t'}|\Gamma_-\rangle = ie^{i\hat{H}t'}\hat{V}e^{-i\hat{H}_0 t'}|\text{in}\rangle \tag{A5}$$

$$\implies |\Gamma_-\rangle = |\text{in}\rangle - i\int_{-T/2}^{0} dt'\, e^{i\hat{H}t'}\hat{V}e^{-i\hat{H}_0 t'}|\text{in}\rangle \tag{A6}$$

The advantage of rewriting $|\Gamma_-\rangle$ as above is that it makes it evident that $|\Gamma_-\rangle$ does not depend on $-T/2$ (as long as $-T/2$ is sufficiently negative). The reason is that $\hat{V}$ acting on $e^{-i\hat{H}_0 t'}|\text{in}\rangle$ returns 0 unless the wavepacket of the photon has some spatial overlap with the material. This observation is the key physics input in the $\hat{\mathcal{T}}$-matrix formalism. In the setting we are imagining, the light comes close to the material only around $t=-t_C<0$ for some time-scale $t_C \ll T/2$. Whatever happens before $-t_C$ does not contribute to the above equation. We will soon use this useful fact. Let's suppose

$$|\text{in}\rangle = \sum_j \phi_j^{\text{in}}|\Psi_j^0\rangle \text{ and } |\text{out}\rangle = \sum_j \phi_j^{\text{out}}|\Psi_j^0\rangle \tag{A7}$$

where $|\Psi_j^0\rangle$ is an eigenstate of $\hat{H}_0$ with energy E_j^0. We assume that the ϕ_j's are narrowly peaked around energy $E_{\text{in},0}$. Also inserting in Eq. (A6) a resolution of identity in terms of $|\Psi_J\rangle$ which are eigenstates of $\hat{H}$ with eigenvalue $\mathcal{E}_J$, i.e., $\sum_J |\Psi_J\rangle\langle\Psi_J|$, we get:

$$|\Gamma_-\rangle = |\text{in}\rangle - i\sum_j \phi_j^{\text{in}}\sum_J |\Psi_J\rangle\langle\Psi_J|\hat{V}|\Psi_j^0\rangle$$
$$\times \int_{-T/2}^{0} dt'\, e^{i(\mathcal{E}_J-E_j^0)t'}$$
$$= |\text{in}\rangle + \sum_j\sum_J |\Psi_J\rangle\langle\Psi_J|\hat{V}|\Psi_j^0\rangle\phi_j^{\text{in}} \tag{A8}$$
$$\times \frac{2\sin^2\left[\frac{(\mathcal{E}_J-E_j^0)T/2}{2}\right]+i\sin\left[(\mathcal{E}_J-E_j^0)T/2\right]}{E_j^0-\mathcal{E}_J}$$

Let us now make sense of the expression $\frac{2\sin^2((\mathcal{E}_J-E_j^0)T/4)+i\sin\left((\mathcal{E}_J-E_j^0)T/2\right)}{E_j^0-\mathcal{E}_J}$ that appears above. We suppose that $T/2 \gg \frac{1}{\delta E_{\text{in}}^0}$, (where δE_{in}^0 is the spread in E_{in}^0), i.e., $T/2$ is so large that as E_j^0 runs through the different eigen-components of the $|\text{in}\rangle$ states, the real part of the numerator goes through several cycles of the $\sin^2()$ function. We also suppose that $|E_j^0-\mathcal{E}_J| \gg \delta E_{\text{in}}^0$ (consequently $|E_j^0-\mathcal{E}_J| \gg 2/T$). Then the fluctuations in the numerator are much stronger than the fluctuations of the denominator. Hence, we can replace the real part of the numerator by its average which is $2 \times 1/2$. Thus, the real part of the expression is $1/(E_j^0-\mathcal{E}_J)$. But when $|E_j^0-\mathcal{E}_J| \ll 2/T$, we can see that the real part tends to 0. Hence the real part can be approximated by $\mathcal{P}\frac{1}{E_j^0-\mathcal{E}_J}$ for large $T/2$. Here, $\mathcal{P}$ stands for principal value and $\mathcal{P}\frac{1}{z}$ is defined as $\lim_{\eta\to 0}\frac{1}{2}\left(\frac{1}{z+i\eta}+\frac{1}{z-i\eta}\right)$. Next, we consider the imaginary part $-\frac{\sin\left((\mathcal{E}_J-E_j^0)T/2\right)}{\mathcal{E}_J-E_j^0}$. As $T/2$ increases, this function becomes more and more sharply peaked around $E_j^0-\mathcal{E}_J=0$. As $T/2\to\infty$, it becomes $-\pi\delta(E_j^0-\mathcal{E}_J)$. Thus, in Eq. (A8), we can make the following replacement

$$\frac{2\sin^2\left[\frac{(\mathcal{E}_J-E_j^0)T/2}{2}\right]+i\sin\left[(\mathcal{E}_J-E_j^0)T/2\right]}{E_j^0-\mathcal{E}_J}$$
$$\to \mathcal{P}\frac{1}{E_j^0-\mathcal{E}_J}-i\pi\delta(E_j^0-\mathcal{E}_J) \tag{A9}$$
$$= \lim_{\eta\to 0^+}\frac{1}{E_j^0-\mathcal{E}_J+i\eta}$$

This agrees with the intuition provided above that $|\Gamma_-\rangle$ should not depend on $T/2$ as long as it is sufficiently large. Thus, we get:

$$|\Gamma_-\rangle = \sum_j \phi_j^{\text{in}}\left(|\Psi_j^0\rangle + \frac{1}{E_j^0-\hat{H}+i0^+}\hat{V}|\Psi_j^0\rangle\right). \tag{A10}$$

Now, we need to evolve $|\Gamma_-\rangle$ forward in time till $t = T/2$ using $\hat{H}$. This is simple because $|\Psi_j^0\rangle + \frac{1}{E_j^0 - \hat{H} + i0^+}\hat{V}|\Psi_j^0\rangle$ is actually an eigenstate of $\hat{H}$ with eigenvalue E_j^0. To see this, if we replace $\hat{V}$ with $\hat{H} - \hat{H}_0$, then we get

$$
\begin{aligned}
&\left|\Psi_j^0\right\rangle + \frac{1}{E_j^0 - \hat{H} + i0^+}\hat{V}\left|\Psi_j^0\right\rangle \\
&= \lim_{\eta \to 0^+} \frac{i\eta}{E_j^0 - \hat{H} + i\eta}\left|\Psi_j^0\right\rangle \\
&= \lim_{\eta \to 0^+} \sum_J \frac{i\eta}{E_j^0 - \mathcal{E}_J + i\eta}\left|\Psi_J\right\rangle\left\langle\Psi_J|\Psi_j^0\right\rangle \quad \text{(A11)}
\end{aligned}
$$

We see that as we take the limit $\eta \to 0^+$, the only J's that survive are those with $\mathcal{E}_J = E_j^0$. Thus we get

$$
\begin{aligned}
&\left|\Psi_j^0\right\rangle + \frac{1}{E_j^0 - \hat{H} + i0^+}\hat{V}\left|\Psi_j^0\right\rangle \\
&= \sum_J \delta_{\mathcal{E}_J = E_j^0}\left|\Psi_J\right\rangle\left\langle\Psi_J|\Psi_j^0\right\rangle
\end{aligned}
\quad \text{(A12)}
$$

Therefore,

$$
\begin{aligned}
&e^{-i\hat{H}T/2}\left|\Gamma_-\right\rangle \\
&= \sum_j \phi_j^{\text{in}}\left\{e^{-iE_j^0 T/2}\left(\left|\Psi_j\right\rangle + \frac{1}{E_j^0 - \hat{H} + i0^+}\hat{V}\left|\Psi_j\right\rangle\right)\right\}
\end{aligned}
\quad \text{(A13)}
$$

Before proceeding, we make one more formal manipulation (in the style of Dyson equations):

$$
\begin{aligned}
&(E_j^0 - \hat{H} + i0^+)^{-1} \\
&= \left(E_j^0 - \hat{H}_0 + i0^+\right)^{-1}\left\{\hat{\mathbb{1}} + \hat{V}(E_j^0 - \hat{H} + i0^+)^{-1}\right\}
\end{aligned}
\quad \text{(A14)}
$$

Therefore,

$$
\begin{aligned}
&\frac{1}{E_j^0 - \hat{H} + i0^+}\hat{V} \\
&= \frac{1}{E_j^0 - \hat{H}_0 + i0^+}\left\{\hat{V} + \hat{V}\frac{1}{E_j^0 - \hat{H} + i0^+}\hat{V}\right\}.
\end{aligned}
\quad \text{(A15)}
$$

We now define the $\hat{\mathcal{T}}$-matrix as

$$
\begin{aligned}
\hat{\mathcal{T}} &\equiv \hat{V} + \hat{V}\frac{1}{E_{\text{in}}^0 - \hat{H} + i0^+}\hat{V} \\
&\equiv \hat{V} + \hat{V}\frac{1}{E_{\text{in}}^0 - \hat{H}_0 - \hat{V} + i0^+}\hat{V}
\end{aligned}
\quad \text{(A16)}
$$

where E_{in}^0 is the energy of the eigenstate of $\hat{H}_0$ appearing in the expansion of $|\text{in}\rangle$ on which $\hat{\mathcal{T}}$ is acting. For example, in the above equation, $\hat{\mathcal{T}}$ is acting on $\left|\Psi_j^0\right\rangle$ and hence we should use $E_{\text{in}}^0 = E_j^0$. With this definition at

hand, we rewrite Eq. (A13) as

$$
\begin{aligned}
&e^{-i\hat{H}T/2}\left|\Gamma_-\right\rangle \\
&= \sum_j \phi_j^{\text{in}}\left\{e^{-iE_j^0 T/2}\left(\left|\Psi_j^0\right\rangle + \frac{1}{E_j^0 - \hat{H}_0 + i0^+}\hat{\mathcal{T}}\left|\Psi_j^0\right\rangle\right)\right\}.
\end{aligned}
\quad \text{(A17)}
$$

Recall that we are interested in calculating $|\text{out}\rangle = e^{i\hat{H}_0 T/2}e^{-i\hat{H}T/2}|\Gamma_-\rangle$. We have

$$
\begin{aligned}
&|\text{out}\rangle \\
&= \sum_{j,k}\left|\Psi_k^0\right\rangle\phi_j^{\text{in}}\left\{\delta_{kj} + \frac{e^{-i(E_j^0 - E_k^0)T/2}}{(E_j^0 - E_k^0) + i0^+}\left\langle\Psi_k^0|\hat{\mathcal{T}}|\Psi_j^0\right\rangle\right\}
\end{aligned}
\quad \text{(A18)}
$$

Now, by the same argument used before about using the time at which wavepacket of the light overlaps with the material, the above expression should be independent of $T/2$ when $T/2 >> 1/(\delta E_{\text{out}}^0)$. Therefore, let us extract the $T/2$-independent piece from the above equation.

$$
\begin{aligned}
&\frac{e^{-i(E^j - E_k^0)T/2}}{(E_j^0 - E_k^0) + i0^+} \\
&= e^{-i(E_j^0 - E_k^0)T/2}\mathcal{P}\frac{1}{(E_j^0 - E_k^0)} - i\pi\delta(E_j^0 - E_k^0) \\
&= \mathcal{P}\frac{\cos\left((E_j^0 - E_k^0)T/2\right)}{(E_j^0 - E_k^0)} - i\frac{\sin\left((E_j^0 - E_k^0)T/2\right)}{(E_j^0 - E_k^0)} \\
&\quad - i\pi\delta(E_j^0 - E_k^0)
\end{aligned}
\quad \text{(A19)}
$$

In the limit $T/2 \to \infty$, the first term above averages to 0, and hence does not contribute to the T-independent piece. The second term gets more and more sharply peaked and goes to $-i\pi\delta(E_j^0 - E_k^0)$. Therefore, in the large $T/2$ limit,

$$
\frac{e^{-i(E_j^0 - E_k^0)T/2}}{(E_j^0 - E_k^0) + i0^+} \to -2\pi i\delta(E_j^0 - E_k^0). \quad \text{(A20)}
$$

Therefore,

$$
\begin{aligned}
&|\text{out}\rangle \\
&= |\text{in}\rangle - \sum_{j,k} 2\pi i\delta(E_j^0 - E_k^0)\left|\Psi_k^0\right\rangle\left\langle\Psi_k^0\right|\hat{\mathcal{T}}\left|\Psi_j^0\right\rangle\left\langle\Psi_j^0|\text{in}\right\rangle.
\end{aligned}
\quad \text{(A21)}
$$

The above equation is a generalization of Fermi's Golden Rule that works to all orders in $\hat{V}$.

Appendix B: When the incoming laser is modeled as a coherent state instead of a Fock state

In Eq. (36) of the main text, we supposed that the radiation part of the $|\text{in}\rangle$ state was in a Fock state (photon-number eigenstate) with $\mathcal{N}_L$ photons in mode L. In this appendix, we examine the case when the initial state of the radiation sector is a coherent state. Our purpose is

two-fold – to clarify the definition of the coupling constant g_L and to write an expression for the $|\text{out}\rangle$ state.

Let us define a coherent state in the radiation sector $|\phi_L\rangle$ as:

$$|\phi_L\rangle \equiv e^{\phi_L \hat{a}_L^\dagger - \phi_L^* \hat{a}_L} |0,\dots,0\rangle. \tag{B1}$$

Then the full $|\text{in}\rangle$ state is

$$|\text{in}\rangle = |I\rangle_M \otimes e^{\phi_L \hat{a}_L^\dagger - \phi_L^* \hat{a}_L} |0,\dots,0\rangle \tag{B2}$$

$$= |I\rangle_M \otimes e^{-\frac{|\phi_L|^2}{2}} \sum_{\mathcal{N}_L} \frac{(\phi_L)^{\mathcal{N}_L}}{\sqrt{\mathcal{N}_L!}} |0,\dots,\mathcal{N}_L,\dots 0\rangle. \tag{B3}$$

In Eq. (6), when introducing the $\hat{\mathcal{T}}$ matrix machinery, we assumed an $|\text{in}\rangle$ state that was an eigenstate of $\hat{H}_0$. When $|\text{in}\rangle$ is not an energy eigenstate, as is the case above, one can decompose it into its energy eigenstates, and for each of them, linearly add up the corresponding $|\text{out}\rangle$ states.

We argued in the main text that within our approximation, the only processes contributing to $G^{(1)}$ that we keep are those where exactly one photon is absorbed from the laser and one photon is emitted into a different mode. Similarly, the only processes that we keep for $G^{(2)}$ are those where exactly two photons are absorbed from the laser and two are emitted. Therefore, the matrix elements of $\frac{1}{E_{\text{in}}^0 - \hat{H}_0}$ are independent of the number of photons $\mathcal{N}_L$ in the initial state. The only dependence of $|\text{out}\rangle$ on the initial state thus comes from the action of $\hat{a}_L$. Therefore, if we make a replacement from a Fock state to a coherent state, we just need to replace $\sqrt{\mathcal{N}_L}$ by ϕ_L in expressions for $G^{(1)}$ and $\sqrt{\mathcal{N}_L(\mathcal{N}_L - 1)}$ by ϕ_L^2 in expressions for $G^{(2)}$. For a Fock state, we used $I_L = \frac{\mathcal{N}_L \omega_L c}{\mathcal{V}}$. For a coherent state, we can instead use $I_L = \frac{|\phi_L|^2 \omega_L c}{\mathcal{V}}$.

Now, we come to the laser-matter coupling. For a Fock state input, in expressions for $G^{(2)}$, we make the identification

$$g_L^2 \leftrightarrow \frac{\sqrt{\mathcal{N}_L(\mathcal{N}_L - 1)} q_e^2 \mathsf{a}^2}{2\varepsilon \mathcal{V} \omega_L}. \tag{B4}$$

On the other hand, for expressions for $G^{(1)}$, we make the identification

$$g_L \leftrightarrow \frac{\sqrt{\mathcal{N}_L} q_e \mathsf{a}}{\sqrt{2\varepsilon \mathcal{V} \omega_L}}. \tag{B5}$$

This means that for Fock state input, our definition of g_L is slightly different for $G^{(1)}$ when compared to $G^{(2)}$. But for a coherent state input, the effective laser-matter coupling constants agree.

Now, we are in a position to write an expression for the $|\text{out}\rangle$ state that works for both a Fock state and a coherent state input. We suppose $|\text{in}\rangle = |I\rangle_M \otimes |\psi_L^{(0)}\rangle_R$, as defined in Eq. (36) in the main text. Recall from Eq. (5) and (6), that $|\text{out}\rangle$ can be computed using the $\hat{\mathcal{T}}$-matrix. In Eq. (34) and Eq. (35), we simplified the terms of the

$\hat{\mathcal{T}}$-matrix for processes corresponding to absorption and emission of one and two photons respectively. Combining these with the discussion in the above paragraph, we get Eq. (39) in the main text.

Appendix C: Explicit calculation for matter operator $\hat{R}^{(2)}$

Our goal here is to calculate $\hat{R}_{\lambda_1,\lambda_2}^{(2)}$ defined in Eq. (35) by expanding $\hat{V}_P \hat{\mathbb{G}}_0 \hat{V}_P \hat{\mathbb{G}}_0 \hat{V}_P \hat{\mathbb{G}}_0 \hat{V}_P + \hat{V}_P \hat{\mathbb{G}}_0 \hat{V}_D \hat{\mathbb{G}}_0 \hat{V}_P$, as promised in Sec. V. Recall from Eq. (26) that $\hat{\mathbb{G}}_0 = \left(E_{\text{in}} - \hat{H}_0\right)^{-1}$. Also, see Eq. (28) and Eq. (30) for definitions of $\hat{V}_P$ and $\hat{V}_D$ respectively.

In the $\hat{\mathcal{T}}$-matrix, each insertion of $\hat{V}_P$ can lead to a photon emission ($\hat{a}_\lambda^\dagger$) or absorption ($\hat{a}_\lambda$). Let us write $\hat{V}_P \equiv \hat{V}_P^+ + \hat{V}_P^-$, where $\hat{V}_P^+$ only consists of photon creation operators and $\hat{V}_P^-$ only consists of photon annihilation operators. Similarly, $\hat{V}_D \equiv \hat{V}_D^{+-} + \hat{V}_D^{++} + \hat{V}_D^{--}$, where $\hat{V}_D^{+-}$ is of the form $\hat{a}_\lambda^\dagger \hat{a}_{\lambda'}$ and so on. Then we see that Fig. 5(a) and 5(b) come from $\hat{V}_P^+ \hat{\mathbb{G}}_0 \hat{V}_P^- \hat{\mathbb{G}}_0 \hat{V}_P^+ \hat{\mathbb{G}}_0 \hat{V}_P^-$, i.e., a photon is first absorbed, then emitted, then absorbed and then emitted. Let us denote the contribution from this process to $R_{\lambda_1,\lambda_2}^{(2)}$ as $\hat{R}_{\lambda_1,\lambda_2}^{(2)}\big|_{a+b}$. Similarly, Fig. 5(c) comes from $\hat{V}_P^+ \hat{\mathbb{G}}_0 \hat{V}_P^+ \hat{\mathbb{G}}_0 \hat{V}_P^- \hat{\mathbb{G}}_0 \hat{V}_P^-$. Let us denote the contribution from this process as $\hat{R}_{\lambda_1,\lambda_2}^{(2)}\big|_c$. Fig. 5(d) comes from $\hat{V}_P^+ \hat{\mathbb{G}}_0 \hat{V}_D^{+-} \hat{\mathbb{G}}_0 \hat{V}_P^-$ and we denote its contribution to $R_{\lambda_1,\lambda_2}^{(2)}$ as $\hat{R}_{\lambda_1,\lambda_2}^{(2)}\big|_d$. Therefore,

$$\hat{R}_{\lambda_1,\lambda_2}^{(2)} = \hat{R}_{\lambda_1,\lambda_2}^{(2)}\Big|_{a+b} + \hat{R}_{\lambda_1,\lambda_2}^{(2)}\Big|_c + \hat{R}_{\lambda_1,\lambda_2}^{(2)}\Big|_d. \tag{C1}$$

1. Processes in Fig. 5(a) and 5(b)

These processes are shown pictorially in Fig. 6(a_1-a_6). Let us first expand out $\hat{V}_P^+ \hat{\mathbb{G}}_0 \hat{V}_P^- \hat{\mathbb{G}}_0 \hat{V}_P^+ \hat{\mathbb{G}}_0 \hat{V}_P^-$, keeping the terms that will contribute to $G^{(2)}$:

$$\hat{V}_P^+ \hat{\mathbb{G}}_0 \hat{V}_P^- \hat{\mathbb{G}}_0 \hat{V}_P^+ \hat{\mathbb{G}}_0 \hat{V}_P^-$$
$$= (g\mathsf{t})^4 \sum_{\boldsymbol{\mu}_1, \boldsymbol{\mu}_2, \boldsymbol{\mu}_1', \boldsymbol{\mu}_2'} (\bar{\boldsymbol{\mu}}_1' \cdot \mathbf{e}_L)(\bar{\boldsymbol{\mu}}_2' \cdot \mathbf{e}_L) \hat{a}_L^2$$
$$\times \sum_{\substack{\lambda_1,\lambda_2 \\ K,J,K',F}} \Bigg\{ \hat{a}_{\lambda_2}^\dagger \hat{a}_{\lambda_1}^\dagger \frac{(\bar{\boldsymbol{\mu}}_1 \cdot \mathbf{e}_{\lambda_1}^*)(\bar{\boldsymbol{\mu}}_2 \cdot \mathbf{e}_{\lambda_2}^*)}{\omega_L - E_{K'I} + i0^+}$$
$$\times \frac{|F\rangle\langle F| \hat{\mathcal{J}}_{\boldsymbol{\mu}_2} |K\rangle\langle K| \hat{\mathcal{J}}_{\boldsymbol{\mu}_2'} |J\rangle\langle J| \hat{\mathcal{J}}_{\boldsymbol{\mu}_1} |K'\rangle\langle K'| \hat{\mathcal{J}}_{\boldsymbol{\mu}_1'}}{(\omega_L - E_{JI} - \omega_{\lambda_1} + i0^+)(2\omega_L - E_{KI} - \omega_{\lambda_1} + i0^+)} \Bigg\}. \tag{C2}$$

See Eq. (27) for the definition of $\hat{\mathcal{J}}_{\boldsymbol{\mu}}$. Here, we sum over $|J\rangle$, $|K'\rangle$, $|K\rangle$ and $|F\rangle$ that are many-body energy eigenstates of the Hubbard model. For convenience, we have

defined $E_{JI} \equiv E_J - E_I$. The overall energy-conservation constraint for each λ_1 and λ_2, imposed by the δ-function in Eq. (41) is

$$E_I + 2\omega_L = E_F + \omega_{\lambda_1} + \omega_{\lambda_2}. \tag{C3}$$

Now consider the three energy dependent factors $(2\omega_L - E_{KI} - \omega_{\lambda_1} + i0^+)^{-1}$, $(\omega_L - E_{JI} - \omega_{\lambda_1} + i0^+)^{-1}$ and $(\omega_L - E_{K'I} + i0^+)^{-1}$. Of these, the first two factors contain ω_{λ_1}, a variable that we integrate over, so we cannot estimate them just yet. But we can estimate the third factor – it is dominated by states $|K'\rangle$ in the single doublon-hole sector. For such states, the factor is of order $1/(\omega_L - U)$. Within this sector, relative variations in this factor are of order $\mathtt{t}/|\omega_L - U|$ that we neglect. We drop contributions from outside this sector because they come with an addition suppression of order $|U - \omega_L|/U$ (see Fig. 5). Since Eq. (C2) now becomes independent of $E_{K'}$, we can replace $\sum_{K'} |K'\rangle\langle K'|$ by the identity. Next, $|J\rangle$ should be in the spin sector. For this to happen, the bond $(\mathbf{r}'_1, \boldsymbol{\mu}'_1)$ along which the first hop occurs should be the same as the bond $(\mathbf{r}_1, \boldsymbol{\mu}_1)$ along which the second hop occurs. Using this fact, we can use the identities (C4) and (C5) given below to simplify the expression in Eq. (C2):

$$\hat{c}^\dagger_\alpha \hat{c}_\beta = \delta_{\beta\alpha} \frac{\hat{n}}{2} + \left(\hat{\mathbf{S}} \cdot \boldsymbol{\sigma}\right)_{\beta\alpha} \tag{C4}$$

$$\hat{c}_\alpha \hat{c}^\dagger_\beta = \delta_{\alpha\beta} \left(1 - \frac{\hat{n}}{2}\right) - \left(\hat{\mathbf{S}} \cdot \boldsymbol{\sigma}\right)_{\alpha\beta}. \tag{C5}$$

We then arrive at the following relation

$$\langle J|\hat{\mathcal{J}}_{\boldsymbol{\mu}} \hat{\mathcal{J}}_{\boldsymbol{\mu}'}|I\rangle \approx \langle J| \delta_{\boldsymbol{\mu},\boldsymbol{\mu}'} \sum_{\mathbf{r}} \left(4\hat{\mathbf{S}}_{\mathbf{r}} \cdot \hat{\mathbf{S}}_{\mathbf{r}+\boldsymbol{\mu}} - 1\right)|I\rangle \tag{C6}$$

if both $|I\rangle$ and $|J\rangle$ are in the spin-sector.

Using this in Eq. (C2), then symmetrizing the resultant expression between indices λ_1 and λ_2, and reading off $\hat{R}^{(2)}_{\lambda_1,\lambda_2}$, we get

$$\langle F|\hat{R}^{(2)}_{\lambda_1,\lambda_2}\Big|_{a+b}|I\rangle$$

$$= \frac{g_L^2 g^2 \mathtt{t}^4}{\omega_L - U} \sum_{\boldsymbol{\mu}_1,\boldsymbol{\mu}_2,\boldsymbol{\mu}'_2} \sum_{K,J} \Bigg\{$$

$$\left[\frac{(\bar{\boldsymbol{\mu}}'_2 \cdot \mathbf{e}_L)(\bar{\boldsymbol{\mu}}_2 \cdot \mathbf{e}^*_{\lambda_2})}{\omega_{\lambda_1} - (2\omega_L - E_{KI} + i0^+)} \frac{1}{\omega_{\lambda_1} - (\omega_L - E_{JI} + i0^+)}\right.$$

$$\left. + \left(\lambda_1 \leftrightarrow \lambda_2\right)\right] \times \langle F| \hat{\mathcal{J}}_{\boldsymbol{\mu}_2} |K\rangle\langle K| \hat{\mathcal{J}}_{\boldsymbol{\mu}'_2} |J\rangle$$

$$\times \langle J| \sum_{\mathbf{r}_1,\boldsymbol{\mu}_1} \left(4\hat{\mathbf{S}}_{\mathbf{r}_1} \cdot \hat{\mathbf{S}}_{\mathbf{r}_1+\boldsymbol{\mu}_1} - 1\right)(\bar{\boldsymbol{\mu}}_1 \cdot \mathbf{e}^*_{\lambda_1})(\bar{\boldsymbol{\mu}}_1 \cdot \mathbf{e}_L)\Bigg\}|I\rangle. \tag{C7}$$

The first term here has two poles, one at $\omega_{\lambda_1} = 2\omega_L - E_{KI} + i0^+$, which corresponds to Fig. 5(a), i.e., the central peak and another at $\omega_{\lambda_1} = \omega_L - E_{JI} + i0^+$, which

corresponds to Fig. 5(b), i.e., the sidebands. The two poles here are reminiscent of the fluorescent triplet of a two-level system studied in Ref. [74]. Our first [Fig. 5(a)] and second [Fig. 5(b)] set of poles loosely correspond to the double Rayleigh process and sidebands respectively of Ref. [74]. The point where the analogy with Ref. [74] breaks is that state $|J\rangle$ in Fig. 5(a) is generically different from $|I\rangle$, and therefore Fig. 5(a) is technically not a double Rayleigh process. Coming back to our calculation, recall from Eq. (41) that the quantity we are interested in is really Eq. (C7) multiplied by $\mathcal{F}_1(\omega_{\lambda_1})\mathcal{F}_2(\omega_{\lambda_2})e^{i\omega_{\lambda_1}\tau}$ and integrated over ω_{λ_1} and ω_{λ_2} with the constraint $2\pi\delta\left(E_{FI} + \omega_{\lambda_1} + \omega_{\lambda_2} - 2\omega_L\right)$. In this work, we will assume that the filter function $\mathcal{F}_i(\omega)$ is narrow enough to prevent the central peak and sidebands from interfering. In this case, we can expand the above expression around the individual poles of ω_{λ_1} (and similarly, of ω_{λ_2}), i.e.,

$$\frac{1}{\omega_{\lambda_1} - (2\omega_L - E_{KI} + i0^+)} \frac{1}{\omega_{\lambda_1} - (\omega_L - E_{JI} + i0^+)}$$

$$\approx \frac{1}{\omega_L - U} \left[\frac{1}{\omega_{\lambda_1} - (\omega_L - E_{JI} + i0^+)}\right.$$

$$\left. - \frac{1}{\omega_{\lambda_1} - (2\omega_L - E_{KI} + i0^+)}\right]. \tag{C8}$$

The upshot is that we only need to look at Eq. (C7) around the two poles, corresponding to either the central peak or the sidebands. With this understanding, we can write $\hat{R}^{(2)}_{\lambda_1,\lambda_2}\Big|_{a+b}$ as a sum of two terms: $\hat{R}^{(2)}_{\lambda_1,\lambda_2}\Big|_a$ and $\hat{R}^{(2)}_{\lambda_1,\lambda_2}\Big|_b$, near the first and second pole respectively. Let us look at them one by one.

a. Process in Fig. 5(a)

Since $\hat{R}^{(2)}_{\lambda_1,\lambda_2}\Big|_a$ is evaluated near $\omega_{\lambda_1} = \omega_L - E_{JI}$, the factor $[\omega_{\lambda_1} - (2\omega_L - E_{KI} + i0^+)]^{-1}$ becomes $[E_{KI} - \omega_L]^{-1}$. This can be approximated as $(U - \omega_L)^{-1}$. Then, the dependence on E_K drops out and we can replace $\sum_K |K\rangle\langle K|$ by the identity. Then, following the same reasoning explained in the paragraph below Eq. (C3), we can simplify the fermionic terms into a spin

singlet projection operator. Doing so, we get

$$
\langle F|\hat{R}^{(2)}_{\lambda_1,\lambda_2}\Big|_a|I\rangle = \frac{-g_L^2 g^2 \mathtt{t}^4}{(\omega_L - U)^2}
$$

$$
\times \sum_J \Bigg\{ \Bigg\{ \frac{1}{\omega_{\lambda_1} - (\omega_L - E_{JI} + i0^+)}
$$

$$
\times \langle F| \sum_{\mathbf{r}_2,\boldsymbol{\mu}_2} \left(4\hat{\mathbf{S}}_{\mathbf{r}_2}\cdot\hat{\mathbf{S}}_{\mathbf{r}_2+\boldsymbol{\mu}_2} - 1\right) (\bar{\boldsymbol{\mu}}_2 \cdot \mathbf{e}_L) (\bar{\boldsymbol{\mu}}_2 \cdot \mathbf{e}^*_{\lambda_2}) |J\rangle
$$

$$
\times \langle J| \sum_{\mathbf{r}_1,\boldsymbol{\mu}_1} \left(4\hat{\mathbf{S}}_{\mathbf{r}_1}\cdot\hat{\mathbf{S}}_{\mathbf{r}_1+\boldsymbol{\mu}_1} - 1\right) (\bar{\boldsymbol{\mu}}_1 \cdot \mathbf{e}_L) (\bar{\boldsymbol{\mu}}_1 \cdot \mathbf{e}^*_{\lambda_1}) \Bigg\} |I\rangle
$$

$$
+ \{\lambda_1 \leftrightarrow \lambda_2\} \Bigg\},
$$

(C9)

where $|J\rangle$ lies in the spin sector. ($|I\rangle$ and $|F\rangle$ lie in the charge-sector, as usual.) As anticipated in Sec. V B, the process in Fig. 5(a) involves operators entirely in the spin sector.

b. Process in Fig. 5(b)

Along similar lines, one can simplify $\hat{R}^{(2)}_{\lambda_1,\lambda_2}\Big|_b$, which is evaluated near $\omega_{\lambda_1} = 2\omega_L - E_{KI}$. As we would expect, this time, it is not possible to rewrite all the fermionic operators in terms of spins. Instead, we get

$$
\langle F|\hat{R}^{(2)}_{\lambda_1,\lambda_2}\Big|_b|I\rangle = \frac{g_L^2 g^2 \mathtt{t}^4}{(\omega_L - U)^2} \Bigg\{ \sum_K \Bigg\{
$$

$$
\times \frac{\langle F|\sum_{\boldsymbol{\mu}_2} (\bar{\boldsymbol{\mu}}_2\cdot\mathbf{e}^*_{\lambda_2}) \hat{\mathcal{J}}_{\boldsymbol{\mu}_2}|K\rangle \langle K|\sum_{\boldsymbol{\mu}'_2} (\bar{\boldsymbol{\mu}}'_2\cdot\mathbf{e}_L)\hat{\mathcal{J}}_{\boldsymbol{\mu}'_2}}{\omega_{\lambda_1} - (2\omega_L - E_{KI} + i0^+)}
$$

$$
\times \sum_{\mathbf{r}_1,\boldsymbol{\mu}_1} \left(4\hat{\mathbf{S}}_{\mathbf{r}_1}\cdot\hat{\mathbf{S}}_{\mathbf{r}_1+\boldsymbol{\mu}_1} - 1\right) (\bar{\boldsymbol{\mu}}_1 \cdot \mathbf{e}_L) (\bar{\boldsymbol{\mu}}_1 \cdot \mathbf{e}^*_{\lambda_1}) \Bigg\} |I\rangle
$$

$$
+ \{\lambda_1 \leftrightarrow \lambda_2\} \Bigg\}
$$

(C10)

where $|K\rangle$ is an energy eigenstate in the single doublon-hole sector. ($|I\rangle$ and $|F\rangle$ lie in the spin-sector, as usual.) Therefore, the process in Fig. 5(b) necessarily includes operators in the charge sector.

2. Process in Fig. 5(c)

We show this process pictorially in Fig. 6(c_1-c'_6). This process, whose energy level schematic is in Fig. 5(c), arises from the term $\hat{V}_P^+ \hat{\mathbb{G}}_0 \hat{V}_P^+ \hat{\mathbb{G}}_0 \hat{V}_P^- \hat{\mathbb{G}}_0 \hat{V}_P^-$. Expanding

it out,

$$
\hat{V}_P^+ \hat{\mathbb{G}}_0 \hat{V}_P^+ \hat{\mathbb{G}}_0 \hat{V}_P^- \hat{\mathbb{G}}_0 \hat{V}_P^-
$$

$$
= (g\mathtt{t})^4 \sum_{\boldsymbol{\mu}_1,\boldsymbol{\mu}'_1,\boldsymbol{\mu}_2,\boldsymbol{\mu}'_2} (\bar{\boldsymbol{\mu}}'_1 \cdot \mathbf{e}_L)(\bar{\boldsymbol{\mu}}'_2\cdot\mathbf{e}_L)\, \hat{a}_L^2
$$

$$
\times \sum_{\substack{\lambda_1,\lambda_2 \\ K,\tilde{J},K',F}} \Bigg\{ \frac{\hat{a}^\dagger_{\lambda_2}\hat{a}^\dagger_{\lambda_1}\left(\bar{\boldsymbol{\mu}}_1\cdot\mathbf{e}^*_{\lambda_1}\right)\left(\bar{\boldsymbol{\mu}}_2\cdot\mathbf{e}^*_{\lambda_2}\right)}{\omega_L - E_{K'I} + i0^+}
$$

$$
\times \frac{|F\rangle\langle F|\,\hat{\mathcal{J}}_{\boldsymbol{\mu}_2}|K\rangle\langle K|\,\hat{\mathcal{J}}_{\boldsymbol{\mu}_1}\left|\tilde{J}\right\rangle\left\langle\tilde{J}\right|\hat{\mathcal{J}}_{\boldsymbol{\mu}'_2}|K'\rangle\langle K'|\hat{\mathcal{J}}_{\boldsymbol{\mu}'_1}}{\left(2\omega_L - E_{\tilde{J}I} + i0^+\right)\left(2\omega_L - E_{KI} - \omega_{\lambda_1} + i0^+\right)} \Bigg\},
$$

(C11)

where $|K'\rangle$ and $|K\rangle$ are in the single doublon-hole sector, $\left|\tilde{J}\right\rangle$ is in the two doublon-hole sector, and $|I\rangle$ and $|F\rangle$ are in the spin sector. Like before, $(\omega_L - E_{K'I})^{-1}$ can be approximated as $(\omega_L - U)^{-1}$. Also, $(2\omega_L - E_{\tilde{J}I})^{-1}$ can be approximated as $(2\omega_L - 2U)^{-1}$. Then the dependence on both $E_{K'}$ and $E_{\tilde{J}}$ drop out. Thus,

$$
\langle F|\hat{R}^{(2)}_{\lambda_1,\lambda_2}\Big|_c|I\rangle = \frac{-g_L^2 g^2 \mathtt{t}^4}{2(\omega_L - U)^2}
$$

$$
\times \Bigg\{ \sum_K \Bigg[\frac{\langle F|\sum_{\boldsymbol{\mu}_2}(\bar{\boldsymbol{\mu}}_2\cdot\mathbf{e}^*_{\lambda_2})\,\hat{\mathcal{J}}_{\boldsymbol{\mu}_2}|K\rangle\langle K|}{\omega_{\lambda_1} - (2\omega_L - E_{KI} + i0^+)}
$$

$$
\times \sum_{\mathbf{r}_1,\boldsymbol{\mu}_1,\sigma_1}(\bar{\boldsymbol{\mu}}_1\cdot\mathbf{e}^*_{\lambda_1})\left(\hat{c}^\dagger_{\mathbf{r}_1+\boldsymbol{\mu}_1,\sigma_1}\hat{c}_{\mathbf{r}_1\sigma_1} - \text{h.c.}\right)
$$

$$
\times \tilde{\sum}_{\tilde{J}}\left|\tilde{J}\right\rangle\left\langle\tilde{J}\right| \sum_{\substack{\mathbf{r}'_2,\boldsymbol{\mu}'_2, \\ \sigma'_2}}(\bar{\boldsymbol{\mu}}'_2\cdot\mathbf{e}_L)\left(\hat{c}^\dagger_{\mathbf{r}'_2+\boldsymbol{\mu}'_2,\sigma'_2}\hat{c}_{\mathbf{r}'_2\sigma'_2} - \text{h.c.}\right)
$$

$$
\times \sum_{\mathbf{r}'_1,\boldsymbol{\mu}'_1,\sigma'_1}(\bar{\boldsymbol{\mu}}'_1\cdot\mathbf{e}_L)\left(\hat{c}^\dagger_{\mathbf{r}'_1+\boldsymbol{\mu}'_1,\sigma'_1}\hat{c}_{\mathbf{r}'_1\sigma'_1} - \text{h.c.}\right) \Bigg] |I\rangle
$$

$$
+ [\lambda_1 \leftrightarrow \lambda_2] \Bigg\},
$$

(C12)

where $\tilde{\sum}_{\tilde{J}}\left|\tilde{J}\right\rangle\left\langle\tilde{J}\right|$ is a projector onto the sector with two doublons and two holes. Consider the first three hops – the first one along bond $(\mathbf{r}'_1,\boldsymbol{\mu}'_1)$, the second one along bond $(\mathbf{r}'_2,\boldsymbol{\mu}'_2)$, and the third along $(\mathbf{r}_1,\boldsymbol{\mu}_1)$. At the end of the second hop, there are two doublons and two holes. At the end of the third hop, there is one doublon and one hole. This can only happen in the two qualitatively distinct ways shown in Fig. 14 and Fig. 15. In Fig. 14, the third hop annihilates the doublon-hole pair created in either the first hop or the second hop.

In Fig. 15 on the other hand, the two doublon-hole pairs created by the first two hops are on neighbouring bonds. The third hop then annihilates a doublon-hole pair, not along either of the previous two bonds, but instead along the bond connecting the first two hops.

Let us analyze the process in Fig. 14 first. Here, the bond $(\mathbf{r}_1,\boldsymbol{\mu}_1)$ is identical to either $(\mathbf{r}'_1,\boldsymbol{\mu}'_1)$ [Fig. 14(e)]
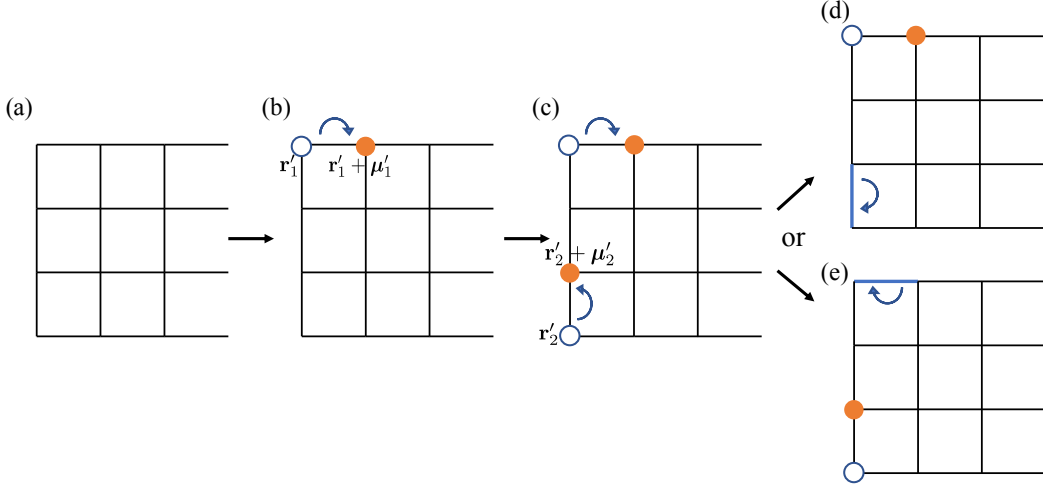
Figure 14. First class of processes contributing to Fig. 5(c). For figures in this paper, an empty circle denotes a hole at the lattice site and a filled circle denotes a doublon. The absence of any circle denotes a spin (whose state is left unspecified). We use a curved blue arrow to denote an electron hopping from the tail to the head of the arrow. The configuration shown in each figure is the *result* of such a hop shown by the arrow on the *same* figure. Here, we show a square lattice for concreteness. But our results hold for any lattice. We suppose $\boldsymbol{\mu}'_1$ and $\boldsymbol{\mu}'_2$ are in the x and y directions respectively. **(a)**: One starts with a spin state. **(b)**: Through a photon absorption, an electron hops from $\mathbf{r}'_1$ to $\mathbf{r}'_1 + \boldsymbol{\mu}'_1$. **(c)**: Through a photon absorption, an electron hops from $\mathbf{r}'_2$ to $\mathbf{r}'_2 + \boldsymbol{\mu}'_2$. At this point, there are two doublon-hole pairs as shown. Now there are two choices of doublon-hole pairs to annihilate via a photon emission – either **(d)**: the one created second, or **(e)**: the one created first.
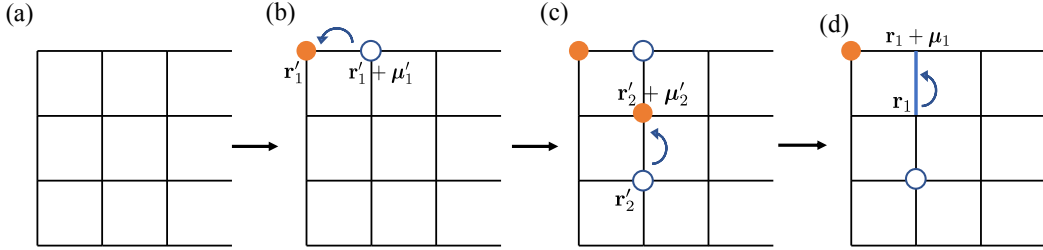

Figure 15. Second class of processes contributing to Fig. 5(c). Here, the doublon-hole pair that is annihilated differs from either of the two pairs that were created, but is instead made of one hole and one doublon from each pair. For this to be possible, the two bonds along which the doublon-hole pairs were created should be connected to each other by another bond. **(a)**: Spin state. **(b)**: Creation of first doublon-hole pair. **(c)**: Creation of second doublon-hole pair. **(d)**: Annihilation of a doublon-hole pair.

or $(\mathbf{r}'_2, \boldsymbol{\mu}'_2)$ [Fig. 14 (d)]. Let us go with the former first. In this case, the bond $(\mathbf{r}'_2, \boldsymbol{\mu}'_2)$ corresponding to the second hop should share no site in common with the bond $(\mathbf{r}_1, \boldsymbol{\mu}_1)$. Therefore, we can replace $\sum_{\mathbf{r}'_2, \sigma'_2} \left(\hat{c}^\dagger_{\mathbf{r}'_2 + \boldsymbol{\mu}'_2, \sigma'_2} \hat{c}_{\mathbf{r}'_2 \sigma'_2} - \hat{c}^\dagger_{\mathbf{r}'_2 \sigma'_2} \hat{c}_{\mathbf{r}'_2 + \boldsymbol{\mu}'_2, \sigma'_2} \right)$ by

$$\mathcal{J}_{\boldsymbol{\mu}'_2} - \sum_{\mathbf{r}'_2, \sigma'_2} \eta^{(\mathbf{r}'_2, \boldsymbol{\mu}'_2)}_{(\mathbf{r}_1, \boldsymbol{\mu}_1)} \left(\hat{c}^\dagger_{\mathbf{r}'_2 + \boldsymbol{\mu}'_2, \sigma'_2} \hat{c}_{\mathbf{r}'_2 \sigma'_2} - \hat{c}^\dagger_{\mathbf{r}'_2 \sigma'_2} \hat{c}_{\mathbf{r}'_2 + \boldsymbol{\mu}'_2, \sigma'_2} \right),$$

where the symbol $\eta^{(\mathbf{r}'_2, \boldsymbol{\mu}'_2)}_{(\mathbf{r}_1, \boldsymbol{\mu}_1)}$ is a function of two bonds $(\mathbf{r}_1, \boldsymbol{\mu}_1)$ and $(\mathbf{r}'_2, \boldsymbol{\mu}'_2)$, and was defined in Eq (49). Once we enforce this constraint, we can drop the projector to the two doublon-hole sector, $\sum_{\tilde{J}} \left| \tilde{J} \right\rangle\!\left\langle \tilde{J} \right|$ in Eq. (C12), since the projector is enforced automatically. Now, we can commute the bond $(\mathbf{r}_1, \boldsymbol{\mu}_1)$ to the right in Eq. (C12)

through the bond $(\mathbf{r}'_2, \boldsymbol{\mu}'_2)$. Then the resulting expression has the currents through two identical bonds next to each other, and we replace it with $\sum_{\mathbf{r}_1} \left(4\hat{\mathbf{S}}_{\mathbf{r}_1} \cdot \hat{\mathbf{S}}_{\mathbf{r}_1 + \boldsymbol{\mu}} - 1 \right)$. It is easy to see that the second option [Fig. 14 (d)] gives the same result. Let us denote the sum of contributions from Fig. 14 (d) and Fig. 14 (e) by $\left\langle F \middle| \hat{R}^{(2)}_{\lambda_1, \lambda_2} \middle|_{c_1} \middle| I \right\rangle$. It thus equals

get

$$\langle F|\hat{R}^{(2)}_{\lambda_1,\lambda_2}\Big|_{c_1}|I\rangle = \frac{-g_L^2 g^2 \mathtt{t}^4}{(\omega_L - U)^2}$$

$$\times \left\{ \sum_K \left\{ \frac{\langle F| \sum_{\boldsymbol{\mu}_2} (\bar{\boldsymbol{\mu}}_2 \cdot \mathbf{e}^*_{\lambda_2}) \hat{\mathcal{J}}_{\boldsymbol{\mu}_2} |K\rangle\langle K|}{\omega_{\lambda_1} - (2\omega_L - E_{KI} + i0^+)} \right.\right.$$

$$\times \sum_{\mathbf{r}_1,\boldsymbol{\mu}_1} \left[\sum_{\boldsymbol{\mu}'_2} (\bar{\boldsymbol{\mu}}'_2 \cdot \mathbf{e}_L) \left(\mathcal{J}_{\boldsymbol{\mu}'_2} - \hat{\mathcal{K}}_{\boldsymbol{\mu}'_2}(\mathbf{r}_1,\boldsymbol{\mu}_1) \right) \right.$$

$$\left. \times \left(4\hat{\mathbf{S}}_{\mathbf{r}_1} \cdot \hat{\mathbf{S}}_{\mathbf{r}_1+\boldsymbol{\mu}_1} - 1 \right) (\bar{\boldsymbol{\mu}}_1 \cdot \mathbf{e}_L)(\bar{\boldsymbol{\mu}}_1 \cdot \mathbf{e}^*_{\lambda_1}) \right] \right\} |I\rangle$$

$$\left. + \{\lambda_1 \leftrightarrow \lambda_2\} \right\},$$

(C13)

where $\hat{\mathcal{K}}_{\boldsymbol{\mu}'_2}(\mathbf{r}_1,\boldsymbol{\mu}_1)$ is an antihermitian local operator supported near the bond $(\mathbf{r}_1,\boldsymbol{\mu}_1)$ in a way that depends on the direction $\boldsymbol{\mu}'_2$. It was defined in Eq. (48) and shown pictorially in Fig. 7.

If we now re-examine Eq. (C10), we find that it actually gets cancelled by part of Eq. (C13). Therefore,

$$\langle F|\hat{R}^{(2)}_{\lambda_1,\lambda_2}\Big|_b + \hat{R}^{(2)}_{\lambda_1,\lambda_2}\Big|_{c_1}|I\rangle = \frac{g_L^2 g^2 \mathtt{t}^4}{(\omega_L - U)^2}$$

$$\times \left\{ \sum_K \left\{ \frac{\sum_{\boldsymbol{\mu}_2} (\bar{\boldsymbol{\mu}}_2 \cdot \mathbf{e}^*_{\lambda_2}) \langle F| \hat{\mathcal{J}}_{\boldsymbol{\mu}_2} |K\rangle\langle K|}{\omega_{\lambda_1} - (2\omega_L - E_{KI} + i0^+)} \right.\right.$$

$$\times \sum_{\mathbf{r}_1,\boldsymbol{\mu}_1} \left[\sum_{\boldsymbol{\mu}'_2} (\bar{\boldsymbol{\mu}}'_2 \cdot \mathbf{e}_L) \hat{\mathcal{K}}_{\boldsymbol{\mu}'_2}(\mathbf{r}_1,\boldsymbol{\mu}_1) \left(4\hat{\mathbf{S}}_{\mathbf{r}_1} \cdot \hat{\mathbf{S}}_{\mathbf{r}_1+\boldsymbol{\mu}_1} - 1 \right) \right.$$

$$\left. \times (\bar{\boldsymbol{\mu}}_1 \cdot \mathbf{e}_L)(\bar{\boldsymbol{\mu}}_1 \cdot \mathbf{e}^*_{\lambda_1}) \right] \right\} |I\rangle + \{\lambda_1 \leftrightarrow \lambda_2\} \right\}.$$

(C14)

Now, let us consider the contribution from the process shown in Fig. 15 to Eq. (C12), that we will denote by $\langle F|\hat{R}^{(2)}_{\lambda_1,\lambda_2}\Big|_{c_2}|I\rangle$. In this process, the bonds $(\mathbf{r}'_2,\boldsymbol{\mu}'_2)$, $(\mathbf{r}_1,\boldsymbol{\mu}_1)$ and $(\mathbf{r}'_1,\boldsymbol{\mu}'_1)$ form a train, when put together successively (see Fig. 15(d)). The result of this process is a back-and forth hopping of an electron across the bond $(\mathbf{r}_1,\boldsymbol{\mu}_1)$ as well as the transport of an electron from $\mathbf{r}'_2$ to $\mathbf{r}'_1$ or vice-versa. Thus, the resulting operator only involves spin (and is not charged) at sites $\mathbf{r}_1$ and $\mathbf{r}_1 + \boldsymbol{\mu}_1$, but involves charged operators at sites adjacent to the bond $(\mathbf{r}_1,\boldsymbol{\mu}_1)$. Simplifying Eq. (C12) for this process, we

$$\langle F|\hat{R}^{(2)}_{\lambda_1,\lambda_2}\Big|_{c_2}|I\rangle = \frac{g_L^2 g^2 \mathtt{t}^4}{(\omega_L - U)^2}$$

$$\times \left\{ \sum_K \left\{ \frac{\sum_{\boldsymbol{\mu}_2} (\bar{\boldsymbol{\mu}}_2 \cdot \mathbf{e}^*_{\lambda_2}) \langle F| \hat{\mathcal{J}}_{\boldsymbol{\mu}_2} |K\rangle\langle K|}{\omega_{\lambda_1} - (2\omega_L - E_{KI} + i0^+)} \right.\right.$$

$$\times \sum_{(\mathbf{r}_1,\boldsymbol{\mu}_1),\boldsymbol{\mu}'_1,\boldsymbol{\mu}'_2} \left[(\bar{\boldsymbol{\mu}}_1 \cdot \mathbf{e}^*_{\lambda_1})(\bar{\boldsymbol{\mu}}'_1 \cdot \mathbf{e}_L)(\bar{\boldsymbol{\mu}}'_2 \cdot \mathbf{e}_L) \right.$$

$$\times \left(\hat{\boldsymbol{\mathcal{S}}}_{\boldsymbol{\mu}'_1,\boldsymbol{\mu}'_2}(\mathbf{r}_1,\boldsymbol{\mu}_1) \cdot \left(\frac{\hat{\mathbf{S}}_{\mathbf{r}_1} - \hat{\mathbf{S}}_{\mathbf{r}_1+\boldsymbol{\mu}_1}}{2} - i\hat{\mathbf{S}}_{\mathbf{r}_1} \times \hat{\mathbf{S}}_{\mathbf{r}_1+\boldsymbol{\mu}_1} \right) \right.$$

$$\left.\left. + \hat{\mathcal{C}}_{\boldsymbol{\mu}'_1,\boldsymbol{\mu}'_2}(\mathbf{r}_1,\boldsymbol{\mu}_1) \left(\hat{\mathbf{S}}_{\mathbf{r}_1} \cdot \hat{\mathbf{S}}_{\mathbf{r}_1+\boldsymbol{\mu}_1} - \frac{1}{4} \right) \right) \right] \right\} |I\rangle$$

$$\left. + \{\lambda_1 \leftrightarrow \lambda_2\} \right\},$$

(C15)

where $\hat{\boldsymbol{\mathcal{S}}}_{\boldsymbol{\mu}'_1,\boldsymbol{\mu}'_2}(\mathbf{r}_1,\boldsymbol{\mu}_1)$ and $\hat{\mathcal{C}}_{\boldsymbol{\mu}'_1,\boldsymbol{\mu}'_2}(\mathbf{r}_1,\boldsymbol{\mu}_1)$ are operators that result in tunneling of charge from one site adjacent to the bond $(\mathbf{r}_1,\boldsymbol{\mu}_1)$ to another adjacent to the same bond, for example, from the empty circle to the filled circle in Fig. 15(d). These operators were defined in Eq. (51) and Eq. (52), and shown pictorially in Fig. 8.

Both of the above operators are symmetric under exchanging the bond directions $\boldsymbol{\mu}'_1$ with $\boldsymbol{\mu}'_2$. Under reversing the orientation of the bond $(\mathbf{r}_1,\boldsymbol{\mu}_1)$, i.e., by replacing it with $(\mathbf{r}_1 + \boldsymbol{\mu}_1, -\boldsymbol{\mu}_1)$, the operator $\hat{\boldsymbol{\mathcal{S}}}_{\boldsymbol{\mu}'_1,\boldsymbol{\mu}'_2}(\mathbf{r}_1,\boldsymbol{\mu}_1)$ remains invariant, while $\hat{\mathcal{C}}_{\boldsymbol{\mu}'_1,\boldsymbol{\mu}'_2}(\mathbf{r}_1,\boldsymbol{\mu}_1)$ flips sign, as is needed for consistency of Eq. (C15). Also, note that $\hat{\boldsymbol{\mathcal{S}}}_{\boldsymbol{\mu}'_1,\boldsymbol{\mu}'_2}(\mathbf{r}_1,\boldsymbol{\mu}_1)$ and $\hat{\mathcal{C}}_{\boldsymbol{\mu}'_1,\boldsymbol{\mu}'_2}(\mathbf{r}_1,\boldsymbol{\mu}_1)$ transform as spin triplet and spin singlet respectively under spin rotation.

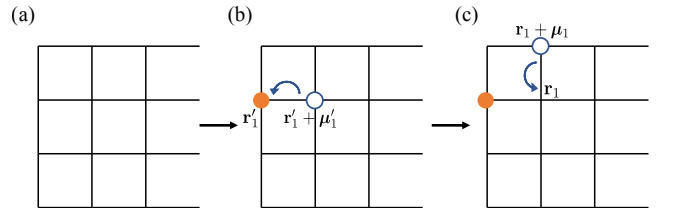### 3. Process in Fig. 5(d): Diamagnetic term

Figure 16. **(a)**: Spin state. **(b)**: First doublon-hole pair is created via the paramagnetic term. **(c)**: A hole moves via the diamagnetic term.

Let us finally look at $\hat{R}^{(2)}_{\lambda_1,\lambda_2}\Big|_d$, i.e., the contribution from $\hat{V}^+_P \hat{\mathbb{G}}_0 \hat{V}^{+-}_D \hat{\mathbb{G}}_0 \hat{V}^-_P$, in other words, the process shown in Fig. 5(d). This process involves the diamagnetic term,

and is illustrated pictorially in Fig. 6(d$_1$-d$_5$). We have,

$$\langle F| \hat{R}^{(2)}_{\lambda_1,\lambda_2}\Big|_d |I\rangle = -g_L^2 g^2 \mathtt{t}^3$$

$$\times \sum_{K,K'} \left\{ \sum_{\boldsymbol{\mu}_2} \left(\bar{\boldsymbol{\mu}}_2 \cdot \mathbf{e}^*_{\lambda_2}\right) \langle F| \hat{\mathcal{J}}_{\boldsymbol{\mu}_2} |K\rangle\!\langle K| \right.$$

$$\times \sum_{\substack{\mathbf{r}_1,\boldsymbol{\mu}_1,\sigma_1 \\ \mathbf{r}'_1,\boldsymbol{\mu}'_1,\sigma'_1}} \frac{\left(\bar{\boldsymbol{\mu}}'_1 \cdot \mathbf{e}_L\right)\left(\bar{\boldsymbol{\mu}}_1 \cdot \mathbf{e}_L\right)\left(\bar{\boldsymbol{\mu}}_1 \cdot \mathbf{e}^*_{\lambda_1}\right)}{\left(\omega_L - E_{K'I} + i0^+\right)\left(2\omega_L - E_{KI} - \omega_{\lambda_1} + i0^+\right)}$$

$$\times \left(\hat{c}^\dagger_{\mathbf{r}_1+\boldsymbol{\mu}_1,\sigma_1}\hat{c}_{\mathbf{r}_1,\sigma_1} + \hat{c}^\dagger_{\mathbf{r}_1,\sigma_1}\hat{c}_{\mathbf{r}_1+\boldsymbol{\mu}_1,\sigma_1}\right)|K'\rangle\!\langle K'|$$

$$\times \left. \left(\hat{c}^\dagger_{\mathbf{r}'_1+\boldsymbol{\mu}'_1,\sigma'_1}\hat{c}_{\mathbf{r}'_1,\sigma'_1} - \hat{c}^\dagger_{\mathbf{r}'_1,\sigma'_1}\hat{c}_{\mathbf{r}'_1+\boldsymbol{\mu}'_1,\sigma'_1}\right)|I\rangle + \left[\lambda_1 \leftrightarrow \lambda_2\right] \right\}.$$
(C16)

Here, $|K'\rangle$ and $|K\rangle$ are in the single doublon-hole sector, and $|I\rangle$ and $|F\rangle$ are in the spin sector. Like before, $(\omega_L - E_{K'I})^{-1}$ can be approximated as $(\omega_L - U)^{-1}$. The pattern of electron hopping in this process is depicted in Fig. 16.

To ensure that state $|K\rangle$ remains in the single doublon-hole subspace, the process leading from Fig. 16(b) to (c) should be just a hopping of a doublon or a hole, and should not result in the formation of an additional doublon-hole pair. Therefore, the bonds $(\mathbf{r}_1, \boldsymbol{\mu}_1)$ and $(\mathbf{r}'_1, \boldsymbol{\mu}'_1)$ should have exactly one site in common. Therefore, either $\mathbf{r}'_1 = \mathbf{r}_1$ or $\mathbf{r}'_1 = \mathbf{r}_1 - \boldsymbol{\mu}_1$. This allows us to simplify Eq. (C16) to

$$\langle F| \hat{R}^{(2)}_{\lambda_1,\lambda_2}\Big|_d |I\rangle = \frac{g_L^2 g^2 \mathtt{t}^3}{\omega_L - U}$$

$$\times \left\{ \sum_K \left\{ \sum_{\boldsymbol{\mu}_2} \frac{\left(\bar{\boldsymbol{\mu}}_2 \cdot \mathbf{e}^*_{\lambda_2}\right)\langle F| \hat{\mathcal{J}}_{\boldsymbol{\mu}_2} |K\rangle\!\langle K|}{\omega_{\lambda_1} - \left(2\omega_L - E_{KI} + i0^+\right)} \right. \right.$$

$$\times \sum_{\boldsymbol{\mu}',\boldsymbol{\mu}} \sum_{\substack{s,s'=\pm 1 \\ s\boldsymbol{\mu} \neq s'\boldsymbol{\mu}'}} \left[\left(\bar{\boldsymbol{\mu}}' \cdot \mathbf{e}_L\right)\left(\bar{\boldsymbol{\mu}} \cdot \mathbf{e}_L\right)\left(\bar{\boldsymbol{\mu}} \cdot \mathbf{e}^*_{\lambda_1}\right) s s' \right.$$

$$\times \left. \left. \left. \sum_{\mathbf{r}} \left[-\frac{\hat{\mathcal{H}}_{\mathbf{r}+s'\boldsymbol{\mu}',\mathbf{r}+s\boldsymbol{\mu}}}{2} + \hat{\boldsymbol{\mathcal{J}}}^S_{\mathbf{r}+s'\boldsymbol{\mu}',\mathbf{r}+s\boldsymbol{\mu}} \cdot \hat{\mathbf{S}}_{\mathbf{r}} \right] \right] \right\} \right\} |I\rangle$$

$$+ \left\{\lambda_1 \leftrightarrow \lambda_2\right\} \right\},$$
(C17)

where $\hat{\mathcal{H}}_{\mathbf{r},\mathbf{r}'}$ and $\hat{\boldsymbol{\mathcal{J}}}^S_{\mathbf{r},\mathbf{r}'}$ were defined in Eq. (46) and (47) respectively.

After all the simplifications in the previous subsection, we are now ready to write an expression for the total two-photon amplitude

$$\langle F| \hat{R}^{(2)}_{\lambda_1,\lambda_2} |I\rangle = \langle F| \hat{R}^{(2)}_{\lambda_1,\lambda_2}\Big|_a |I\rangle + \langle F| \hat{R}^{(2)}_{\lambda_1,\lambda_2}\Big|_b |I\rangle$$
$$+ \langle F| \hat{R}^{(2)}_{\lambda_1,\lambda_2}\Big|_c |I\rangle + \langle F| \hat{R}^{(2)}_{\lambda_1,\lambda_2}\Big|_d |I\rangle .$$
(C18)

The result leads to Eq. (56) in the main text.

Thus, Eq. (56), combined with the definitions in Eq. (53),(55) and (54), gives the amplitude to find two photons – one in mode λ_1 and another in mode λ_2, entirely in terms of the matrix elements of matter operators between initial matter eigenstate $|I\rangle$ and final matter eigenstate $|F\rangle$. Now, we would like to get rid of the explicit dependence on the intermediate states $|J\rangle$ and $|K\rangle$ in Eq. (56). To do so, we use the following identity (for some ω and ω_0): $\frac{1}{\omega-\omega_0-i0^+} = i \int_{-\infty}^{\infty} \mathrm{d}t\, \theta(t) e^{-i(\omega-\omega_0-i0^+)t}$, where $\theta(t)$ is a step function that is 1 for $t > 0$ and 0 otherwise. By using the constraint $\omega_{\lambda_2} = 2\omega_L - \omega_{\lambda_1} - E_{FI}$, Eq. (56) can be viewed as a function of only one frequency ω_{λ_1}. We then use the above identity to trade the denominators in Eq. (56) in favor of the t-dependent phases. Now, these phases can be absorbed into the Heisenberg evolution of the operators $\hat{A}_j$ and $\hat{B}_j$ (defined as $\hat{A}_j(t) = e^{i\hat{H}_0 t}\hat{A}_j e^{-i\hat{H}_0 t}$). This allows us to rewrite Eq. (56) as Eq. (57) in the main text.

4. Second order photon number conserving homodyne correlator X^{-+}

Let us now consider the second order photon number conserving homodyne correlator $X^{-+}_{d_1,d_2}(\tau) = \langle \text{out}| \hat{a}^\dagger_{d_2}(\tau)\hat{a}_{d_1}(0) |\text{out}\rangle$. If detectors d_1 and d_2 are identical, this is the same as $G^1_{d_1}(\tau)$. Using the expression in Eq. (44), we obtain

$$\left\langle \hat{a}^\dagger_{d_2}(\tau)\hat{a}_{d_1}(0)\right\rangle_{\text{out}} \approx e^{i\omega_L \tau} \iint_{-\infty}^{\infty} \mathrm{d}t_1\, \mathrm{d}t_2 \left\{ \tilde{\mathcal{F}}_1(t_1)\left[\tilde{\mathcal{F}}_2(t_2)\right]^* \right.$$

$$\times \left. e^{i[(\omega_L-\omega_1)t_1 - (\omega_L-\omega_2)t_2]} \left\langle \hat{A}^\dagger_2(-t_2+\tau)\hat{A}_1(-t_1)\right\rangle_0 \right\},$$
(C19)

where the operators $\hat{A}_i$, defined in Eq. (53) are the same operators appearing in $G^{(1)}$ and X^+. Specializing to a Lorentzian filter function given in Eq. (59), we get

$$\left\langle \hat{a}^\dagger_{d_2}(\tau)\hat{a}_{d_1}(0)\right\rangle_{\text{out}} \approx \frac{i\mathtt{K}_1\mathtt{K}^*_2\Gamma_1\Gamma_2 e^{i\omega_L\tau}}{\omega_2 - \omega_1 + i\left(\Gamma_1+\Gamma_2\right)}$$

$$\times \int_{-\infty}^{\infty} \mathrm{d}t \left[e^{-(\Gamma_1+\Gamma_2)\frac{|t|}{2}} e^{i(\omega_2-\omega_1)\frac{|t|}{2}} \right.$$

$$\times \left. e^{it\left(\frac{\omega_1+\omega_2}{2}-\omega_L\right)} \left\langle \hat{A}^\dagger_2(\tau-t)\hat{A}_1(0)\right\rangle_0 \right]$$
(C20)

As the detectors become more frequency selective, i.e., as Γ_1,Γ_2 go to 0, this correlator is non-negligible only when the frequencies selected by the two detectors ω_1 and ω_2 are equal. In the opposite limit of broad frequency filters, i.e., as $\Gamma_1,\Gamma_2 \to \infty$,

$$\left\langle \hat{a}^\dagger_{d_2}(\tau)\hat{a}_{d_1}(0)\right\rangle_{\text{out}}\Big|_{\Gamma_1,\Gamma_2\to\infty}$$
$$\approx \mathtt{K}_1\mathtt{K}^*_2 e^{i\omega_L\tau} \left\langle \hat{A}^\dagger_2(\tau)\hat{A}_1(0)\right\rangle_0 .$$
(C21)

As a sanity check, one can now verify a known relation between the regulated Fourier transform of the above cor-

relator $G^{(1)}(\tau)$ (when the two detectors are identical) for $\Gamma_1 \to \infty$, and $G^{(1)}_{d_1}(0)$ [Eq. (60)] for the case of a narrow frequency filter ($\Gamma_1 \to 0$):

$$\lim_{\Gamma' \to 0^+} \int_{-\infty}^{\infty} d\tau \, \frac{\Gamma' e^{-\Gamma'|\tau|}}{2} e^{-i\omega_1 \tau} \left[G^{(1)}_{d_1}(\tau) \Big|_{\Gamma_1 \to \infty} \right] \quad \text{(C22)}$$
$$= G^{(1)}_{d_1}(0) \Big|_{\Gamma_1 \to 0}.$$

[1] D. Arovas, J. R. Schrieffer, and F. Wilczek, Fractional statistics and the quantum hall effect, Physical review letters **53**, 722 (1984).

[2] X.-G. Wen and Q. Niu, Ground-state degeneracy of the fractional quantum hall states in the presence of a random potential and on high-genus riemann surfaces, Physical Review B **41**, 9377 (1990).

[3] X. G. Wen, E. Dagotto, and E. Fradkin, Anyons on a torus, Physical Review B **42**, 6110 (1990).

[4] X.-G. Wen, Topological orders and chern-simons theory in strongly correlated quantum liquid, International Journal of Modern Physics B **5**, 1641 (1991).

[5] J. Nakamura, S. Liang, G. C. Gardner, and M. J. Manfra, Direct observation of anyonic braiding statistics, Nature Physics **16**, 931 (2020).

[6] H. Bartolomei, M. Kumar, R. Bisognin, A. Marguerite, J.-M. Berroir, E. Bocquillon, B. Placais, A. Cavanna, Q. Dong, U. Gennser, *et al.*, Fractional statistics in anyon collisions, Science **368**, 173 (2020).

[7] M. B. Hastings, Lieb-schultz-mattis in higher dimensions, Physical review b **69**, 104431 (2004).

[8] M. Oshikawa, Commensurability, excitation gap, and topology in quantum many-particle systems on a periodic lattice, Physical review letters **84**, 1535 (2000).

[9] E. Lieb, T. Schultz, and D. Mattis, Two soluble models of an antiferromagnetic chain, Annals of Physics **16**, 407 (1961).

[10] A. Kitaev, Anyons in an exactly solved model and beyond, Annals of Physics **321**, 2 (2006).

[11] J. Knolle and R. Moessner, A field guide to spin liquids, Annual Review of Condensed Matter Physics **10**, 451 (2019).

[12] L. Savary and L. Balents, Quantum spin liquids: a review, Reports on Progress in Physics **80**, 016502 (2016).

[13] P. A. Lee, From high temperature superconductivity to quantum spin liquid: progress in strong correlation physics, Reports on Progress in Physics **71**, 012501 (2007).

[14] P. A. Lee, N. Nagaosa, and X.-G. Wen, Doping a mott insulator: Physics of high-temperature superconductivity, Reviews of modern physics **78**, 17 (2006).

[15] C. Broholm, R. Cava, S. Kivelson, D. Nocera, M. Norman, and T. Senthil, Quantum spin liquids, Science **367**, eaay0668 (2020).

[16] L. Clark and A. H. Abdeldaim, Quantum spin liquids from a materials perspective, Annual Review of Materials Research **51**, 495 (2021).

[17] B. Keimer, S. A. Kivelson, M. R. Norman, S. Uchida, and J. Zaanen, From quantum matter to high-temperature superconductivity in copper oxides, Nature **518**, 179 (2015).

[18] E. Y. Andrei, D. K. Efetov, P. Jarillo-Herrero, A. H. MacDonald, K. F. Mak, T. Senthil, E. Tutuc, A. Yazdani, and A. F. Young, The marvels of moiré materials, Nature Reviews Materials **6**, 201 (2021).

[19] K. F. Mak and J. Shan, Semiconductor moiré materials, Nature Nanotechnology **17**, 686 (2022).

[20] T. P. Devereaux and R. Hackl, Inelastic light scattering from correlated electrons, Reviews of modern physics **79**, 175 (2007).

[21] D. Wulferding, Y. Choi, W. Lee, and K.-Y. Choi, Raman spectroscopic diagnostic of quantum spin liquids, Journal of Physics: Condensed Matter **32**, 043001 (2019).

[22] B. S. Shastry and B. I. Shraiman, Theory of raman scattering in mott-hubbard systems, Physical review letters **65**, 1068 (1990).

[23] B. S. Shastry and B. I. Shraiman, Raman scattering in mott-hubbard systems, International Journal of Modern Physics B **5**, 365 (1991).

[24] W.-H. Ko, Z.-X. Liu, T.-K. Ng, and P. A. Lee, Raman signature of the u (1) dirac spin-liquid state in the spin-1 2 kagome system, Physical Review B **81**, 024414 (2010).

[25] G. Nambiar, D. Bulmash, and V. Galitski, Monopole josephson effects in a dirac spin liquid, Physical Review Research **5**, 013169 (2023).

[26] Y. Wan and N. Armitage, Resolving continua of fractional excitations by spinon echo in thz 2d coherent spectroscopy, Physical review letters **122**, 257401 (2019).

[27] F. Mahmood, D. Chaudhuri, S. Gopalakrishnan, R. Nandkishore, and N. Armitage, Observation of a marginal fermi glass, Nature Physics **17**, 627 (2021).

[28] M. Fava, S. Biswas, S. Gopalakrishnan, R. Vasseur, and S. Parameswaran, Hydrodynamic nonlinear response of interacting integrable systems, Proceedings of the National Academy of Sciences **118**, e2106945118 (2021).

[29] W. Choi, K. H. Lee, and Y. B. Kim, Theory of two-dimensional nonlinear spectroscopy for the kitaev spin liquid, Physical Review Letters **124**, 117205 (2020).

[30] R. M. Nandkishore, W. Choi, and Y. B. Kim, Spectroscopic fingerprints of gapped quantum spin liquids, both conventional and fractonic, Physical Review Research **3**, 013254 (2021).

[31] O. Hart and R. Nandkishore, Extracting spinon self-energies from two-dimensional coherent spectroscopy, Physical Review B **107**, 205143 (2023).

[32] E. König, P. Coleman, and A. M. Tsvelik, Spin magnetometry as a probe of stripe superconductivity in twisted bilayer graphene, Physical Review B **102**, 104514 (2020).

[33] Z.-L. Li, M. Oshikawa, and Y. Wan, Photon echo from lensing of fractional excitations in tomonaga-luttinger spin liquid, Physical Review X **11**, 031035 (2021).

[34] G. Sim, J. Knolle, and F. Pollmann, Nonlinear spectroscopy of bound states in perturbed ising spin chains, Physical Review B **107**, L100404 (2023).

[35] G. Sim, F. Pollmann, and J. Knolle, Microscopic details of two-dimensional spectroscopy of one-dimensional quantum ising magnets, Physical Review B **108**, 134423 (2023).

[36] M. K. Negahdari and A. Langari, Nonlinear response of the kitaev honeycomb lattice model in a weak magnetic field, Physical Review B **107**, 134404 (2023).

[37] Q. Gao, Y. Liu, H. Liao, and Y. Wan, Two-dimensional coherent spectrum of interacting spinons from matrix product states, Physical Review B **107**, 165121 (2023).

[38] M. Potts, R. Moessner, and O. Benton, Exploiting polarization dependence in two-dimensional coherent spectroscopy: Examples of ce 2 zr 2 o 7 and nd 2 zr 2 o 7, Physical Review B **109**, 104435 (2024).

[39] Z. Zhang, F. Y. Gao, J. B. Curtis, Z.-J. Liu, Y.-C. Chien, A. von Hoegen, M. T. Wong, T. Kurihara, T. Suemoto, P. Narang, *et al.*, Terahertz field-induced nonlinear coupling of two magnon modes in an antiferromagnet, Nature Physics , 1 (2024).

[40] S. Parameswaran and S. Gopalakrishnan, Asymptotically exact theory for nonlinear spectroscopy of random quantum magnets, Physical review letters **125**, 237601 (2020).

[41] F. Gerken, T. Posske, S. Mukamel, and M. Thorwart, Unique signatures of topological phases in two-dimensional thz spectroscopy, Physical Review Letters **129**, 017401 (2022).

[42] E. Z. Zhang, C. Hickey, and Y. B. Kim, Disentangling spin excitation continua in classical and quantum magnets using 2d nonlinear spectroscopy, arXiv preprint arXiv:2404.16935 (2024).

[43] O. Krupnitska and W. Brenig, Finite-temperature second harmonic generation in kitaev magnets, Physical Review B **108**, 075120 (2023).

[44] Y. Watanabe, S. Trebst, and C. Hickey, Revealing quadrupolar excitations with non-linear spectroscopy, arXiv preprint arXiv:2405.14954 (2024).

[45] T. P. Devereaux, M. Claassen, X.-X. Huang, M. Zaletel, J. E. Moore, D. Morr, F. Mahmood, P. Abbamonte, and Z.-X. Shen, Angle-resolved pair photoemission theory for correlated electrons, Physical Review B **108**, 165134 (2023).

[46] M. McGinley, M. Fava, and S. Parameswaran, Signatures of fractional statistics in nonlinear pump-probe spectroscopy, Physical Review Letters **132**, 066702 (2024).

[47] M. McGinley, M. Fava, and S. Parameswaran, Anomalous thermal relaxation and pump-probe spectroscopy of two-dimensional topologically ordered systems, Physical Review B **109**, 075108 (2024).

[48] Y.-R. Shen, *Principles of nonlinear optics* (Wiley-Interscience, New York, NY, USA, 1984).

[49] A. Gelzinis, R. Augulis, V. Butkus, B. Robert, and L. Valkunas, Two-dimensional spectroscopy for non-specialists, Biochimica et Biophysica Acta (BBA)-Bioenergetics **1860**, 271 (2019).

[50] C. L. Smallwood and S. T. Cundiff, Multidimensional coherent spectroscopy of semiconductors, Laser & Photonics Reviews **12**, 1800171 (2018).

[51] K. Kobayashi and M. Hashisaka, Shot noise in mesoscopic systems: From single particles to quantum liquids, Journal of the Physical Society of Japan **90**, 102001 (2021).

[52] L. Saminadayar, D. Glattli, Y. Jin, and B. c.-m. Etienne, Observation of the e/3 fractionally charged laughlin quasiparticle, Physical Review Letters **79**, 2526 (1997).

[53] R. De-Picciotto, M. Reznikov, M. Heiblum, V. Umansky, G. Bunin, and D. Mahalu, Direct observation of a fractional charge, Physica B: Condensed Matter **249**, 395 (1998).

[54] K. M. Bastiaans, D. Chatzopoulos, J.-F. Ge, D. Cho, W. O. Tromp, J. M. van Ruitenbeek, M. H. Fischer, P. J. de Visser, D. J. Thoen, E. F. Driessen, *et al.*, Direct evidence for cooper pairing without a spectral gap in a disordered superconductor above t c, Science **374**, 608 (2021).

[55] P. Zhou, L. Chen, Y. Liu, I. Sochnikov, A. T. Bollinger, M.-G. Han, Y. Zhu, X. He, I. Bozović, and D. Natelson, Electron pairing in the pseudogap state revealed by shot noise in copper oxide junctions, Nature **572**, 493 (2019).

[56] L. Chen, D. T. Lowder, E. Bakali, A. M. Andrews, W. Schrenk, M. Waas, R. Svagera, G. Eguchi, L. Prochaska, Y. Wang, *et al.*, Shot noise in a strange metal, Science **382**, 907 (2023).

[57] D. E. Chang, V. Vuletić, and M. D. Lukin, Quantum nonlinear optics—photon by photon, Nature Photonics **8**, 685 (2014).

[58] R. H. Brown and R. Q. Twiss, Correlation between photons in two coherent beams of light, Nature **177**, 27 (1956).

[59] Up to a correction due to retardation, see Eq. (8) in Sec. III B.

[60] V. Kalmeyer and R. Laughlin, Equivalence of the resonating-valence-bond and fractional quantum hall states, Physical review letters **59**, 2095 (1987).

[61] X.-G. Wen, F. Wilczek, and A. Zee, Chiral spin states and superconductivity, Physical Review B **39**, 11413 (1989).

[62] S.-S. Gong, W. Zhu, and D. Sheng, Emergent chiral spin liquid: Fractional quantum hall effect in a kagome heisenberg model, Scientific reports **4**, 6317 (2014).

[63] Y.-C. He, D. Sheng, and Y. Chen, Chiral spin liquid in a frustrated anisotropic kagome heisenberg model, Physical review letters **112**, 137202 (2014).

[64] C. Hickey, L. Cincio, Z. Papić, and A. Paramekanti, Haldane-hubbard mott insulator: From tetrahedral spin crystal to chiral spin liquid, Physical review letters **116**, 137202 (2016).

[65] A. Wietek and A. M. Läuchli, Chiral spin liquid and quantum criticality in extended s= 1 2 heisenberg models on the triangular lattice, Physical Review B **95**, 035141 (2017).

[66] T. Cookmeyer, J. Motruk, and J. E. Moore, Four-spin terms and the origin of the chiral spin liquid in mott insulators on the triangular lattice, Physical review letters **127**, 087201 (2021).

[67] P. A. Lee and N. Nagaosa, Gauge theory of the normal state of high-t c superconductors, Physical Review B **46**, 5621 (1992).

[68] X.-Y. Song, C. Wang, A. Vishwanath, and Y.-C. He, Unifying description of competing orders in two-

dimensional quantum magnets, Nature communications **10**, 4254 (2019).

[69] M. Hafezi, D. E. Chang, V. Gritsev, E. A. Demler, and M. D. Lukin, Photonic quantum transport in a nonlinear optical fiber, Europhysics Letters **94**, 54006 (2011).

[70] A. V. Gorshkov, J. Otterbach, M. Fleischhauer, T. Pohl, and M. D. Lukin, Photon-photon interactions via rydberg blockade, Physical review letters **107**, 133602 (2011).

[71] D. P. Arovas, E. Berg, S. A. Kivelson, and S. Raghu, The hubbard model, Annual review of condensed matter physics **13**, 239 (2022).

[72] M. Qin, T. Schäfer, S. Andergassen, P. Corboz, and E. Gull, The hubbard model: A computational perspective, Annual Review of Condensed Matter Physics **13**, 275 (2022).

[73] P. Fleury and R. Loudon, Scattering of light by one- and two-magnon excitations, Physical Review **166**, 514 (1968).

[74] J. Dalibard and S. Reynaud, Correlation signals in resonance fluorescence: interpretation via photon scattering amplitudes, Journal de Physique **44**, 1337 (1983).

[75] L. Masters, X.-X. Hu, M. Cordier, G. Maron, L. Pache, A. Rauschenbeutel, M. Schemmer, and J. Volz, On the simultaneous scattering of two photons by a single two-level atom, Nature Photonics **17**, 972 (2023).

[76] V. V. Orre, E. A. Goldschmidt, A. Deshpande, A. V. Gorshkov, V. Tamma, M. Hafezi, and S. Mittal, Interference of temporally distinguishable photons using frequency-resolved detection, Physical review letters **123**, 123603 (2019).

[77] P. A. Lee and N. Nagaosa, Proposal to use neutron scattering to access scalar spin chirality fluctuations in kagome lattices, Physical Review B—Condensed Matter and Materials Physics **87**, 064423 (2013).

[78] F. Gallagher and S. Mazumdar, Excitons and optical absorption in one-dimensional extended hubbard models with short-and long-range interactions, Physical Review B **56**, 15025 (1997).

[79] F. H. Essler, F. Gebhard, and E. Jeckelmann, Excitons in one-dimensional mott insulators, Physical Review B **64**, 125119 (2001).

[80] P. Wróbel and R. Eder, Excitons in mott insulators, Physical Review B **66**, 035111 (2002).

[81] T. Tohyama, H. Onodera, K. Tsutsui, and S. Maekawa, Resonant two-magnon raman scattering and photoexcited states in two-dimensional mott insulators, Physical review letters **89**, 257405 (2002).

[82] A. Maeda, M. Ono, H. Kishida, T. Manako, A. Sawa, M. Kawasaki, Y. Tokura, and H. Okamoto, Third-order nonlinear susceptibility spectra of cuo chain compounds investigated by the z-scan method, Physical Review B **70**, 125117 (2004).

[83] H. Matsueda, T. Tohyama, and S. Maekawa, Excitonic effect on the optical response in the one-dimensional two-band hubbard model, Physical Review B **71**, 153106 (2005).

[84] M. Ono, H. Kishida, and H. Okamoto, Direct observation of excitons and a continuum of one-dimensional mott insulators: A reflection-type third-harmonic-generation study of ni-halogen chain compounds, Physical review letters **95**, 087401 (2005).

[85] T. Tohyama, Symmetry of photoexcited states and large-shift raman scattering in two-dimensional mott insulators, Journal of the Physical Society of Japan **75**, 034713 (2006).

[86] A. Gössling, R. Schmitz, H. Roth, M. Haverkort, T. Lorenz, J. Mydosh, E. Müller-Hartmann, and M. Grüninger, Mott-hubbard exciton in the optical conductivity of ytio 3 and smtio 3, Physical Review B **78**, 075122 (2008).

[87] F. Novelli, D. Fausti, J. Reul, F. Cilento, P. H. Van Loosdrecht, A. A. Nugroho, T. T. Palstra, M. Grüninger, and F. Parmigiani, Ultrafast optical spectroscopy of the lowest energy excitations in the mott insulator compound yvo 3: Evidence for hubbard-type excitons, Physical Review B **86**, 165135 (2012).

[88] J. Kim, M. Daghofer, A. Said, T. Gog, J. Van den Brink, G. Khaliullin, and B. Kim, Excitonic quasiparticles in a spin–orbit mott insulator, Nature communications **5**, 4453 (2014).

[89] S. Zhou, Y. Wang, and Z. Wang, Doublon-holon binding, mott transition, and fractionalized antiferromagnet in the hubbard model, Physical Review B **89**, 195119 (2014).

[90] T.-S. Huang, C. Baldwin, M. Hafezi, and V. Galitski, Spin-mediated mott excitons, Physical Review B **107**, 075111 (2023).

[91] O. Mehio, X. Li, H. Ning, Z. Lenarčič, Y. Han, M. Buchhold, Z. Porter, N. J. Laurita, S. D. Wilson, and D. Hsieh, A hubbard exciton fluid in a photo-doped antiferromagnetic mott insulator, Nature Physics , 1 (2023).

[92] M. L. Goldberger and K. M. Watson, *Collision theory* (Courier Corporation, 2004).

[93] M. O. Scully and M. S. Zubairy, *Quantum optics* (Cambridge university press, 1997).

[94] D. F. Walls and G. J. Milburn, *Quantum optics* (Springer Berlin, Heidelberg, 2008).

[95] J. Li, D. Golez, G. Mazza, A. J. Millis, A. Georges, and M. Eckstein, Electromagnetic coupling in tight-binding models for strongly correlated light and matter, Physical Review B **101**, 205140 (2020).

[96] O. Dmytruk and M. Schiró, Gauge fixing for strongly correlated electrons coupled to quantum light, Physical Review B **103**, 075131 (2021).

[97] It may appear from the definition of $G^{(2)}(\tau)$ that this phase is $e^{-i(\omega_{\lambda_2} + E_F + (\mathcal{N}_L - 2)\omega_L)\tau}$. But this reduces to $e^{i\omega_{\lambda_1}\tau}$ after using the δ-function that imposes energy conservation, and after getting rid of overall phases independent of indices F, λ_1, λ_2.

[98] For Eq. (65, 66) to hold, we want $\Gamma_j < |\omega_L - U|$, so that the spin operators ($\hat{A}_j$) do not interfere with the charge operators ($\hat{B}_j$, $\hat{C}_j$). Therefore, the approximation $\theta(t)\Gamma_j e^{-\Gamma_j t} \approx \delta(t)$ is justified, only if $|\omega_L - U|$ is much greater than the bandwidth of matter excitations. Since this bandwidth can be at most the tunneling $\mathtt{t}$, the approximation is justified in our setting.

[99] T. Holstein and H. Primakoff, Field dependence of the intrinsic domain magnetization of a ferromagnet, Physical Review **58**, 1098 (1940).

[100] A. Altland and B. D. Simons, *Condensed matter field theory* (Cambridge university press, 2010).

[101] Being in different symmetry channels, $\hat{A}_1^\dagger$ cannot annihilate anyons created by $\hat{A}_2$ and vice-versa.

[102] A. Bohrdt, L. Homeier, C. Reinmoser, E. Demler, and F. Grusdt, Exploration of doped quantum magnets with ultracold atoms, Annals of Physics **435**, 168651 (2021).

[103] A. H. MacDonald, S. M. Girvin, and D. t. Yoshioka, t u expansion for the hubbard model, Physical Review B **37**, 9753 (1988).

[104] C. Kuhlenkamp, W. Kadow, A. Imamoğlu, and M. Knap, Chiral pseudospin liquids in moiré heterostructures, Physical Review X **14**, 021013 (2024).

[105] S. Divic, T. Soejima, V. Crépel, M. P. Zaletel, and A. Millis, Chiral spin liquid and quantum phase transition in the triangular lattice hofstadter-hubbard model, arXiv preprint arXiv:2406.15348 (2024).

[106] T. Graß, U. Bhattacharya, J. Sell, and M. Hafezi, Two-dimensional excitons from twisted light and the fate of the photon's orbital angular momentum, Physical Review B **105**, 205202 (2022).

[107] D. Session, M. J. Mehrabad, N. Paithankar, T. Grass, C. J. Eckhardt, B. Cao, D. G. S. Forero, K. Li, M. S. Alam, K. Watanabe, *et al.*, Optical pumping of electronic quantum hall states with vortex light, arXiv preprint arXiv:2306.03417 (2023).

[108] M. Liu, A. J. Sternbach, and D. Basov, Nanoscale electrodynamics of strongly correlated quantum materials, Reports on Progress in Physics **80**, 014501 (2016).